Disorder dominated singular behaviour in random quantum and classical systems

PhD thesis

written by

Róbert Juhász

supervised by

Prof. Dr. Ferenc Iglói

Institute for Theoretical Physics
University of Szeged
2002

Contents

Chapter 1

Introduction

The bulk of substances and processes in nature is often characterized by certain degree of inhomogeneity: one might say, it is rather the rule than the exception. The most frequently mentioned example is the almost always inevitable presence of impurities or other lattice defects in crystals. The theoretical description of this kind of feature of real systems established the concept of *disorder*, and started on its way the investigation of the—nowadays wide-spread—*disordered models*, which is gently developing to be an independent discipline.

From a theoretical point of view, in systems with many degrees of freedom one has to distinguish between two cases on the ground of dynamics of random impurities. If the characteristic relaxation time associated to impurities t_d is comparable to that of thermal degrees of freedom t_t, i.e. $t_d \sim t_t$, then in the theoretical description randomness appears just as an additional parameter among other parameters characterizing the thermal degrees of freedom. In this case disorder is termed *annealed.*

The situation is very different, however, if impurities relax much slower than thermal degrees of freedom: $t_d >> t_t$. In the theoretical approaches randomness is now considered to be time-independent. This is the case of *quenched* or *frozen disorder.* As a consequence disorder has to be treated separately from thermal degrees of freedom: averaging procedure decomposes into the calculation of thermal expectational value and the averaging over disorder. In the sequel we always think of *quenched* disorder if it is not specified.

Among disordered models special attention was payed for models which exhibit a *phase transition*, where the obvious question arises, what consequences the introduction of disorder has (if it has at all) on the properties of *pure* (e.i. homogeneous) system. According to the experiences quenched disorder has effects on the nature of phase transitions in varying degrees. It may lead to the elimination of the transition by smearing out singularities. Or it may cause the change of order of the transition: a first order transition can turn to a continuous one. In case of a continuous transition (which is not "smeared out" by randomness), a basic question was, how *universal* properties, such as critical exponents are influenced by disorder. Here, a heuristic relevance-irrelevance criterion was formulated by Harris for diluted systems, which was generalized to other kinds of random models [43]. Intensive numerical and analytical work has started to clarify the universality class of various disordered models, including those which have a discontinuous transition in their pure form.

Besides classical transitions, also zero-temperature *quantum phase transitions* attracted much interest, where the critical behavior in random systems is formed by the interplay between disorder and *quantum fluctuations* instead of thermal ones, leading to a new mechanism for phase transitions, which differs in many respects from the activated dynamics in thermally driven transitions. Quantum fluctuations are more pronounced in low-dimensional systems, such as spin chains, where a remarkable progress was achieved by an asymptotically exact real-space renormalization group scheme developed for the random Heisenberg chain by Ma, Dasgupta and Hu [89]. This method was then extended to other random quantum spin chains including the random transverse-field Ising spin chain by Fisher [33, 31, 32]. In these systems a new type of coarse-grained behaviour was found. By coarse-graining, most systems flow toward a fixed point, where the ratio of local parameters in the Hamiltonian remains finite. Contrary to this it turned out, that in these quantum spin chains, the distribution of parameters becomes arbitrarily broad on a logarithmic scale as the fixed point is approached. The ratio of parameters is typically infinite or zero here, and the system is governed by an *infinite-randomness fixed point.*

Disorder was found however to influence not only the critical behaviour. Griffiths and McCoy pointed out in the random classical [37] and quantum Ising model [91], respectively, that there exists an extended region around the critical point, where several physical quantities are singular. The origin of *Griffiths phase* (also termed as a line of "semicritical fixed points") are the fluctuations of disorder. The so called Griffiths-McCoy singularities are much more enhanced in quantum systems, where statics and dynamics are inherently linked. According to a phenomenological scaling theory the origin of singular behaviour of all quantities studied so far, were reduced to a common physical ground.

One might think, among disordered models those with infinite randomness are less tractable. For models governed by a finite-randomness fixed point, disorder can be treated as a perturbation of the pure behaviour, and perturbative methods are sometimes applicable. For the study of models with infinitely strong randomness, perturbative techniques obviously cannot be developed. Instead of this, a large amount of information can be extracted from these systems, (surprisingly, in certain cases more is known about disordered models than about corresponding pure ones), via methods exploiting that disorder completely dominates and prescribes the physics close to the fixed point.

This latter type of randomness, i.e. the infinitely strong one, is the main subject of the present work. We shall discuss two related issues. In the first part of the thesis we deal with the singular behaviour of random quantum spin chains at criticality and in the Grrifiths phase, whereas in the second part a classical model, the random-bond q-state Potts model is studied in a special limit, where thermal fluctuations become irrelevant. A common feature of both problems, that the critical behaviour is strongly dominated by fluctuations of disorder as opposed to quantum fluctuations (resp. thermal fluctuations in the classical model). The new results presented in this work were published in Refs. [54, 112, 55, 53, 70].

The outline of the thesis is the following. In Chapter 2 we shortly summerize the theory of critical phenomena in disordered classical and quantum systems, and give a general phenomenological description of Griffiths phase.

In Chapter 3 previously known results on the random transverse-field Ising chain are reviewed, including the free-fermion description of the model, the

relation with random walk, and the phenomenological scaling theory of the so called *rare events.*

In Chapter 4 we present our numerical and phenomenological results on the Griffiths phase of random transverse-field Ising spin chain. We consider here quantities, the singular behaviour of which is not trivially related to that of the energy gap, such as the second energy gap, non-linear susceptibility, and energy-density autocorrelation function. By using phenomenological scaling arguments we relate the exponents describing the singular behaviour of the above quantities to the dynamical exponent. In the free-fermion picture closed forms for these quantities are derived, which are then analysed numerically. The numerical results support the validity of scaling considerations.

Subsequently we extend the Ma-Dasgupta-Hu type real-space renormalization group scheme to the Griffiths phase, which is presented in Chapter 5. We give an analytic solution for the flow equations of the random transverse-field Ising chain in the Griffiths region, where we show that the procedure is asymptotically exact, and the dynamical exponent stays invariant during renormalization. By the help of this an exact expression for the determination of dynamical exponent is given. On the ground of phenomenological considerations we propose the above assertions to be generally valid for quantum spin chains. In order to check this we solve numerically the renormalization group flow equations of random quantum Potts chain. Our results are compatible with theoretical considerations.

Chapter 6. is devoted to the study of random XY- and random dimerized XX chain. Here, we develop a phenomenological theory of average quantities, which relies on the scaling behaviour of rare events. Establishing a relation with random walks, rare events are identified as regions corresponding to *surviving walks.* By the help of this theory we determine the complete set of bulk- and surface critical exponents. These are than compared to numerical results on operator-profiles obtained by using the free-fermion representation. We find critical order parameter profiles follow the conformal predictions, if we use the exponents obtained from phenomenology. Furthermore we determine the average behaviour and the distribution of dynamical correlations at criticality and in the Griffiths phase. Using the decoupling of models under study into two Ising chains, we give an analytical expression for the dynamical exponent.

In Chapter 7 we turn to study the q-state random Potts model, where after appropriate parameterization the $q \to \infty$ limit is sensible, and the magnetization exponent is known to converge to a finite value. Contrary to previous finite-q calculations we perform here a *direct* investigation in the $q \to \infty$ limit by the help of *random cluster representation* of the model. We show that in this limit thermal fluctuations becomes irrelevant, and critical behaviour is determined by a single dominant graph in the geometric representation of the model. To find this graph is equivalent to an optimization problem of a non-convex cost-function defined on the set of graphs. We solve this problem by a stochastic- and a combinatorial optimization method, and analysing the fractal properties of dominant graph, we give a more accurate estimation for critical exponents, than previously.

Chapter 2

Criticality and disorder

2.1 Critical phenomena

In the present work we deal with continuous phase transitions of disordered models. These phase transitions have to be discussed in the light of critical phenomena in pure systems, irrespective whether the corresponding pure system undergoes a first- or a second order transition. Therefore we review a few basic notions connected with critical phenomena in pure systems, before we turn to discuss the consequences of randomness in the next section.

2.1.1 Critical exponents

We consider here a pure system with many degrees of freedom and short-range interactions between them, which possesses a continuous phase transition. To quantify the deviation from criticality one introduces a *control parameter* δ, which is zero at the transition. In thermally driven phase transitions it is the reduced temperature, but in general it may be some other parameter of the Hamiltonian.

The system is characterized by a continuous function of δ, the *order parameter*, which is non-zero at one side of the transition ($\delta < 0$), called *ordered phase*, and vanishes otherwise. The opposite side of critical point is termed *disordered phase*. In the sequel we deal with magnetic phase transitions, which are connected with the vanishing of magnetization. Here the local order parameter density is the local magnetization

$$\langle \hat{m}(\mathbf{r}) \rangle = -\frac{\partial f}{\partial h}, \tag{2.1}$$

where the local external field $h(\mathbf{r})$ couples to to the local magnetization operator $\hat{m}(\mathbf{r})$ in the free energy density $f(\mathbf{r})$. Here and in the following $\langle \ldots \rangle$ denotes thermal expectation value, which reduces at zero temperature to ground state expectational value.

The bulk two-point correlation function for the magnetization operator is obtained by taking the functional derivative of the free energy with respect to the position-dependent field

$$C(r, \delta) \equiv \langle \hat{m}(0)\hat{m}(\mathbf{r}) \rangle = \frac{\delta^2 F}{\delta h(0) \delta h(\mathbf{r})}. \tag{2.2}$$

It has the asymptotic behaviour $\lim_{r\to\infty} C(r,\delta) = \langle\hat{m}(0)\rangle\langle\hat{m}(\mathbf{r})\rangle$, since the local order parameters are asymptotically uncorrelated. The ordered phase is characterized by $\langle\hat{m}(\mathbf{r})\rangle \neq 0$, meaning, there is *long-range order* (LRO), while in the disordered phase $\langle\hat{m}(\mathbf{r})\rangle = 0$ and there is *short-range order* (SRO). Considering the connected part of correlation function, i.e. the spatial correlation of fluctuations around the average, $C_{\text{con}}(r,\delta) = \langle(\hat{m}(0) - \langle\hat{m}(0)\rangle)(\hat{m}(\mathbf{r}) - \langle\hat{m}(\mathbf{r})\rangle)\rangle$, one observes in both phases:

$$C_{\text{con}}(r, \delta \neq 0) \sim e^{-r/\xi}, \tag{2.3}$$

where ξ is the *correlation length.* This is the distance over which the fluctuations of microscopic degrees of freedom (here the local order parameters) are significantly correlated with each other. (Note that $C_{\text{con}}(r) \equiv C(r)$ for $\delta \geq 0$.)

Close to criticality the singular part of thermodynamic quantities are described by power-laws, where the powers are called *critical exponents.* A critical point is hallmarked by an infinite correlation length, which close to the transition diverges as

$$\xi \sim |\delta|^{-\nu}, \tag{2.4}$$

where ν is the correlation length exponent. Strictly at criticality ($\delta = 0$) ξ is infinite, and the bulk correlation of the order parameter has an algebraic decay,

$$C(r, 0) \sim r^{-\eta}, \tag{2.5}$$

where η is the decay exponent. This type of behaviour of correlation is called *quasi-long-range order* (QLRO). The bulk order parameter (simply denoted by m) vanishes in the ordered phase close to the transition as

$$m \sim (-\delta)^{\beta}, \tag{2.6}$$

where β is the order parameter exponent. The specific heat $c = \frac{\partial^2 f}{\partial \delta^2}$ diverges as

$$c \sim |\delta|^{-\alpha}, \tag{2.7}$$

with α, the specific heat exponent. Perturbing the system by an external magnetic field h, leads to the divergence of the susceptibility $\chi = \frac{\partial^2 f}{\partial h^2}$ following the scaling law

$$\chi \sim |\delta|^{-\gamma}, \qquad h \to 0. \tag{2.8}$$

At $\delta = 0$ the order parameter vanishes with h like

$$m \sim h^{1/\delta_h}. \tag{2.9}$$

Close to the surfaces of the system (if there are any) various properties may behave differently as in the bulk. This necessitates the introduction of the analogous *surface critical exponents*, through the singular behaviour of corresponding surface quantities, e.g. $m_s \sim (-\delta)^{\beta^s}$, where m_s is the surface magnetization.

In most cases the critical exponents are fully specified by the symmetry properties of the model under consideration, and do not depend on microscopic details of interaction. This allows phase transitions to be categorized into different *universality classes.*

2.1.2 Scaling

The power-low form of quantities in terms of parameters δ, h etc. measuring the deviation from critical point, is linked to the self-similarity of critical fluctuations inside the correlation volume ξ^d. The system is then covariant under a global change of the length-scale and singular quantities are homogeneous functions of their arguments. These properties form the basis of the scaling hypothesis.

When lengths are rescaled by a factor $b > 1$, i.e. when $\mathbf{r} \to \mathbf{r}/b$, the scaling fields ($\delta$, h) are changed by a factor b^{d-x} where x is the *scaling dimension* of conjugate quantities. When $d - x > 0$ (< 0) the corresponding scaling field grows (decreases) under rescaling. Such a field is said to be relevant (irrelevant) whereas it is marginal when $x = d$. The system becomes invariant under rescaling only when the relevant scaling fields vanish which corresponds to the critical point. Since irrelevant variables finally vanish under rescaling, only relevant and marginal scaling fields influence the critical properties, the marginal ones generally leading to varying exponents.

Assuming that the only relevant scaling fields are δ and h, the free energy density is a homogeneous function of its variables and transforms as

$$f\left(\delta, h, \frac{1}{L}\right) = b^{-d} f\left(b^{1/\nu}\delta, b^{d-x_m}h, \frac{b}{L}\right), \tag{2.10}$$

where x_m is the scaling dimension of magnetization. The critical behaviour of conjugate quantities and their derivatives can be deduced from (2.10), and the corresponding exponents are all related to x_m and ν, as follows:

$$\begin{aligned}
\alpha &= 2 - d\nu && (2.11)\\
\beta &= \nu x_m && (2.12)\\
\gamma &= \nu(d - 2x_m) && (2.13)\\
\delta_h &= \frac{d}{x_m} - 1 && (2.14)\\
\eta &= 2x_m. && (2.15)
\end{aligned}$$

Relation (2.12) can be recovered from the second δ derivative of both sides of (2.10) at $h = 1/L = 0$ and taking $b = \delta^{-\nu}$. From (2.10) it follows for the scaling form of magnetization

$$m\left(\delta, h, \frac{1}{L}\right) = b^{-x_m} m\left(b^{1/\nu}\delta, b^{d-x_m}h, \frac{b}{L}\right). \tag{2.16}$$

Taking now $h = 1/L = 0$ and $b = \delta^{-\nu}$ one gets (2.13). Similarly, putting $\delta = 1/L = 0$ and $b = h^{\frac{1}{x_m - d}}$ one obtains (2.15). From (2.10) the scaling form of susceptibility is

$$\chi\left(\delta, h, \frac{1}{L}\right) = b^{d-2x_m} \chi\left(b^{1/\nu}\delta, b^{d-x_m}h, \frac{b}{L}\right). \tag{2.17}$$

Taking $h = 1/L = 0$ and $b = t^{-\nu}$ one arrives to (2.14). The transformation law of the two-point function follows from (2.10) and (2.2)

$$C(r, \delta) = b^{-2x_m} C(\frac{r}{b}, b^{1/\nu}\delta). \tag{2.18}$$

Now with the choice $\delta = 0$ and $b = r$ relation (2.15) is recovered. At the critical point singularities are supressed by a finite L. *Finite-size scaling* exploits the way they develop when $L \to \infty$ in order to determine the critical exponents. For example choosing $\delta = h = 0$ and $b = L$ in (2.16) gives

$$m \sim L^{-x_m}. \tag{2.19}$$

2.1.3 Conformal invariance

Covariance under conformal transformations [11, 46] is expected to hold at the critical point of systems with short-range interactions, which possess translational and rotational symmetry and are invariant under uniform scaling.

A conformal transformation $\mathbf{r} \to \mathbf{r}'(\mathbf{r})$ can be viewed as a generalization of uniform scaling, where the local structure of the lattice (i.e. angles between curves) is preserved, but the rescaling factor $b(\mathbf{r})$ is a smooth function of position. It follows from the Jacobian of the transformation as $b(\mathbf{r})^{-d} = \det(\partial\mathbf{r}'/\partial\mathbf{r})$. Since local fields transform as $h(\mathbf{r}) \to h'(\mathbf{r}') = b(\mathbf{r})^{d-x}h(\mathbf{r})$, two point correlation function in (2.2) transforms like

$$\langle \hat{m}(\mathbf{r}_1)\hat{m}(\mathbf{r}_2)\rangle = b(\mathbf{r}_1)^{-x_m} b(\mathbf{r}_2)^{-x_m} \langle \hat{m}(\mathbf{r}'_1)\hat{m}(\mathbf{r}'_2)\rangle \tag{2.20}$$

under a conformal transformation. The conformal group for $d > 2$ is finite-dimensional and contains rotations, uniform dilatations, translations, inversions and the special conformal transformation

$$\frac{\mathbf{r}'}{(r')^2} = \frac{\mathbf{r}}{r^2} + \mathbf{a}, \tag{2.21}$$

which is a composition of previous ones. It is especially useful, since a semi-infinite system with a flat surface containing the origin is invariant under (2.21) if $\mathbf{a}$ parallel with the surface, and the covariance under such an infinitesimal transformation determines the form of critical two-point functions.

In two dimensions the conformal group is isomorfic with the group of complex analytic functions $w(z)$. Therefore it is infinite-dimensional and the local dilatation factor is $|dw/dz|^{-1}$. A frequently used conformal mapping in two dimensions is the *logarithmic transformation*

$$w = \frac{L}{2\pi} \ln z, \tag{2.22}$$

which maps the infinite z plane onto a periodic strip of width L and infinite length. Applying (2.22) on the correlation function (2.18) at criticality, it can be shown, that the correlation length ξ along the strip is related to the scaling dimension x_m via

$$\xi^{-1} = \frac{2\pi}{L} x_m. \tag{2.23}$$

Furthermore the above procedure allows to determine the boundary-induced operator profiles [57, 129, 56].

If a disordered system has the required symmetry properties on average, then the results of conformal invariance are expected to hold for the corresponding average quantities. When some of the symmetries quoted above are broken, then some of the results associated to conformally invariant systems still hold, like the relation (2.23) as observed in specific examples [57].

2.2 The effects of disorder

In this section we discuss the question how randomness affects the phase transitions. We shall use through and through the terminology of renormalization group (RG) theory which is a useful tool in the theory of phase transitions. Generally in real-space RG methods a partial trace (i.e. trace over a fraction of degrees of freedom) in the patition sum is performed. After this in some cases it can be replaced by an effective Hamiltonian which has the same structure as the original one, however with different parameters and a reduced number of degrees of freedom. The iteration of this procedure is then leads to the changing of parameters in the Hamiltonian, which can be illustrated in the parameter space by the so called *RG trajectories.* A point in the parameter space which is left invariant by the transformation is called a *fixed point.* The phase diagram can be divided into attractive basins of fixed points, from any point of which the system flows to the same fixed point. In such a region the large-scale behaviour is described by the properties of the fixed point. The decreasing of degrees of freedom during the RG transformation corresponds to the rescaling of correlation length. Therefore in a fixed point the correlation length must be either zero or infinite. The former ones are called trivial fixed points and these control the ordered and disordered phases, whereas the latter are the critical fixed points controlling the system on the critical surface.

Relevance-irrelevance criteria For continuous phase transitions perturbation expansions were developed [86, 87, 88, 28, 82] to treat the effect of weak disorder and also a heuristic relevance-irrelevance criterion on the stability of a pure system fixed point against weak disorder is known[43], which was originally derived in diluted systems, but can be generalized to other kinds of random systems. The *Harris-criterion* predicts the randomness, which couples to the energy density, to be relevant, if

$$\nu < d/2, \tag{2.24}$$

where ν is the correlation length exponent of the *pure* system. In this case the system flows to a new disordered fixed point in the parameter space (see later). While if $\nu > d/2$, randomness is irrelevant, and the critical behaviour is governed by the pure system fixed point. Note that the above criterion takes into account only the immediate vicinity of the pure system fixed point, i.e. it concerns only *weak* disorder. It can happen that a model is stable against weak disorder, however sufficiently strong randomness brings it to a new fixed point. Such a behaviour can be observed e.g. in the one-dimensional Ashkin-Teller model and the quantum-clock model [13].

The effect of quenched disorder at a first-order transition point is comparatively less understood than the same phenomena at a continuous transition point. Here neither a general relevance criterion, nor a consistent perturbation expansion is known to apply around the discontinuity fixed point of the pure model. One remarkable exception is the stability criterion by Aizenman and Wehr [2] (based on an idea of Imry and Wortis [64], see also by Hui and Berker [50]), which rigorously states that in two dimensions any amount of quenched disorder will soften the first-order transition in the pure system into a continuous one. In three dimension the same criterion predicts a cross-over phenomenon:

generally the transition stays discontinuous for weak disorder, whereas it turns to a second-order one for sufficiently strong disorder [21].

Irrelevant disorder If quenched disorder is irrelevant, the system is spatially inhomogeneous on a microscopic scale, but by coarse-graining it, becomes asymptotically homogeneous on macroscopic scales. The coarse-grained behaviour is thus equivalent with that of the corresponding pure system, and the system belongs to the pure system universality class.

If randomness is relevant, the resulting disordered fixed points can be further classified on the basis of the coarse-grained behaviour of the system in the low-energy and long-wavelength limit[96].

Finite randomness fixed points One possibility for the system by coarse-graining it is to remain inhomogeneous also on macroscopic scales, however with *finite* relative magnitude of inhomogenities (i.e. ratio of parameters in the Hamiltonian) in the long-wavelength limit. In this case the system is said to be governed by a finite randomness fixed point.

Infinite-randomness fixed points An other possible scenario by coarse-graining a random system is that the relative magnitude of inhomogenities does not remain finite, but grows without limits. In these systems the distributions of the logarithmic magnitudes of the terms in the Hamiltonian become arbitrarily broad, as the energy scale tends to zero. The critical behaviour is controlled by an *infinite-randomness fixed point* (IRFP). Broad distributions involve the lack of self-averaging. Considering finite samples of size N, the thermal average of a quantity X is obviously sample-dependent in a quenched random system. Therefore, if one is interested in the average quantity, one has to perform an additional average over the disorder configurations, which is called *quenched disorder average*. We shall denote by $[\ldots]_{av}$ in the following. The sample-to-sample fluctuations of X can be described by the normalized variance:

$$D_N(X) = \frac{[X^2]_{av} - [X]_{av}^2}{[X]_{av}^2}. \tag{2.25}$$

If $D_N(X) \to 0$ in the thermodynamic limit $N \to \infty$, then X is said to be *self-averaging* and a sufficiently large sample is a good representative of the whole ensemble. Contrary if $D_N(X)$ tends to a finite limit, the sample-to-sample fluctuations remains finite, and any sample, no matter how large, is never a good representative of the ensemble. In this case X is called non-self-averaging, and in order to characterize X, its whole distribution is needed.

There are only few models known, where the critical behaviour is controlled by an IRFP. Most of them are one-dimensional quantum chains at zero temperature: random singlet states of certain antiferromagnetic chains, the quantum critical point of random transverse-field Ising (and Potts) chains or the Haldane state in the random spin-1 Heisenberg chain. In addition to chains we mention here spin-$\frac{1}{2}$ ladders, which exhibit essentially one-dimensional behaviour, as well [84, 97]. Later it turned out that also the quantum critical behaviour of higher-dimensional systems, such as the $d = 2$ and $d = 3$ random ferromagnetic transverse-field Ising model, is governed by an IRFP [96].

2.3 Classical spin models with quenched disorder

Here, we introduce two simple but non-trivial classical spin systems, which are basic for the theoretical study of critical behaviour with quenched disorder. The simplest and historically first studied spin system having a continuous phase transition, is the *Ising model* [65]. It is defined by the Hamiltonian

$$H = -J \sum_{\langle ij \rangle} \sigma_i \sigma_j - h \sum_i \sigma_i, \tag{2.26}$$

where $\sigma_i = \pm 1$ is a classical Ising spin attached to site i of a d-dimensional lattice, and the first sum is taken only over nearest-neighbour spins. The short-range interaction tends to align neighbouring spins if $J > 0$ (the case of Ising ferromagnet), while for $J < 0$ antiparallel orientation is favorable (Ising antiferromagnet). Below a critical temperature T_c, the system possesses two ordered phases with non-zero per site magnetization $m = \langle \sigma \rangle$. (See the phase diagram in Fig. 2.1.) The phase boundary $h = 0$ ends in a critical point at $T = T_c$.

Disorder is introduced in (2.26) via the parameters J and h:

$$H = -\sum_{<ij>} J_{ij} \sigma_i \sigma_j - \sum_i h_i \sigma_i, \tag{2.27}$$

where, now, J_{ij} and h_i are quenched random variables. Hereby one obtains the various random Ising models.

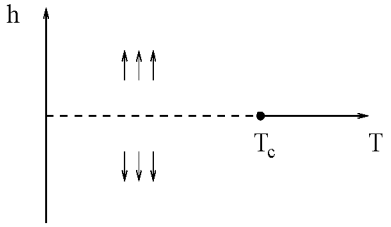

Figure 2.1: Phase diagram of the Ising ferromagnet. Crossing the dashed line the system undergoes a first order transition. A critical point is located at $T = T_c$, $h = 0$.

An important generalization of (2.26) (in the sense that more than two values of spin variables are allowed) is the *q-state Potts model*,

$$H_{Potts} = -\sum_{\langle ij \rangle} J_{ij} \delta(\sigma_i, \sigma_j) - \sum_i h_i \delta(\sigma_i, 1), \tag{2.28}$$

where the classical Potts spin σ_i, is allowed to take q different values $\sigma_i = 1, 2, \ldots, q$ and $\delta(i, j)$ is the Kronecker symbol. For $q = 2$ one recovers the Ising Hamiltonian (2.26) up to a multiplicative and an additive constant. Other notable special case of (2.28) is *bond-percolation*, which can be regarded as the suitably defined $q \to 1$ limit of q-state Potts model [132].

For $h = 0$ the pure Potts model has a low temperature ordered and a high temperature disordered phase. In between them a phase transition point takes place, which is of first order, if q is above some dimension-dependent critical value $q_c(d) \leq q$, otherwise it is continuous. However, even in the former case the transition softens to a continuous one in the random bond Potts model [2].

Diluted models

The simplest realizations of systems with quenched disorder are the *diluted magnets*. These systems may be interpreted as a binary alloy with a magnetic and a non-magnetic component, which occupy the lattice sites randomly. The two

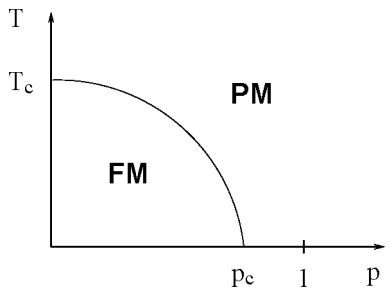

Figure 2.2: Phase diagram of a diluted ferromagnet. The ferromagnetically ordered phase is denoted by FM, whereas the paramagnetic phase by PM.

relevant parameters of such a system are the temperature and the concentration of, say, the non-magnetic component p. The phase diagram is depicted in Fig. 2.2. The line $T = 0$ of the phase diagram corresponds to the problem of *site-percolation*. Decreasing p from one towards zero, p_c is the first value where an infinite cluster of magnetic atoms appears (in an infinite system). The singular point, p_c, is a geometric analogon of continuous phase transitions. For example the density of the spanning cluster playing the role of order parameter vanishes as $\rho \sim (p_c - p)^{\beta_p}$ close to p_c. Below a certain concentration, p_c, the system has a long-range ordered phase at low enough temperature, while above p_c there does not exist any long-range order. Crossing the separatrix a continuous phase transition occurs, which belongs to different universality classes at $T = 0$ (percolation) and at $p = 0$ (pure ferromagnetic system). In the intermediate region $0 < p < p_c$ the critical exponents are constant. If dilution is irrelevant, the systems on the separatrix flows to the attractive pure system fixed point and the exponents agree with that of pure one. If dilution is relevant, a new attractive fixed point appears on the phase boundary which controls the whole region $0 < p < p_c$, and characterized by different exponents than that of pure one.

A particular diluted model is the bond-diluted Ising ferromagnet, obtained by putting $h_i = 0$ and $J_{ij} = 0$ with probability p and $J_{ij} = J > 0$ with probability $1 - p$ in (2.27).

Random field models

The second important class is the family of *random field models*. Considering (2.27) with $J_{ij} = J$ and h_i's as independent random variables with zero mean, (drawn from, e.g. a Gaussian distribution with variance h_0) one obtains the random field Ising model. There is a competition between the two terms in the Hamiltonian at $T = 0$: the interaction tends to align neighbouring spins, while external fields try to pin the spins according to the sign of local field. Fixing the the value of the exchange coupling J, the two relevant parameters are the variance of the field distribution h_0 and the temperature T. The phase diagram looks similar to that of diluted models (one should replace p by h_0). For sufficiently small h_0 and T the interaction term wins and the system is in its ferromagnetic phase with non-vanishing magnetization. As opposed to dilution, random field is always a relevant perturbation. Finding the ground

state is an optimization problem and since the $T = 0$ fixed point controls the whole critical line, the structure of the ground-state gives some insight into the finite-temperature behaviour, as well.

Spin glasses

The paradigms of quenched disordered systems are the *spin glasses* [6]. These are different from other random systems in many respects: at the transition the *non-linear* response functions diverges, dynamics is rather slow in the spin-glass phase and near the transition, they are characterized by a "random" order parameter and the "chaotic" behaviour of correlations as a function of temperature can be observed.

A particular spin glass model is the Ising spin glass. It can be originated from (2.27) by choosing $h_i = 0$ and $J_{ij} = \pm J$ with probability $1 - p$ and p, respectively. So both ferromagnetic and antiferromagnetic couplings are allowed between pairs of spins.

The phase diagram (Fig. 2.3) is richer than that of diluted models. In addition to ferromagnetic, antiferromagnetic, and paramagnetic phases a *spin glass (SG) phase* appears at low enough temperature and at intermediate concentration of antiferromagnetic couplings. The two main physical ingredients controlling this region are the quenched disorder and the *frustration*. This later means that not all terms in the Hamiltonian can be minimized simultaneously. These lead to a rugged multi-valley structure of the energy-landscape with exponentially many local minima having approximately the same energy. The finding of the true minimum (or minima if degeneracy is possible) is an optimization procedure again. The microscopic picture behind the spin-glass behaviour is that the samples consist of small ferromagnetically ordered islands, the momenta of which point to random directions. Therefore in this phase the conventional order parameter is zero $[\langle\sigma\rangle]_{av} = 0$. However $[\langle\sigma\rangle^2]_{av} \neq 0$, while in the paramagnetic phase it vanishes, so this quantity is suitable for order parameter.

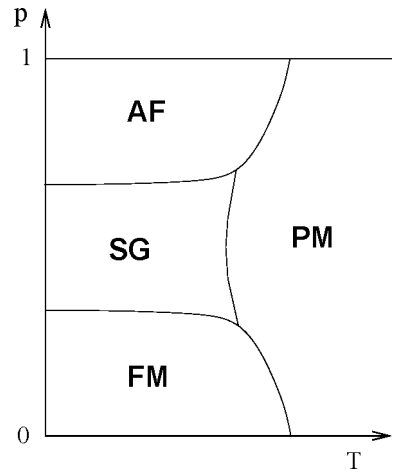

Figure 2.3: Phase diagram of the three-dimensional Ising spin glass on a cubic lattice. In between ferromagnetic- (FM) and antiferromagnetic (AF) phase a spin glass phase (SG) takes place, where $[\langle\sigma\rangle^2]_{av} \neq 0$.

2.4 Phase transitions in quantum systems

So far we quoted examples for phase transitions in classical (spin) systems. Now we turn to the survey of phase diagrams of quantum-mechanical systems. First we deal with features, which are characteristic also for *pure* quantum models, while phenomena caused by randomness are discussed in the next section.

In the classical disordered systems in the previous section two antagonistic effects are present: On the one hand there were short-range interactions between spins, which enforce ordering, and on the other hand thermal fluctuations, which try to destroy the order. At criticality these two conflicting effects are in some sence in equilibrium. Furthermore there was an other ingredient, a parameter (dilution, variation of random fields, concentration of antiferromagnetic couplings), which can be used in order to tune the critical temperature. In a quantum-mechanical model all these effects may be present, as well. What makes the situation much different is that the Hamiltonian describing the system contains non-commuting local terms. This leads to *quantum fluctuations* and gives an entirelly different way for the relaxation of the system, via quantum tunelling.

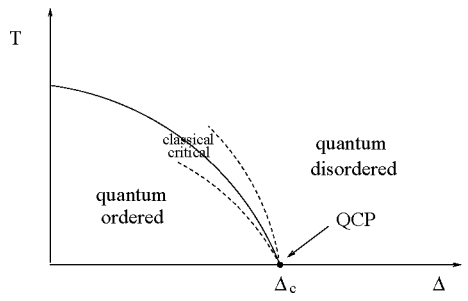

Figure 2.4: Phase diagram of a quantum system. A quantum critical point (QCP) is located at $T = 0$, $\Delta = \Delta_c$.

We now discuss the influence of quantum fluctuations on the critical behaviour of the system. We first argue that they are irrelevant at finite-temperature transitions. In order to do this, one has to compare the magnitude of thermal fluctuations with that of quantum fluctuations. The former is given by the thermal energy per degree of freedom, which is of order $k_B T_c$, while the later is measured by the zero-point quantum of energy, which is $\hbar\omega_c$, if the characteristic frequency of fluctuations is ω_c. It is known, that close to the transition the correlation length ξ, becomes infinite, according to (2.4). At the same time fluctuations become very slow, and the relaxation time diverges, which is known as "critical slowing-down". The characteristic time scale, which is set by the relaxation time close to criticality, and the characteristic length scale, given by the correlation length, are connected as

$$\tau \sim \xi^z, \tag{2.29}$$

where the exponent z, defined in this way, is called *dynamical exponent.* By the help of (2.4) and (2.29) one obtains for the characteristic frequency

$$\omega_c \sim \frac{1}{\tau} \sim |\delta|^{\nu z}. \tag{2.30}$$

At a finite T_c quantum fluctuations are negligible if $\hbar\omega_c \ll k_B T_c$, or equivalently

$$|\delta| \ll T_c^{\frac{1}{\nu z}}, \tag{2.31}$$

which can always be satisfied close enough to the transition for finite T_c. Hence for any finite T_c the transition is therefore classical.

Suppose there is a parameter Δ, by which the transition temperature can be tuned, and after all, at some value Δ_c, T_c is forced to zero. (See phase diagram in Fig. 2.4.) We see, that the width of the region, where (2.31) is valid,

shrinks to zero as $T_c \to 0$ (Fig. 2.4). If $T_c = 0$ a new universality class emerges, which differs from the classical one. Changing Δ along the line $T = 0$ a *quantum phase transition* (QPT) occurs at $\Delta = \Delta_c$, which is triggered purely by quantum fluctuations. At $T = 0$ no heat bath exists, and thermally activated hopping in the energy landscape is replaced by tunelling through barriers. A so called *quantum control parameter* measuring the deviation from quantum critical point can be conveniently defined as $\delta = \frac{\Delta_c - \Delta}{\Delta}$.

So for finite T_c the critical behaviour of a d-dimensional quantum system is equivalent with that of a d-dimensional classical system. Contrary to this, strictly at the quantum critical point (QCP) the physics is described by a $(d+1)$-dimensional classical action, where the extra dimension corresponds to the imaginary time $\tau = it$ of the quantum-mechanical problem. The reason for this connection is the Suzuki-Trotter transformation [125]. The main idea of Suzuki-Trotter mapping is, that the imaginary time evolution operator of a d-dimensional quantum model, which is Hermitian, can be viewed as a transfer-matrix of a $(d+1)$-dimensional classical model, in the anisotropic limit where the lattice spacing in the transfer direction vanishes. In this case the quantum model is called the *Hamiltonian limit* of the classical model, while the later is the *lattice representation* of the former. The extension of the classical system in the transfer direction is $\hbar/k_B T$, where T is the temperature of the quantum model. For $T_c \neq 0$ the correlation length in the imaginary time direction is limited by $\hbar/k_B T_c$, and the critical behaviour is controlled by the diverging correlation length in space dimensions. So the behaviour is like that of a d-dimensional classical system. For $T_c = 0$, however, correlations in the temporal direction can grow unlimitedly. Therefore the system behaves as a $(d+1)$-dimensional classical one.

In quantum models relation (2.29) is a consequence of the fact, that statics and dynamics are inextricably connected, since both statical properties and dynamics of the system are determined by the Hamiltonian. According to Suzuki-Trotter mapping the imaginary time of a quantum model can be viewed as additional spatial dimension of a classical model. Thus, it is supposed that the correlation length in this direction (the relaxation time) diverges simultaneously with spatial correlation length near criticality, as given in (2.29). In pure systems the dynamical exponent is one, $z = 1$, which corresponds to the equivalence of time and space, and also corresponds to a linear dispersion relation, which is indeed the case for the exactly solvable one-dimensional transverse-field Ising model.

In order to illustrate the relevance of QPT's one mentions the metal-insulator transition in three-dimensional doped semiconductors [81] or the superconducting-insulator transition [85]. In both cases the control parameter is the concentration of impurities. Other examples are the quantum spin glasses [117, 6], where the control parameter is an external thermodynamical parameter, such as the strenght of the magnetic field.

2.4.1 Transverse-field Ising model and quantum Potts model

For concreteness we introduce here the simplest model possessing a QPT. As the prototype of thermal phase transitions is the classical Ising model, the protoype of systems possessing a QPT, is the transverse-field Ising model (TIM). It is

defined by the Hamiltonian:

$$H = -\sum_{<ij>} J_{ij}\sigma_i^x\sigma_j^x - \sum_i h_i\sigma_i^z, \tag{2.32}$$

where σ_i^x and σ_i^z are Pauli matrices, representing a spin sitting on site i of a d-dimensional hypercubic lattice. The first sum in (2.32) runs over only nearest-neighbour pairs of sites. This model is the Hamiltonian limit of the classical Ising model in (2.27). For later convenience we introduce here immediately the random version of TIM, where exchange couplings, J_i and external fields h_i are independent random variables.

Since $[\sigma_i^x, \sigma_i^z] \neq 0$ for all i, (2.32) is genuinely a quantum-mechanical model. The interaction term tends to order the spins along the x-axis, while the transverse fields, coupled to σ_i^z, try to flip them to the z-axis hence they tend to destroy the order. If the exchange couplings are positive, the interaction prefers a parallel orientation of neighbouring spins, and the order is ferromagnetic, while if they are negative, the antiparallel alignment is favourable, and it is the case of an antiferromagnet. By allowing both ferromagnetic and antiferromagnetic couplings, one gets the quantum Ising spin glass. (The sign of h_i's can always be gauged away by local spin rotations around the x-axis.)

Now we consider the pure ferromagnetic TIM, i.e. $J_{ij} = J > 0$ and $h_i = h$. Fixing J, the quantum control parameter is defined as $\delta = \frac{h-h_c}{h_c}$, where h_c is the dimension-dependent critical value of the field h. In any dimension at zero temperature the TIM has a ferromagnetically ordered phase with non-zero magnetization for $\delta < 0$, while if $\delta > 0$ the system is in its paramagnetic phase with vanishing magnetization. The two regions are separated by a quantum critical point at $\delta = 0$. If the dimensionality of the system is below the lower critical dimension d_c, which is between two and three, the system is paramagnetic at any finite temperature, while if $d > d_c$, the ferromagnetic order holds on also for finite temperatures.

Quantum fluctuations are introduced in this model by the presence of transverse terms: If h was zero, the interaction term would be diagonal in the x-representation, the σ^x operators could be replaced by its eigenvalues, and the model would be equivalent to the classical Ising model, with a unique ground state (in small symmetry breaking longitudinal field). On the other hand if interaction were switched off, the spins would be pinned by external fields, and the ground state would be classical again.

If J is non-zero, and the field is switched on, H is no longer diagonal in the x-representation, and the model becomes quantum-mechanical. The ground-state will be a superposition of classical states, which describes the quantum-mechanical tunelling between local minima of the classical energy-landscape. Quantum fluctuations which manifests itself in tunelling are the strongest at the critical point $\delta = 0$.

As we have already mentioned, the lattice representation of (2.32) is a classical $d+1$-dimensional Ising model with ferromagnetic interactions in the extra, temporal direction:

$$\beta H_{\text{classical}} = -\sum_\tau \sum_{<ij>} K_{ij}\sigma_i(\tau)\sigma_j(\tau) - \sum_\tau \sum_i K_i\sigma_i(\tau)\sigma_i(\tau+1), \tag{2.33}$$

where $\tau = 1, 2, \ldots, L_\tau$ refers to slices of the (imaginary) time direction. The reduced interactions, K_{ij} are the same in all time slices. The couplings in (2.33)

are related to that of the quantum Ising model, as $K_{ij} = \Delta\tau J_{ij}$, $\exp(-2K_i) = \tanh(\Delta\tau h_i)$, where $\Delta\tau$ is the width of a time slice. The extension in this direction is equal to the temperature of the quantum model: $L_\tau \Delta\tau = \beta$. Performing the Hamiltonian limit $\Delta\tau \to 0$ leads to $K_{ij} \to 0$ and $K_i \to \infty$ in (2.33). At criticality the universal properties are not affected by $\Delta\tau$, and (2.33) belongs to the same universality class as the TIM.

A generalization of TIM is the *q-state quantum Potts model.* It is defined by the Hamiltonian

$$H = -\sum_{\langle ij \rangle} q J_{ij} \delta(n_i, n_j) - \sum_i \frac{1}{q} h_i \sum_{k=1}^{q-1} M_i^k, \tag{2.34}$$

where the $q \times q$ matrix M_i given in (B.3) flips the Potts spin at site i, the states of which are labelled by $|n_i\rangle$, $n_i = 1, 2, \ldots, q$. This model is the Hamiltonian limit of the classical q-state Potts model given in (2.28), and it reduces to (2.32) for $q = 2$.

2.4.2 Quantum phase transitions in the presence of disorder

So far we have concentrated on the quantum critical behaviour of *pure* systems. Now we sketch here what differences to the pure quantum critical behaviour may arise by the introduction of disorder. We illustrate this through the random variant of TIM in (2.32), where the exchange interactions J_{ij} and external fields h_i are independent, random variables, drawn from some distributions, $\pi(J)dJ$ and $\rho(h)dh$, respectively.

Throughout this work we are dealing with lattice models, in which random variables at different lattice sites are uncorrelated, although the question of correlated disorder is also a subject of intensive research[130, 111]. Another feature is that, random variables are identically distributed in space. The problem of "inhomogeneous disorder", when variables are drawn from position-dependent distributions, has also attracted much interest, but it is not discussed here. For a recent study of this issue in the RTIC with algebraic decaying surface inhomogeneous disorder see Ref. [72].

As we have already discussed in Section 2.2, a pure system fixed point may be eighter stable against disorder or unstable, if the system flows to a new, disordered fixed point. For deciding the relevance of disorder one invokes the Harris-criterion, which indicates the pure quantum Ising critical point to be unstable against weak disorder if $d < 4$.

As we have already mentioned, time scale and length scale are connected in quantum systems according to (2.29), and pure critical behaviour is isotropic in the sence that $z = 1$. This is not necessarily true in the vicinity of a disordered quantum critical point. This follows from the fact, that randomness is uncorrelated in spatial directions, however the quenched (time-independent) randomness is perfectly correlated along the time direction. The anisotropy in time direction is manifesting itself in a dynamic exponent differing from one. A conventional finite randomness fixed point is characterised by a finite dynamical exponent, while an IRFP is characterised by extremly strong anisotropy, with a formally infinite dynamical exponent. The random transverse-field Ising ferromagnet in one-, two- and three spatial dimensions were found to be governed

by an IRFP with $z = \infty$ [106, 113, 63, 96]. The IRFP was argued to be attractive also for quantum Ising spin glasses for strong disorder [96], but in contrary to this, Monte-Carlo results predicted a conventional fixed point with finite z [38, 115]. For a possible explanation of this controversy see Ref. [13].

2.5 Griffiths phase

A surprising feature of disordered quantum (and also classical) systems, which has no counterpart in pure systems, is the presence of an extended region around the critical point, the so called *Griffiths phase*, where several physical quantities are singular (Griffiths-McCoy singularities). Such anomalous behaviour was first found by Griffiths in the paramagnetic phase of the site-diluted classical Ising ferromagnet [37]. While in classical systems these singularities are only essential, in a quantum system they can by rather strong, as was pointed out by McCoy, who found the divergence of susceptibility in the McCoy-Wu model [93, 92] (which is the lattice representation of the one-dimensional random TIM) in an extended region above the critical point [91]. Although such a singular phase exists also in the ferromagnetic side of the critical point, we shall focus on the paramagnetic region in the following.

The underlying physics behind Griffiths-McCoy singularities is that there exist such rare regions in the sample, which contain much stronger couplings than the average. These strongly coupled domains (SCD) tend to order locally even if the whole system is in the disordered phase. The spins sitting in such a locally ordered cluster, are frozen together, and act collectively, as a giant spin. These give a strong response for external perturbations, which may lead to the divergence of average response functions, e.g. the susceptibility. Besides, to such a well-localised ordered formation a small energy gap is associated, since one knows from the exact solution of the homogeneous transverse-field Ising chain, that the gap vanishes (exponentially in an open chain) with the system size, in the ordered phase.

The vanishing energy gap involves the anomalous behaviour of dynamical quantities. Locally ordered clusters contain small fields, which corresponds to large temporal couplings in the lattice representation of the model, which tend to order the spins ferromagnetically in the time direction, so relaxation time is consequently large. These rare, exponential slowly relaxing domains lead to power-law-tail distributions of relaxation time $\tau_{\rm rel}$, and other quantities related to it. The broad distribution of $\tau_{\rm rel}$ implies the algebraic decay of average autocorrelations. This is reminescent of a critical point, however the characteristic spatial extent of the strongly coupled domains is still finite and spatial correlations fall off exponentially with a finite correlation length. Therefore Griffiths phase is termed as a line of "semicritical fixed points". This anisotropy is also reflected in the dynamical exponent, which differs from one, and varies continuously in the Griffiths phase, tending to a limiting value as the critical point is approached. This limiting value was found to coincide with the value obtained at criticality, in the one- and two-dimensional random TIM, indicating, that also the critical behaviour is dominated by the rare strong clusters.

Depending on the type of disorder distribution, the Griffiths phase may extend to the whole paramagnetic phase, but in some cases it has a finite upper boundary δ_G, above which (i.e. for $\delta > \delta_G$) the forming of SCD-s, i.e. locally

ordered regions is impossible. In the one-dimensional RTIM for example, where $h_c = J$ in the pure case, SCD-s cannot exist if $\max\{J_{ij}\} < \min\{h_i\}$. Thus δ_G depends on the form of coupling and field distributions. So does z, which is exactly known in the one-dimensional random TIM, and was found to be non-universal in the Griffiths region. At the upper limit of the Griffiths phase δ_G we have $z = 1$, thus the isotropy of time and space axes is restored.

There exists a phenomenological theory [126, 39] of the Griffiths phase, by the help of which the origin of singular behaviour of various quantities is reduced to a common physical ground. We shall introduce this in the following section.

2.5.1 Phenomenological description

Consider the quantity $P_L(N)$, which measures the probability, that in a finite d-dimensional sample of volume $V \equiv L^d$ there is a cluster of $N \equiv l^d \ll V$ strongly coupled spins. Here, l is the typical linear size of the SCD. Since N consecutive strong bonds can be found with exponentially small probability $\sim \exp(-AN)$, whereas the cluster could be placed at $\sim V$ different sites, we have

$$P_L(N) \sim V \exp(-AN), \tag{2.35}$$

where A is some positive constant. The imaginary relaxation time of such a SCD is, however, exponentially large in the volume, which can be seen as follows. The vanishing of temporal correlation corresponds to the insertion of a domain wall perpendicular to the time axis in the lattice representation of the quantum model under consideration. This costs an energy proportional to the volume of the SCD $E = -BN$, where B is a positive constant. The probability of such an event (i.e. the formation of a domain wall), and thus the characteristic length between walls, which gives the relaxation time, is proportional to the Boltzmann factor

$$\tau_{\rm rel} \sim \exp(BN). \tag{2.36}$$

Combining (2.35) and (2.36) one obtains a broad power-law distribution of imaginary relaxation times

$$P_L(\tau_{\rm rel}) \sim V \tau_{\rm rel}^{-\frac{A}{B}-1}. \tag{2.37}$$

The power depends on the microscopic details, so it is expected to vary smoothly in the Griffiths-phase.

For a classical system with activated dynamics the difference is that in the relaxation time (2.36) not the volume but the surface of the SCD appears $\tau_{\rm rel} \sim \exp(B' N^{\frac{d-1}{d}})$. This leads to a much narrower, stretched exponential distribution $P_L^{\rm class}(\tau_{\rm rel}) \sim \exp(-A(\ln \tau_{\rm rel})^{\frac{d}{d-1}})$. Therefore Griffiths-McCoy singularities are rather weak in classical systems and it is hard to observe them by numerical simulations.

The energy gap is related to the relaxation time as $\epsilon_1 \sim \frac{1}{\tau_{\rm rel}}$, hence (2.37) implies the algebraic decay of its distribution $\tilde{P}_L(\epsilon_1) \sim V \epsilon_1^{\frac{A}{B}-1}$. The following argumentation sheds light upon an another physical meaning of $\frac{A}{B}$. The dimensionless probability distribution is

$$P_L(\ln \epsilon_1) = \epsilon_1 \tilde{P}_L(\epsilon_1) \sim L^d \epsilon_1^{\frac{A}{B}} = (L \epsilon_1^{1/z})^d, \tag{2.38}$$

where in the last expression the dynamical exponent z appears, which relates the time scale to the length scale by definition. Comparing the last two expressions in (2.38), one obtains $A/B = d/z$. Hence the linearized form of the low energy tail of distribution reads as:

$$\ln[P_L(\ln \epsilon_1)] = \frac{d}{z} \ln \epsilon_1 + \text{const.} \tag{2.39}$$

Another singular quantity related to τ_{rel}, is the local susceptibility χ_l at site l, defined through the local magnetization

$$m_l = - \lim_{H_l \to 0} \frac{\partial E_0}{\partial H_l} \tag{2.40}$$

as:

$$\chi_l = \lim_{H_l \to 0} \frac{\partial m_l}{\partial H_l} \, . \tag{2.41}$$

H_l is the strength of the local longitudinal field, which enters the Hamiltonian (2.32) via an additional term $H_l \sigma_l^x$, and E_0 is the ground-state energy of the system. One knows from the one-dimensional TIM, that χ_l is inversely proportional to the energy gap (see (4.1)), therefore one expects

$$\ln[P_L(\ln \chi_l)] = -\frac{d}{z} \ln \chi_l + \text{const.} \tag{2.42}$$

It may happen that the linear response is analytical in the Griffiths-phase and singularity arises only in the non-linear response (e.g. in higher-dimensional quantum spin glasses). Therefore one often investigates the local non-linear susceptibility, defined as

$$\chi_l^{\text{nl}} = \lim_{H_l \to 0} \frac{\partial^3 m_l}{\partial H_l^3} \, , \tag{2.43}$$

which is the first non-vanishing higher derivative of m_l, since m_l is an odd function of H_l.

In the one-dimensional TIM χ_l^{nl} contains the third power of gap in the denominator (see (4.3)), hence one assumes that the tail of its distribution is

$$\ln[P_L(\ln \chi_l^{\text{nl}})] = -\frac{d}{z^{nl}} \ln \chi_l^{\text{nl}} + \text{const}, \tag{2.44}$$

with

$$z^{\text{nl}} = 3z. \tag{2.45}$$

From (2.42) it is obvious, that the average local susceptibility diverges if $z > d$, while the condition for the divergence of non-linear susceptibility follows from (2.44) as $z > \frac{d}{3}$.

Now we deduce the scaling form of singular thermodynamic quantities for a finite but small temperature T and external field H. The average susceptibility can be obtained using (2.42) and expecting a cutoff in the distribution of order T^{-1}:

$$[\chi]_{av}(T) \sim T^{d/z-1}. \tag{2.46}$$

The same result can be deduced from the asymptotic decay of the average spin-spin autocorrelation function

$$[G]_{av}(\tau) \equiv [\langle \sigma_l^x \sigma_l^x(\tau) \rangle]_{av} \sim \int e^{-\tau/\tau_{\text{rel}}} P_L(\tau_{\text{rel}}) d\tau_{\text{rel}} \sim \int_\tau^\infty P_L(\tau_{\text{rel}}) d\tau_{\text{rel}} \sim \tau^{-d/z}. \tag{2.47}$$

Using the sum rule for susceptibility, $[\chi]_{av} = \int_0^{T^{-1}} [G]_{av}(\tau)d\tau$, one recovers (2.46).

The scaling form of average susceptibility in the presence of a small longitudinal field of strength H, when the appropriate scaling variable is T/H, is expected to be

$$[\chi]_{av}(T,H) = T^{\frac{d}{z}-1}\tilde{\chi}(T/H), \tag{2.48}$$

where $\tilde{\chi}(x)$ is some smooth scaling function. Putting $H = T$ in (2.48) yields

$$[\chi]_{av}(T=0,H) \sim H^{\frac{d}{z}-1}. \tag{2.49}$$

Integrating (2.49) by H, one gets the scaling form of average local magnetization

$$[m^x]_{av}(T=0,H) \sim H^{\frac{d}{z}}. \tag{2.50}$$

Since the magnetization is related to the ground state energy according to (2.40), integrating (2.50) over H once again yields for the scaling form of average internal energy at small T and H:

$$E(T,H) = H^{\frac{d}{z}+1}\tilde{E}(T/H), \tag{2.51}$$

where $\tilde{E}(x)$ is a smooth scaling function. With the choice $T = H$ one obtains

$$E(T,H=0) \sim T^{\frac{d}{z}+1}. \tag{2.52}$$

This yields for the scaling behaviour of specific heat:

$$c(T,H=0) = \frac{\partial E}{\partial T}(T,H=0) \sim T^{\frac{d}{z}}. \tag{2.53}$$

Thus all above Griffiths-McCoy singularities are characterized with a single exponent z, which varies continuously with the control parameter in the Griffiths phase.

2.6 Experimental realizations

In this work we restrict ourselves mainly to the study of disordered one-dimensional quantum systems. There are a few magnetic materials for the description of which the three-dimensional version of our models are adequate. Since special phenomena (Griffiths-phase etc.) are present also in the less complicated one-dimensional models, the investigation of them helps us to understand the behaviour of more realistic two- and three-dimensional systems better. In fact the special features arising from the interplay between disorder and quantum fluctuations, are more pronounced in one-dimension than in higher dimensional systems.

For three-dimensional Ising-model an experimental realization is the compound $LiHo_xY_{1-x}F_4$, an insulating magnetic material [134, 133]. It is an isostructural derivative of the dipolar-coupled Ising ferromagnet $LiHoF_4$, where non-magnetic Y^{3+} ions and magnetic Ho^{3+} ions occupy randomly the rare-earth sites. Applying an external magnetic field of strength Γ perpendicular to the easy magnetic axis, results in the splitting of the ground-state doublets of Ho^{3+}

ions, and makes for the system possible to tunnel between these states. This diluted system can be described by a random transverse-field Ising spin glass with transverse-field $h \sim \Gamma^2$. In this system studied with $x = 0.167$ a spin-glass phase appears below a temperature $T_g(\Gamma)$, which depends on the applied field, Γ. Crossing the phase boundary at $T = 98mK$ the divergence of non-linear susceptibility was found, which vanishes at $25mK$ [134] in contrast to theoretical expectations. This discrepancy may originate from the long-range nature of dipolar coupling.

On the other hand one-dimensional models have experimental relevance on their own right, as well. There are special substances in which chains of relative strongly interacting atoms are settled, which interact weakly with each other. One can mention, e.g. the ionic crystal Sr_2CuO_3, in which paramagnetic copper atoms are aligned along lines, and the strength of coupling between them, mediated by oxygen atoms is $2000K$ [36]. The interaction energy between such chains separated by Sr atoms is $5K$. Thus in the temperature range $5K < T < 2000K$ this system is quasi-one-dimensional, and can be described by the antiferromagnetic Heisenberg chain. Other examples are Sr_3CuPtO_6, where antiferromagnetic couplings between Cu atoms are provided by Pt, while in Sr_3CuIrO_6 the interaction mediated by Ir is ferromagnetic. The isostructural compound $Sr_3CuPt_{1-x}Ir_xO_6$ is a realization of a one-dimensional spin-glass. Other examples are the various tetracyano-quinodimethanide(TCNQ)-salts, such as quinolinium-$(TCNQ)_2$. These are one-dimensional insulating compounds, in which positive ions have two states. They can be described by a Hubbard model with half-filling of electrons. When hopping term is much larger than Coulomb-repulsion term, the latter model is equivalent to a Heisenberg antiferromagnet.

Measurements on the susceptibility of quinolinium-$(TCNQ)_2$ came to the low temperature behaviour $\chi \sim T^{-\alpha}$ with $\alpha < 1$ universal [127]. This, together with other results of measurements on dynamical properties [128] was interpreted as evidence that the above compound is a random-exchange Heisenberg antiferromagnet.

An interesting relation of the random transverse-field Ising models to the non-Fermi liquid behaviour of f-electron compounds, such as U and Ce intermetallics. In these systems the the low temperature properties of the Kondo impurities have been mapped onto an effective random transverse-field Ising chain with random bonds and fields having power-law decaying spatial correlations [14, 15, 111].

Chapter 3

The random transverse-field Ising chain

In this chapter we review the known results on the random transverse-field Ising spin chain (RTIC) with free ends:

$$H = -\sum_{i=1}^{L-1} J_i \sigma_i^x \sigma_{i+1}^x - \sum_{i=1}^{L} h_i \sigma_i^z, \tag{3.1}$$

where J_i and h_i are independent random variables, drawn from distributions $\pi(J)dJ$ and $\rho(h)dh$, respectively. The sign of J_i and h_i can be chosen to be positive without loss of generality, since it is always possible to make the sign disappear by a gauge transformation $\sigma_i^x \to -\sigma_i^x$, $\sigma_i^z \to -\sigma_i^z$ on the appropriate sites, which is a consequence of the absence of frustration in one dimension. Thus the one dimensional transverse-field Ising ferromagnet, antiferromagnet and spin-glass are equivalent. In higher dimensions it is no longer true because of frustration. The random transverse-field Ising chain is self-dual. The transformation

$$\begin{aligned} \tilde{\sigma}_i^z &= \sigma_i^x \sigma_{i+1}^x \\ \tilde{\sigma}_i^x &= \prod_{j=1}^{i} \sigma_j^z \end{aligned} \tag{3.2}$$

maps (3.1) into the same Hamiltonian however with parameters $J_i' = h_i$ and $h_i' = J_{i-1}$, thus bonds and fields are formally interchanged.

3.1 Phase diagram with non-random couplings

The transverse-field Ising chain with non-random couplings $J_{ij} = J$ and $h_i = h$ is exactly solvable by mapping it to free fermions [83, 104]. Its lattice representation, the two-dimensional classical Ising model was firstly solved by Onsager in a more complicated way [100].

Introducing the quantum control parameter $\delta = \ln \frac{h}{J}$, the phase diagram looks as shown in Fig 3.1. At zero temperature and $\delta < 0$ the system is in its

ferromagnetic phase with longe-range order and non-vanishing magnetization. The energy gap vanishes exponentially with the system size in the thermodynamic limit. (The way ϵ_1 vanishes in this phase depends on the boundary condition [9].)

If $\delta > 0$ or $T > 0$ there is short-range order with zero magnetization and the system is paramagnetic. Here the energy gap is finite.

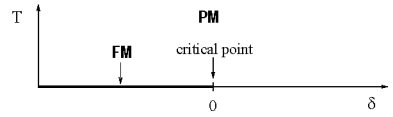

Figure 3.1: Phase diagram of the homogeneous transverse-field Ising chain.

At $T = 0$ the two phases are separated by a quantum critical point at $\delta = 0$. Its location also follows from the self-duality of the model. This point is characterized by quasi-long-range order, and by critical exponents $\nu = 1$, $x_m = \frac{1}{8}$ and $z = 1$. According to the Harris-criterion in (2.24) this model is unstable against weak randomness and is driven to a new fixed point.

3.2 Phase diagram of the random model

The quantum control parameter of the random model is

$$\delta = \frac{[\ln h]_{av} - [\ln J]_{av}}{\mathrm{var}[J] + \mathrm{var}[h]}, \tag{3.3}$$

where $\mathrm{var}[x]$ denotes the variance of x. The phase diagram is similar to that of non-random one (see Fig 3.2). A striking difference is the appearance of Griffiths phase. For the random model there exists a large amount of exact, conjectured and numerical results, which we shall briefly summerize below.

3.2.1 Critical region

According to Fisher's renormalization group (RG) treatment [33], which will be introduced in detail in Chapter 5, the critical behaviour of the model is controlled by an IRFP, with extremely (logarithmically) broad distribution of quantities. The average bulk magnetization vanishes close to the transition as $[m]_{av} \sim (-\delta)^{\beta}$ with the conjectured exponent

$$\beta = 2 - \phi, \qquad \phi = \frac{(1+\sqrt{5})}{2}. \tag{3.4}$$

The corresponding surface exponent is

$$\beta_s = 1, \tag{3.5}$$

which is an exact result of McCoy [91]. From the RG treatment the zero-temperature scaling form of magnetization in a small applied longitudinal field H is exactly known for $\delta \ll 1$ (see Ref. [33]). At criticality ($\delta = 0$) the bulk magnetization behaves as $[m]_{av}(H) \sim \frac{1}{|\ln H|^{2-\Phi}}$, for $H \ll 0$.

The relation between the RTIC and random walk (see Section 3.5.1) can be used in order to calculate the finite-size scaling of surface magnetization [59]:

$$[m_s^x]_{av} \sim L^{-x_m^s}, \qquad x_m^s = \frac{1}{2}. \tag{3.6}$$

The RG method leads to the following results on correlations [33]. The spin-spin correlation function

$$C^x(r) = \langle \sigma_i^x \sigma_{i+r}^x \rangle \tag{3.7}$$

behaves typically at criticality as $-\ln C^x(r) = Ar^{1/2}$ for large r, where the constant A is broadly distributed. For $|\delta| \ll 1$ $C^x(r)$ decays typically as $-\ln C^x(r) \approx r/\xi_{\rm typ}$ and the typical correlation length $\xi_{\rm typ}$ diverges as

$$\xi_{\rm typ} \sim \frac{1}{|\delta|^{\nu_{\rm typ}}}, \qquad \nu_{\rm typ} = 1. \tag{3.8}$$

This was found also by Shankar and Murthy [121] via transfer matrix calculations.

The *average* correlations, which are measurable, are dominated by the rare, strongly correlated regions with order unity correlations, and therefore behave differently. At criticality the power-law decay of mean correlation

$$[C^x(r)]_{av} \sim \frac{1}{r^{2-\Phi}} \tag{3.9}$$

was found, while for $|\delta| \ll 0$ the true correlation length diverges faster than $\xi_{\rm typ}$:

$$\xi \sim \frac{1}{\delta^\nu}, \qquad \nu = 2. \tag{3.10}$$

The critical point characterized by extreme anisotropy. Time scale is related to length scale as

$$\ln \tau \sim \xi^{1/2}, \tag{3.11}$$

which corresponds to an infinite dynamical exponent $z = \infty$ [33].

According to phenomenological and numerical results [109] the critical autocorrelation function $G^x(\tau) = \langle \sigma_i^x(\tau)\sigma_i^x(0)\rangle$ typically falls off faster than any power-law, while the average decays logarithmically slowly

$$[G^x]_{av}(\tau) \sim (\ln \tau)^{-2x_m}. \tag{3.12}$$

The critical transverse spin correlation function $C_e(r) = \langle \sigma_i^z \sigma_{i+r}^z \rangle$ is a self-averaging quantity and at criticality its average behaves as $-\ln[C^e(r)]_{av} \sim r^{1/2}$, like its typical value [109]. The critical average transverse spin autocorrelation function $[G^e(\tau)]_{av} = [\langle \sigma_i^z(\tau)\sigma_i^z(0)\rangle]_{av}$ decays as $[G^e(\tau)]_{av} \sim \tau^{-\eta_e}$ [109].

3.2.2 Griffiths phase

In the paramagnetic phase the disordered Griffiths phase is located in the region $0 < \delta < \delta_G$, where free energy is a non-analytic function of T and H, as it was discussed in Section 2.5.

This region extends to δ_G, above which all transverse-fields are bigger than couplings. The exact value of the dynamical exponent is known [59]. It is the positive root of the equation

$$\left[\left(\frac{J}{h}\right)^{1/z}\right]_{av} = 1. \tag{3.13}$$

The dynamical exponent generally depends both on δ and on the distributions $\pi(J)$ and $\rho(J)$. However it becomes universal, i.e. distribution independent, in the vicinity of the critical point where $z(\delta) \approx 1/(2\delta)$, $|\delta| \ll 1$, in accordance with the RG results [33, 31]. On the other hand $z = 1$ as $\delta \to \delta_G^-$.

The phenomenological argumentations on scaling behaviour of singular quantities achieved for the RTIM in general dimension d in Section 2.5, also hold here with $d = 1$. The numerical results on different singular quantities in the Griffiths phase are all in agreement with the analytical formula in (3.13) and the observed small deviations are attributed to finite-size corrections [138, 58].

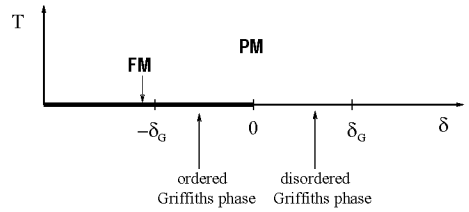

Figure 3.2: Phase diagram of the RTIC.

Below the critical point lies the ordered Griffiths phase, exhibiting similar singularities as its disordered counterpart. The underlying physics of singularities in this region is understood due to duality, which connects the point in the paramagnetic phase at δ to the point in the ferromagnetic phase at $-\delta$. The formations corresponding to SCD's in the paramagnetic side of critical point, are the weakly coupled domains (WCD) in the ferromagnetic phase, which contain smaller bonds and stronger fields than the average, and are locally in the disordered phase. A WCD effectively cuts the system inty two very weakly interacting parts and thus reduces the surface order enormously. The dual object, i.e. a SCD is known to be associated with a very small energy gap, ϵ_1. Thus in the tails of the distributions, m_s^x and ϵ_1 are dual quantities, and one expects the following singularity of surface magnetization in the ordered Griffiths phase:

$$P(\ln m_s^x) \sim (m_s^x)^{1/z}, \quad m_s^x \to 0 \; . \tag{3.14}$$

This scaling relation, which can be proven exactly for the RTIC (see Section 3.4), is expected to hold also for other one-dimensional disordered quantum chains.

3.3 Free fermion description of RTIC

The problem of diagonalization of (3.1) is equivalent to the eigenvalue problem of a $2^L \times 2^L$ matrix if one would expand H in the tensoral product space of spin states. However considerable simplification can be achieved by mapping H through a Jordan-Wigner transformation and a following canonical transformation to a free fermion model:

$$H = \sum_{q=1}^{L} \epsilon_q \left(\eta_q^+ \eta_q - \frac{1}{2} \right) \; , \tag{3.15}$$

in terms of the η_q^+ (η_q) fermion creation (annihilation) operators. The energy of modes ϵ_q is obtained through the solution of an eigenvalue problem, which necessitates the diagonalization of a $2L \times 2L$ tridiagonal matrix with non-vanishing matrix-elements $T_{2i-1,2i} = T_{2i,2i-1} = h_i$, $i = 1, 2, \ldots, L$ and $T_{2i,2i+1} = T_{2i+1,2i} = J_i$, $i = 1, 2, \ldots, L-1$, and the components of the eigenvectors V_q are denoted as $V_q(2i-1) = -\phi_q(i)$ and $V_q(2i) = \psi_q(i)$, $i = 1, 2, \ldots, L$,

i.e.

$$\mathbf{T} = \begin{pmatrix} 0 & h_1 & & & & & \\ h_1 & 0 & J_1 & & & & \\ 0 & J_1 & 0 & h_2 & & & \\ & & h_2 & 0 & \ddots & & \\ & & & \ddots & \ddots & J_{L-1} & \\ & & & & J_{L-1} & 0 & h_L \\ & & & & & h_L & 0 \end{pmatrix}, \qquad V_q = \begin{pmatrix} -\Phi_q(1) \\ \Psi_q(1) \\ -\Phi_q(2) \\ \vdots \\ \Psi_q(L-1) \\ -\Phi_q(L) \\ \Psi_q(L) \end{pmatrix}. \tag{3.16}$$

One considers only the $\epsilon_q \geq 0$ part of the spectrum. The details of this standard method can be found in Appendix A.2. The eigenvalue problem of (3.16) is analytically solvable only for the pure model [104]. However it is a powerful tool also for the numerical study of the random model, since the dimensionality of the problem is reduced from 2^L to $2L$.

In the following we derive expressions for various quantities in the free fermion picture, which are needed later.

3.3.1 Critical point

First we give a justification of criticality condition given by (3.3). The critical point for the RTIC can be obtained from the condition that the energy gap, which is inversely proportional to the relaxation time, must vanish in the thermodynamic limit. From Eq.(A.15) one obtains that a non-trivial solution with zero eigenvalue exists if $\det((\mathbf{A}-\mathbf{B})(\mathbf{A}+\mathbf{B})) = 0$. Or simply $\det(\mathbf{A}-\mathbf{B}) = 0$, since $(\mathbf{A}-\mathbf{B})^T = (\mathbf{A}+\mathbf{B})$. The exact solution of the pure model tells us, that with periodic boundaries the first gap can be zero even in a *finite* chain. Therefore one considers here the corresponding matrix for the cyclic chain, which reads as

$$\mathbf{A}_c - \mathbf{B}_c = \begin{pmatrix} h_1 & 0 & & & & & J_L \\ J_1 & h_2 & 0 & & & & \\ & J_2 & h_3 & \ddots & & & \\ & & \ddots & \ddots & & & \\ & & & \ddots & \ddots & & \\ & & & & & 0 & \\ & & & & & J_{L-1} & h_L \end{pmatrix}. \tag{3.17}$$

The determinant of (3.17) vanishes if $\prod_{i=1}^{L} h_i = \prod_{i=1}^{L} J_i$. In the $L \to \infty$ limit, when boundary effects are irrelevant, this yields the criticality condition also for the free chain:

$$[\ln h]_{av} = [\ln J]_{av}. \tag{3.18}$$

For a special case the validity of Eq. (3.18) follows from the self-duality of the model. Assuming that there exist only a single phase transition in the system, where physical properties are singular, it must be located at the fixed point of the transformation (3.2) [80]. Thus if $\pi(J)$ and $\rho(h)$ are identical, the system is expected to be at its criticality, and (3.18) is trivially satisfied.

3.3.2 Magnetization and dynamical correlations

Since the Hamiltonian contains products of two step operators, it commutes with the operator

$$\tilde{Q} = \prod_{i=1}^{L} \sigma_i^z. \tag{3.19}$$

$\tilde{Q}$ has two eigenvalues: $Q = \pm 1$, therefore the space of spin states decomposes into two orthogonal subspaces. In the free fermion picture these two sectors are related to the parity of the fermion number operator $N = \sum_{i=1}^{L} c_i^+ c_i = \frac{1}{2}(\sum_{i=1}^{L} \sigma_i^z + 1)$. If $Q = 1$, N is even, and if $Q = 0$, N is odd. The operator σ_i^x maps a state from one sector to the other, hence the ground state expectation value $\langle 0|\sigma_i^x|0\rangle$ is zero. Consequently $\langle 0|\sigma_i^x|0\rangle$ is not suitable as an order parameter. The true order parameter has to be determined from the asymptotic behaviour of the autocorrelation function $G_l^x(\tau) = \langle 0|\sigma_l^x(\tau)\sigma_l^x(0)|0\rangle$. Using $\sigma_l^x(\tau) = e^{\tau H}\sigma_l^x e^{-\tau H}$, the autocorrelation function assumes the form

$$G_l^x(\tau) = \sum_i |\langle i|\sigma_l^x|0\rangle|^2 \exp\left[-\tau(E_i - E_0)\right], \tag{3.20}$$

where $|i\rangle$ is the i-th eigenstate of H with eigenvalue E_i. Then $\lim_{\tau\to\infty} G_l(\tau) = (m_l^x)^2$, since the magnetization is asymptotically uncorrelated. In the ordered phase the first energy gap vanishes exponentially in the thermodynamic limit, i.e. the first excited state becomes degenerate with the ground-state. Therefore in the large τ limit only the first excited state survives in (3.20) and the local magnetization is given by the off-diagonal matrix element:

$$m_l^{free} = \langle 1|\sigma_l^x|0\rangle, \tag{3.21}$$

where the superscript refers to the boundary condition. In the fermion representation σ_l^x is expressed as

$$\sigma_l^x = A_1 B_1 \ldots A_{l-1} B_{l-1} A_l \tag{3.22}$$

with

$$A_i = \sum_q \phi_q(i)(\eta_q^+ + \eta_q) \quad B_i = \sum_q \psi_q(i)(\eta_q^+ - \eta_q)\,. \tag{3.23}$$

Using $|1\rangle = \eta_1^+|0\rangle$ the matrix-element in (3.21) is evaluated by Wick's theorem. Since for $i \neq j$ $\langle 0|A_i A_j|0\rangle = \langle 0|B_i B_j|0\rangle = 0$, one obtains for the local magnetization

$$m_l^{\text{free}} = \begin{vmatrix} H_1 & G_{11} & G_{12} & \ldots & G_{1l-1} \\ H_2 & G_{21} & G_{22} & \ldots & G_{2l-1} \\ \vdots & \vdots & \vdots & \ddots & \vdots \\ H_l & G_{l1} & G_{l2} & \ldots & G_{ll-1} \end{vmatrix}, \tag{3.24}$$

where

$$\begin{aligned} H_j &= \langle 0|\eta_1 A_j|0\rangle = \Phi_1(j) \\ G_{jk} &= \langle 0|B_k A_j|0\rangle = -\sum_q \Psi_q(k)\Phi_q(j)\,. \end{aligned} \tag{3.25}$$

The surface magnetization can be given in a closed form [58]. One possible route to this is to put $h_L = 0$, what implies that the eigenvalue s_L^x of $S_L^x \equiv \frac{1}{2}\sigma_L^x$ becomes a good quantum number. In the fermion-picture the twofold degeneracy $s_L^x = \pm\frac{1}{2}$ corresponds to the presence of a zero mode, $\epsilon_1 = 0$, with an eigenvector satisfying $V_1(2i) = \Psi_1(i) = 0, i = 1, 2, \ldots, L$. Then the first excited state $|1\rangle$ is degenerate with the ground state $|0\rangle$ and the matrix-element in (3.21) corresponds to the ground-state expectation value of the magnetization:

$$m_l^{free+} = \langle 0|\sigma_l^x|0\rangle, \tag{3.26}$$

which is given by (3.24). The surface magnetization, $m_s^x \equiv m_1^x = \Phi_1(1)$ can easily be obtained by solving $\mathbf{T}V_1 = 0$ with $V_1(2i) = 0$ for $i = 1, \ldots, L$ and using the normalization condition $\sum_i \Phi_1(i)^2 = 1$. This yields

$$m_s^x = \left[1 + \sum_{l=1}^{L-1} \prod \left(\frac{h_j}{J_j}\right)^2\right]^{-1/2}. \tag{3.27}$$

This can be derived also with free boundaries in the $L \to \infty$ limit [102].

The autocorrelation between surface spins can be obtained directly from (3.20) as:

$$G_1^x(\tau) = \sum_q |\Phi_q(1)|^2 \exp(-\tau\epsilon_q)\ , \tag{3.28}$$

whereas bulk autocorrelation function can be given in a more complicated form in terms of a Pfaffian (for details see Ref. [58]).

3.4 Relation with random walks

Another source of exact results is the mathematical equivalence between the RTIC and the Sinai walk [120], which was found by Iglói [59]. Namely, Eq. (A.15) can be transformed into the eigenvalue problem of the Fokker-Planck operator of a one-dimensional random walk (RW) with nearest-neighbour hopping in a random environment [59, 62]. Among others the following correspondances were established:

$$J_i \quad \Leftrightarrow \quad (w_{i+1,i})^{1/2} \tag{3.29}$$

$$h_i \quad \Leftrightarrow \quad (w_{i,i+1})^{1/2} \tag{3.30}$$

$$\epsilon_k^2 \quad \Leftrightarrow \quad -\lambda_k, \tag{3.31}$$

where $w_{i,i\pm1} = w(i \to i \pm 1)$ transition probabilities characterizing the random walk, and λ_k is the k'th eigenvalue of the Fokker-Planck operator.

The free boundaries of RTIC of size L correspond to adsorbing boundaries in the RW problem at site $i = 0$ and $i = L$. The surviving probability $P_{surv}(L)$, i.e. the probability for the walker starting near one of the adsorbing walls not to cross its starting point after L steps, is given in a form similar to (3.27). It was thus established:

$$P_{surv}(L) \Leftrightarrow m_s^2(L). \tag{3.32}$$

The control parameter of the RW is defined as

$$\delta_{RW} = \frac{[\ln w_{\leftarrow}]_{av} - [\ln w_{\rightarrow}]_{av}}{\mathrm{var}[w_{\leftarrow}] + \mathrm{var}[w_{\rightarrow}]}. \tag{3.33}$$

At $\delta_{RW} = 0$ the diffusion is ultra-slow and the averaged mean-square displacement grows as $[\langle X^2(t)\rangle]_{av} \sim \ln^4 t$. Around this point, i.e. for small $\delta_{RW} \neq 0$ takes place the region of *anomalous diffusion*, characterized by

$$[\langle X^2(t)\rangle]_{av} \sim t^{\Psi}, \tag{3.34}$$

with $\Psi < 1$, which is the analogon of Griffiths phase in RTIC. Comparing the finite-size-scaling behaviour of the largest non-zero eigenvalue $\lambda_k(L) \sim L^{-\frac{2}{\Psi}}$ in this region with that of the energy gap of RTIC in the Griffiths-phase $\epsilon_k \sim L^{-z}$, one obtains using Eq. (3.31)

$$z \Leftrightarrow \frac{1}{\Psi}. \tag{3.35}$$

Now exploiting, that Ψ is known exactly [25, 75] in the form

$$\left[\left(\frac{w_{\rightarrow}}{w_{\leftarrow}}\right)^{\frac{\Psi}{2}}\right]_{av} = 1, \tag{3.36}$$

and using (3.29), (3.30) and (3.35), one obtains for the dynamical exponent of the RTIC the implicit equation in (3.13).

Eq. (3.36) follows from the observation, that the product of independent, identically distributed random variables $\lambda = x_1 x_2 x_3 \ldots$ (the so called *Kesten-variable*) has a singular distribution $P(\lambda) \sim \lambda^{-1+\mu}$, with μ given by $[x^{\mu}]_{av} = 1$ [75]. One can also arrive at (3.13) directly by regarding the perturbative expression for the energy gap in (3.42) as a Kesten-variable. Applying this argument to the exact expression of surface magnetization

$$\frac{1}{m_s^2} = 1 + \sum_{l=1}^{L} \prod_{i=1}^{l} \left(\frac{h_i}{J_i}\right)^2, \tag{3.37}$$

one obtains (3.14).

3.5 Phenomenological theory

In random quantum spin chains the critical properties are expected to be controlled by an IRFP, where distributions are extremely broad and as a consequence the average and typical behavior of these quantities are completely different. The average is dominated by such realizations (the so called *rare events*), which have a very large contribution, but their fraction is vanishing in the thermodynamic limit. In this section we identify these rare events for the RTIC model and use their properties to develop a phenomenological theory, on the ground of which we derive some of the results listed in Section 3.2. Later we shall apply this theory with slight modifications to the random XX and XY chains.

3.5.1 Surface order parameter and the mapping to random walks

The surface order parameter is given by the simple formula in (3.27). It is easy to see from (3.27) that in the thermodynamic limit the average surface order

parameter is zero (non-zero), if the geometrical mean of the J_j couplings is (smaller) greater than that of the h_j couplings. From this the definition of the control parameter in (3.3) follows.

Next we compute the average value of the surface order parameter for the extreme binary distribution[1], i.e. the limit $\lambda \to 0$ and $h_0 = 1$ in (4.17). For a random realization of the couplings the surface order parameter at the critical point ($p = q = 1/2$) is zero, if a product of the form of $\prod_{i=1}^{l}(J_i)^{-2}$, $l = 1, 2, \ldots, L$ is infinite, i.e. the number of λ-couplings exceeds the number of λ^{-1}-couplings in any of the $[1, l]$ intervals. Otherwise the surface order parameter has a finite value of $O(1)$. The sequence of couplings J_i can be represented by one-dimensional random walks that start at zero and make the i-th step upwards (for $J_i = \lambda^{-1}$) or downwards (for $J_i = \lambda$). The ratio of walks representing a sample with finite surface order parameter is given by the survival probability of the walk P_{surv}, i.e. the probability of the walker to stay always above the starting point in L steps.

In the vicinity of the critical point, the scaling behavior of the average surface order parameter can be obtained from the survival probabilities of biased random walks [58], where the probability that the walker makes a step towards the adsorbing boundary, q, is different from that of a step off the boundary, p. The control parameter of the walk, $\delta_w = p - q$, is proportional to the quantum control parameter δ in (3.3) evaluated with the binary distribution. Thus the basic correspondences are:

$$[m_s(\delta, L)]_{av} \sim P_{\rm surv}(\delta_w, L), \quad \delta \sim \delta_w. \tag{3.38}$$

We recall the asymptotic properties of $P_{\rm surv}(\delta_w, L)$ [58]. For unbiased walks:

$$P_{\rm surv}(\delta_w = 0, L) \sim L^{-1/2}\,, \tag{3.39}$$

for walks with a drift away from the wall:

$$P_{\rm surv}(\delta_w > 0, L \to \infty) \sim \delta_w\,, \tag{3.40}$$

and for walks with a drift towards the wall:

$$P_{\rm surv}(\delta_w < 0, L) \sim \exp(-L/\xi_w), \quad \xi_w \sim \delta_w^{-2}\,. \tag{3.41}$$

In this way we have identified the rare events for the surface order parameter, which are samples with a coupling distribution which have a surviving walk character. The scaling properties of the average surface order parameter and the correlation length immediately follow from Eqs. (3.39), (3.40) and (3.41).

3.5.2 Scaling of low-energy excitations

The rare events are also important for the low-energy excitations. The results are obtained by using a simple relation for the smallest gap $\epsilon_1(l)$ of an open system of size l with free boundary conditions, expecting that it goes to zero at least as $\sim 1/l$. Then one can neglect the r.h.s. of the eigenvalue problem of $\mathbf{T}$

[1]The extreme binary distribution represents one possible explicit construction of the infinite-randomness fixed point.

in (A.16) and derive approximate expressions for the eigenfunctions Φ_1 and Ψ_1. Finally one arrives at

$$\epsilon_1(l) \sim m_1^x \bar{m}_{l-1}^x h_l \prod_{j=1}^{l-1} \frac{h_j}{J_j} \,. \tag{3.42}$$

(For details see Ref. [61].) Here, the surface order parameter at the other end of the chain $\bar{m}_{l-1}$ is given by replacing h_j/J_j for h_{L-j}/J_{L-j} in Eq. (3.27).

Before using (3.42) we note that (surface) order and the presence of low-energy excitations are inherently related. Samples with an exponentially small gap have finite, $O(1)$, order parameters at both boundaries and the coupling distribution follows a surviving walk picture. Such a coupling configuration represents a SCD, which at the critical point extends over the size of the system, L. In the off-critical situation, in the Griffiths phase the SCD-s have a smaller extent, $l \ll L$, and they can be localized both in the bulk and near the surface of the system. The characteristic excitation energy of a SCD can be estimated from Eq. (3.42) as

$$\epsilon_1(l) \sim \prod_{j=1}^{l-1} \frac{h_j}{J_j} \sim \exp\Big\{-l_{\rm tr}\overline{\ln(J/h)}\Big\} \,, \tag{3.43}$$

where $l_{\rm tr}$ measures the size of *transverse fluctuations* of a surviving walk of length l, defined as the conditional expectation value of the position of the walker after l steps under the condition, that the walker survives until the lth step, whereas $\overline{\ln(J/h)}$ is an average ratio of the couplings.

At the critical point ($\delta = 0$), where $l \sim L$, the size of transverse fluctuations of the couplings in the SCD is $l_{\rm tr} \sim L^{1/2}$ [58]. Consequently one obtains from Eq. (3.43) for the scaling relation of the gap:

$$\epsilon_1(\delta = 0, L) \sim \exp(-\text{const} \cdot L^{1/2}) \,. \tag{3.44}$$

Then the appropriate scaling variable is $\ln \epsilon/\sqrt{L}$ and the distribution of the excitation energy is extremely (logarithmically) broad.

In the Griffiths phase the size of a SCD can be estimated along the lines of Ref. [58] as $l \sim \xi_w \ln L$ and the size of transverse fluctuations is now $l_{\rm tr} \sim l \sim \ln L$. Setting this estimate into Eq. (3.43) we obtain for the scaling relation of the gap:

$$\epsilon_1(L) \sim L^{-z} \,, \tag{3.45}$$

where z is the dynamical exponent.

3.5.3 Scaling theory of correlations

The scaling behavior of critical average correlations is also inherently connected to the properties of rare events. Here the quantity of interest is the probability $P^\mu(l)$, which measures the fraction of rare events of the local order parameter m_l^μ. [2] For the surface order parameter m_1^x it is given by the surviving probability, $P^x(1) = P_{surv}$, according to Eq. (3.38). We start with the equal-time correlations

$$[C^\mu(r)]_{\rm av} = [\langle 0|\sigma_l^\mu \sigma_{l+r}^\mu|0\rangle]_{\rm av} \,. \tag{3.46}$$

[2] Here and throughout the section $\mu = x$ for the RTIC, while considering the XX and XY chains (see later) $\mu = x, y, z$.

In a given sample there should be local order at both reference points of the correlation function in order to have $C^\mu(r) = O(1)$. This is equivalent of having two SCD-s in the sample which occur with a probability of $P_2^\mu(l, l+r)$, which factorizes for large separation $\lim_{r\to\infty} P_2^\mu(l, l+r) = P^\mu(l)P^\mu(l+r)$, since the disorder is uncorrelated. The probability of the occurrence of a SCD at position l, $P^\mu(l)$, has the same scaling behavior as the local order parameter $[m_l^\mu]_{\rm av}$. Generalizing the arguments leading to (3.21), $[m_l^\mu]_{\rm av}$ is given by

$$[m_l^\mu]_{\rm av} = [\langle\phi_\mu|\sigma_l^\mu|0\rangle]_{\rm av}, \tag{3.47}$$

where $|\Phi_\mu\rangle$ denotes the lowest eigenstate of H having a non-vanishing matrix-element of σ_l^μ with the ground state in the ordered phase. It behaves at a bulk point, $0 < l/L < 1$, as:

$$[m_l^\mu(L)]_{\rm av} \sim L^{-x^\mu} , \tag{3.48}$$

whereas for a boundary point, $l = 1$, this relation involves the surface scaling dimension x_1^μ. Consequently $P^\mu(l)$ transforms as $P^\mu(l) = b^{-x^\mu}P^\mu(l/b)$ under a scaling transformation, when lengths are rescaled by a factor $b > 1$. Recalling that for spatial correlations there should be two independent SCD-s we obtain the transformation law:

$$[C^\mu(r)]_{\rm av} = b^{-2x^\mu}[C^\mu(r/b)]_{\rm av} . \tag{3.49}$$

Now taking $b = r$ one obtains power-law decay with the exponent

$$\eta^\mu = 2x^\mu . \tag{3.50}$$

For critical time-dependent correlations the scaling behaviour is different from that in (3.49). This is due to the fact that disorder in the time direction is perfectly correlated and the autocorrelation function in a given sample is $G_l^\mu(\tau) = O(1)$, if there is *one* SCD localized at position l. Therefore the average autocorrelation function $[G_l^\mu(\ln\tau)]_{\rm av}$ scales as the probability of rare events $P^\mu(l)$:

$$[G_l^\mu(\ln\tau)]_{\rm av} = b^{-x^\mu}[G_l^\mu(\ln\tau/b^{1/2})]_{\rm av} , \tag{3.51}$$

where we have used the relation in Eq. (3.11) between relevant length and time at the critical point. Taking the length scale as $b = (\ln\tau)^2$ we obtain for points l in the volume:

$$[G_l^\mu(\tau)]_{\rm av} \sim (\ln\tau)^{-\eta^\mu} , \tag{3.52}$$

whereas for surface spins, $l = 1$, one should use the corresponding surface decay exponent η_1^μ.

Next we turn to study the scaling properties of the average correlation functions in the Griffiths phase, i.e. outside the critical point. For equal-time correlations in a sample $C^\mu(r) = O(1)$, if the SCD extends over a large distance of r, which according to Eq. (3.41) is exponentially improbable. Thus the average spatial correlations decay as

$$[C^\mu(r)]_{\rm av} \sim \exp(-r/\xi), \quad \xi \sim \xi_w , \tag{3.53}$$

where ξ_w is defined in Eq. (3.41). On the other hand the autocorrelation function in a sample is $G^\mu(\tau) = O(1)$, if there is one SCD localized at l, which occurs

with a probability of $P^{\mu}(l) \sim 1/L$. Consequently the average autocorrelation function, which scales as $P^{\mu}(l)$, transforms under a scaling transformation as:

$$[G_l^{\mu}(\tau)]_{\mathrm{av}} = b^{-1}[G_{l/b}^{\mu}(\tau/b^z)]_{\mathrm{av}} \quad \delta > 0 \,, \tag{3.54}$$

where we used the scaling combination τ/b^z in accordance with Eq. (2.29). Now taking $b = \tau^{1/z}$ one obtains

$$[G_l^{\mu}(\tau)]_{\mathrm{av}} \sim \tau^{-1/z} \,, \tag{3.55}$$

both in the volume and at the surface.

Chapter 4

Numerical study of the Griffiths phase

The singular quantities studied so far in the Griffiths phase are all related to the scaling properties of the lowest energy gap. This explains the observation why a single varying exponent is sufficient to characterize the singularities of the different quantities. There are, however, other observables, which are expected to be singular as well, but not connected directly to the first gap. As an example one could consider the distribution of the second (or some higher) gap. By similar reasons as for the first gap these higher excitations are also expected to vanish in the thermodynamic limit and the corresponding probability distributions are described by new exponents valid for small values of the gaps. As another example we consider the connected transverse spin autocorrelation function $G_l^e(\tau)$ In the McCoy-Wu model, this function corresponds to the energy-density correlation function in the direction of correlated disorder. Therefore we adopt in the following this terminology and call $G_l^e(\tau)$ the *energy-density autocorrelation function.* Finally one should mention the non-linear susceptibility whose distribution is expected to be described by a new varying exponent. In the one-dimensional RTIM this quantity has not yet been investigated before.

In this section we extend previous numerical work and study the scaling behavior of the above mentioned singular quantities in the Griffiths phase. We present a phenomenological scaling theory and we confront its predictions by results of numerical calculations, based on the free-fermion representation of the Hamiltonian in (3.1). We show that the physical quantities we studied are characterized by power-law singularities with varying critical exponents, the value of those are connected to the dynamical exponent through scaling relations.

4.1 Free fermion description of dynamical quantities

The local susceptibility defined in (2.41) can be expressed as [58]:

$$\chi_l = 2 \sum_i \frac{|\langle i|\sigma_l^x|0\rangle|^2}{E_i - E_0} \,. \tag{4.1}$$

Using (3.22), for the boundary spin $l = 1$ one has the simple expression:

$$\chi_1 = 2 \sum_q \frac{|\Phi_q(1)|^2}{\epsilon_q} \, . \tag{4.2}$$

Similarly, the local non-linear susceptibility defined in (2.43) can be obtained by perturbation calculation and reads as:

$$\chi_l^{\rm nl} = 24 \left\{ \sum_{i,j,k} \langle 0|\sigma_l^x|i\rangle \frac{1}{E_i - E_0} \langle i|\sigma_l^x|j\rangle \frac{1}{E_j - E_0} \langle j|\sigma_l^x|k\rangle \frac{1}{E_k - E_0} \langle k|\sigma_l^x|0\rangle + \right.$$
$$\left. \sum_i \left(\frac{\langle i|\sigma_l^x|0\rangle}{E_i - E_0} \right)^2 \sum_j \frac{|\langle j|\sigma_l^x|0\rangle|^2}{E_j - E_0} \right\} \, . \tag{4.3}$$

For surface spins, $l = 1$, (4.3) simplifies:

$$\chi_1^{\rm nl} = 24 \left\{ \sum_{p,q} \frac{\Phi_p(1)^2 \Phi_q(1)^2}{(\epsilon_p + \epsilon_q)\epsilon_p} \left(\frac{1}{\epsilon_p} - \frac{1}{\epsilon_q} \right) - \sum_p \left(\frac{\Phi_p(1)}{\epsilon_p} \right)^2 \sum_q \frac{|\Phi_q(1)|^2}{\epsilon_q} \right\} \, . \tag{4.4}$$

Next we consider the connected part of energy-density autocorrelation function at site l, G_l^e, defined by

$$\begin{aligned} G_l^e(\tau) &= \langle 0|\sigma_l^z(\tau)\sigma_l^z(0)|0\rangle - \langle 0|\sigma_l^z(\tau)|0\rangle\langle 0|\sigma_l^z(0)|0\rangle \\ &= \sum_{i>0} |\langle 0|\sigma_l^z|i\rangle|^2 \exp[-\tau(E_i - E_0)] \, . \end{aligned} \tag{4.5}$$

In the free-fermion representation σ_l^z is expressed as [83]:

$$\sigma_l^z = A_l B_l, \tag{4.6}$$

with A_l and B_l given in (3.23). By the help of this $G_l^e(\tau)$ is given by

$$G_l^e(\tau) = \sum_{\delta>\gamma} |\Psi_\delta(l)\Phi_\gamma(l) - \Psi_\gamma(l)\Phi_\delta(l)|^2 \exp[-\tau(\epsilon_\delta + \epsilon_\gamma)] \, , \tag{4.7}$$

which can be expressed for surface spins as

$$G_1^e(\tau) = \sum_{\delta>\gamma} \left[\frac{\epsilon_\delta - \epsilon_\gamma}{h_1} \Phi_\delta(1)\Phi_\gamma(l) \right]^2 \exp[-\tau(\epsilon_\delta + \epsilon_\gamma)] \, . \tag{4.8}$$

4.2 Phenomenological and scaling considerations

Previously, along a phenomenological argumentation, we arrived to the distribution of first energy gap given in (2.39), where now $d = 1$.

Next, we consider the second gap, ϵ_2, which is connected to the existence of a *second* strongly connected cluster of $N' \leq N$ spins, and its value is given according to the argumentations in Section 2.5.1 as

$$\epsilon_2 \sim \exp(-BN') \, . \tag{4.9}$$

The probability with which a cluster of size N' occurs, provided another cluster of size $N \geq N'$ exists, is given by $P'_L(N') \sim L \exp(-AN') \sum_{N=N'}^{L} P_L(N)$. For $N' \ll L$ (or in the infinite system size limit $L \to \infty$) this can be estimated as:

$$P'_L(N') \sim L^2 \exp[-2AN'] \,. \tag{4.10}$$

Thus from (4.9) and (4.10) we have

$$P'_L(\ln \epsilon_2) \sim L^2 \epsilon_2^{1/z'} \,, \tag{4.11}$$

with $1/z' = 2A/B$, thus

$$z' = z/2 \,. \tag{4.12}$$

Note that the scaling combination in the r.h.s. of (4.11) is dimensionless, as it should be. Repeating the above argument for the third, or generally the nth gap the corresponding distribution is described by an exponent $z^{(n)} = z/n$, however the finite size corrections for these gaps are expected to increase rapidly with n.

The scaling behavior of the average spin autocorrelation function is given by:

$$[G_l]_{\rm av}(\tau) = \int P_L(\epsilon_1) |M_l|^2 \exp(-\tau\epsilon_1) {\rm d}\epsilon_1 \,, \tag{4.13}$$

where the factor with the matrix-element is $|M_l|^2 \sim 1/L$, since the probability that a low energy cluster is localized at a given site, l, is inversely proportional to the length of the chain. Then using (2.38) one arrives to the result in (2.47) with $d = 1$, thus establishing the relation between the decay exponent of the spin autocorrelation function and the dynamical exponent.

For energy-density autocorrelations, according to (4.7) and (4.8) the characteristic energy scale is ϵ_2 and the asymptotic behavior of the average energy-density autocorrelation function is given by:

$$[G^e_l]_{\rm av}(\tau) = \int P'_L(\epsilon_2) |M^e_l|^2 \exp(-\tau\epsilon_2) {\rm d}\epsilon_2 \,. \tag{4.14}$$

Now we take the example of the surface autocorrelation function in (4.8) to show that the factor with the matrix-element, $|M^e_1|^2$, is proportional to ϵ_2^2. The remaining factor in (4.8) with the first components of the eigenvectors is expected to scale as $1/L$ due to similar reasons as for the spin autocorrelations, thus $|M^e_l|^2 \sim L^{-1}\epsilon_2^2$ and together with (4.11) one has $P'_L(\epsilon_2)|M^e_l|^2 \sim L\epsilon_2^{1/z'+1}$. Before evaluating the integral in (4.14) we note that for a fixed L the expression in (4.14) stays valid up to $\tau \sim L^z$. Therefore to obtain the L independent asymptotic behavior in τ we should instead vary L, so that according to (4.11) take $L \sim \epsilon_2^{-1/(2z')}$ and in this way we stay within the border of validity of (4.14) for any τ. With this modification we arrive to the algebraic decay of average energy-density autocorrelation function:

$$[G^e]_{\rm av}(\tau) \sim \tau^{-\eta_e} \,, \tag{4.15}$$

with an exponent η_e related to the dynamical exponent as

$$\eta_e = 2 + \frac{1}{z} \,, \tag{4.16}$$

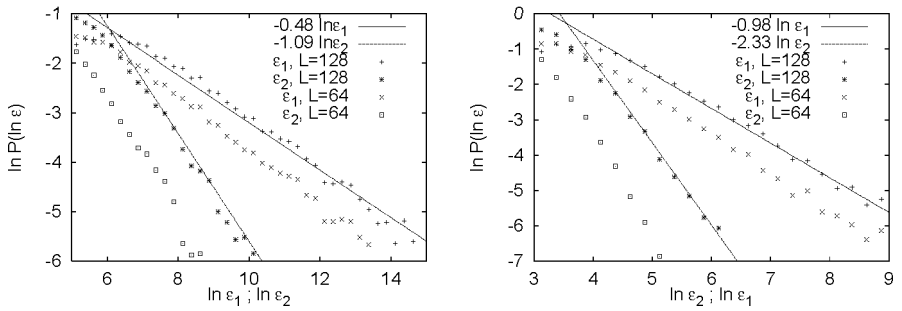

Figure 4.1: Probability distribution of $-\ln \epsilon_1$ and $-\ln \epsilon_2$ for the uniform distribution at $h_0 = 2$ (left) and the binary distribution ($\lambda = 4$) at $h_0 = 2.5$ (right). The slopes of fitted straight lines correspond to $1/z(h_0)$ and $1/z'(h_0)$, respectively. They follow the predicted relation $z'(h_0) = z(h_0)/2$.

where the relation in (4.12) is used. We expect that the factor, $|M_l^e|^2$, has the same type of scaling behavior for any position l, thus the relation in (4.16) stays valid both for bulk and surface spins. We note that the reasoning above (4.16) applies also for the spin autocorrelation function, in which case in (4.13), however there is no explicit L dependence.

In this way we have established a phenomenological scaling theory which connects the unconventional exponents in (4.12), (4.16) to the dynamical exponent. In the next section we confront these relations with numerical results.

4.3 Numerical results

In the numerical calculations we have considered RTIC's with up to $L = 128$ sites and the average is performed over several 10000 realizations, typically we considered 50000 samples. For some cases, where the finite-size corrections were strong, we also made runs with $L = 256$, but with somewhat less realizations.

We have used two types of random distributions. In the *binary distribution* the couplings can take two values $\lambda > 1$ and $1/\lambda$ with probability p and $q = 1-p$, respectively, while the transverse-field is constant:

$$\pi(J) = p\delta(J - \lambda) + q\delta(J - \lambda^{-1}) \,, \qquad \rho(h) = \delta(h - h_0) \,. \tag{4.17}$$

From (3.3) the criticality condition is $(p - q) \ln \lambda = \ln h_0$, whereas for the symmetric binary distribution $p = q = \frac{1}{2}$ it is $h_0 = 1$. In the Griffiths phase, $1 < h_0 < \lambda$, the dynamical exponent from (3.13) is determined by the equation

$$h_0^{\frac{1}{z}} = p\lambda^{\frac{1}{z}} + q\lambda^{-\frac{1}{z}}. \tag{4.18}$$

In the *uniform distribution* both the couplings and the fields have rectangular distributions:

$$\pi(J) = \begin{cases} 1, & \text{for } 0 < J < 1 \\ 0, & \text{otherwise} \end{cases}$$
$$\rho(h) = \begin{cases} h_0^{-1}, & \text{for } 0 < h < h_0 \\ 0, & \text{otherwise} \end{cases} \,. \tag{4.19}$$

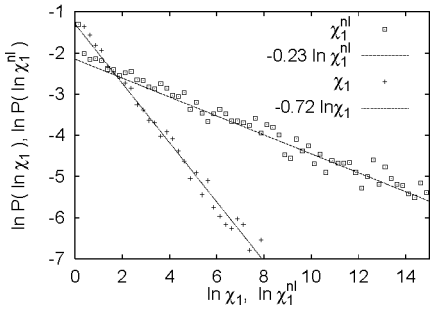

Figure 4.2: Probability distribution of the linear and non-linear susceptibility, $\ln \chi_1$ and $\ln \chi_1^{\rm nl}$, respectively, for the uniform distribution at $h_0 = 3$. The straight lines are fitted to the data for the largest system size, their slopes correspond to $1/z(h_0)$ and $1/z^{\rm nl}(h_0)$, respectively. They follow the predicted relation $z^{\rm nl}(h_0) = 3z(h_0)$.

The critical point is at $h_0 = 1$, whereas the dynamical exponent is given by the solution of the equation

$$z \ln \left(1 - z^{-2}\right) = -\ln h_0. \tag{4.20}$$

The Griffiths phase now extends to $1 < h_0 < \infty$.

We start to present results about the distribution of the first and second gaps.

As illustrated in Fig. 4.1, both for the uniform and the binary distributions, the asymptotic scaling relations for the distribution of the first two gaps in (2.39) and (4.11) are satisfied. From the asymptotic slopes of the distributions we have estimated the $1/z$ and $1/z'$ exponents for the two largest finite systems, $L = 64$ and $L = 128$, which are presented in Fig. 4.3 for different points of the Griffiths phase for the uniform distribution. As seen in the Figure the z exponent calculated from the first gap agrees very well with the analytical results in (4.20). For the z' exponent, as calculated from the distribution of the second gap the scaling result in (4.12) is also well satisfied, although the finite-size corrections are stronger than for the first gap. For the third gap, due to the even stronger finite size effects, we have not made a detailed investigation. Extrapolated results at $h_0 = 2$ are found to follow the scaling result $z^{(3)} = z/3$. Next, we analyzed the distribution of the linear and non-linear local susceptibilities at the surface spin. As demonstrated in Fig. 4.2 both type of distributions satisfy the respective asymptotic relations in (2.42) and (2.44), from which the critical exponents z and $z^{\rm nl}$ are calculated.

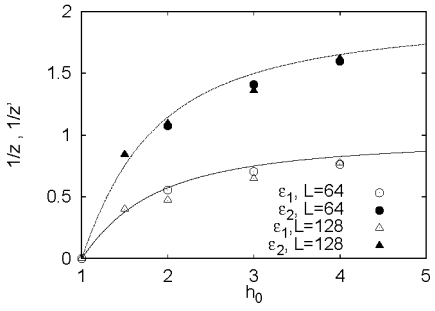

Figure 4.3: The estimates for $1/z$ and $1/z'$ as a function of h_0 for the uniform distribution. The full line for $1/z$ corresponds to the analytical result (3.13), the broken line corresponds to $2/z$.

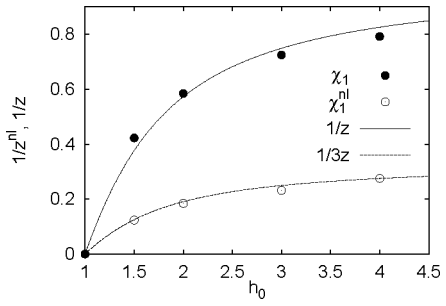

Figure 4.4: The estimates for $1/z$ and $1/z^{\rm nl}$ as a function of h_0 for the uniform distribution. They have been obtained from our analysis of the probability distribution of $\ln \chi_1$ and $\ln \chi_1^{\rm nl}$, respectively, for two system sizes (as exemplified in fig. 3). The full line for $1/z$ corresponds to the analytical result (3.13), the broken line corresponds to $1/3z$, which should be identical with $1/z^{\rm nl}$.

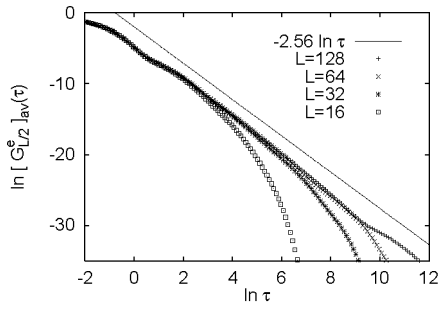

Figure 4.5: The bulk energy-energy autocorrelation function $[G^e_{L/2}]_{\rm av}(\tau)$ for the binary distribution ($\lambda = 4$) at $h_0 = 1.5$ for different system sizes as a function of $\ln \tau$. The slope of the straight line identifies the exponent $\eta_e(h_0)$.

The estimates are shown in Fig. 4.4 at different points of the Griffiths phase. As seen in the Figure the numerical results for the dynamical exponent, z, are again in very good agreement with the analytical results in (4.20) and also the exponent of the non-linear susceptibility, $z^{\rm nl}$, follows fairly well the scaling in (2.45).

Finally, we calculated the average energy-density autocorrelation function. As seen in Fig. 4.5 $[G^e]_{\rm av}(\tau)$ displays a linear region in a log-log plot, the size of which is increasing with L, but its slope, which is just the decay exponent, η_e, has only a weak L dependence. The slope of the curve and thus the corresponding decay exponent η_e has a variation with the parameter h_0, as illustrated in Fig. 4.6. The estimated η_e exponents at the critical point, $h_0 = 1$, and in the Griffiths phase are presented in Fig. 4.7. As seen in this Figure the variation of η_e is well described by the form $\eta_e(\delta) = \eta_e(0) + 1/z(\delta)$. This functional form corresponds to the scaling result in Eq.(4.16), if the critical point correlations decay with

$$\eta_e(0) = 2\,. \tag{4.21}$$

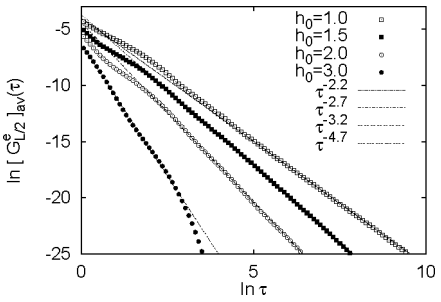

Figure 4.6: The bulk energy-energy autocorrelation function $[G^e_{L/2}]_{\rm av}(\tau)$ for the binary distribution ($\lambda = 4$) at different values for h_0 for $L = 128$ as a function of $\ln \tau$. One observes the variation of the exponent $\eta_e(h_0)$ (identical to the slope of the straight line fits) with increasing h_0.

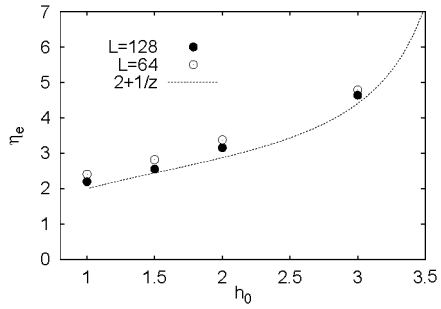

Figure 4.7: The exponent $\eta_e(h_0)$ for the binary distribution ($\lambda = 4$). The full line is the analytical prediction $\eta_e(h_0) = 2 + 1/z(h_0)$ with $z(h_0)$ given by the exact formula (3.13) for the binary distribution with $\lambda = 4$.

The numerical calculations with $L = 128$ give a slightly higher value $\eta_e(0) \approx 2.2$ [109]. However, the finite-size estimates show a slowly decreasing $\eta_e(0)$ with increasing system size. Repeating the calculation with $L = 256$ we got $\eta_e(0) \approx 2.1$. Thus we can conclude that the scaling relation in (4.16) is probably valid and then (4.21) is the exact value of the decay exponent of the average critical energy-density autocorrelations[1].

4.4 Summary

We have considered the random transverse-field Ising spin chain and studied the singular behaviour of susceptibility, non-linear susceptibility, higher gaps, and the energy-density autocorrelation function in the Griffiths phase. Our main

[1] Numerical estimates for the decay exponent of the average energy-density autocorrelation function for *surface* spins at the critical point are $\eta_e^s \approx 2.5$ with $L = 128$ [109], which is somewhat larger than for bulk autocorrelations. Discrepancies between estimates for z from surface and bulk quantities have been observed before [58]. They can be attributed to corrections to scaling effects which are different for different quantities, see also Fig. 6 in Ref. [138]

conclusion is that all the above singular quantities can be characterized by power-law singularities and the corresponding varying critical exponents can be related to the dynamical exponent $z(\delta)$ and, for energy-density autocorrelations, to the $\eta_e(0)$ critical point exponent. Since the exact value of $z(\delta)$ is known in (3.13) and we expect that also the relation in (4.21) is valid, we have a complete, analytical description of the Griffiths phase of the RTIM in one dimension. Much of the reasoning of our phenomenological scaling considerations in Section 4.2 stay valid for other random quantum systems. Especially the scaling behavior of the higher gaps and the corresponding relation in (4.12) should be valid even for higher dimensions and the same is true for the distribution of the non-linear susceptibility and the corresponding relation in (2.45).

Chapter 5

RG study of the Griffiths phase

Among the theoretical methods developed to study random quantum systems the renormalization group (RG) scheme introduced by Ma, Dasgupta and Hu[89] plays a special role. For a class of systems, the critical behavior of those is controlled by an infinite randomness fixed point, the RG method becomes asymptotically exact during iteration. For some one-dimensional models, e.g. the random transverse-field Ising model [33] and the random XXZ model [32], Fisher has obtained analytical solution of the RG equations and in this way many new exact results and new physical insight about the critical behavior of these models have been gained. Subsequent analytical [58] and numerical [137, 58] investigations of the models are in agreement with Fisher's results. The RG-scheme has been numerically implemented in higher dimensions [96, 84], as well, to study the critical behavior of the RTIM and reasonable agreement with the results of quantum Monte-Carlo simulations[106] has been found. Considering the Griffiths-phase of random quantum spin chains here the RG-scheme has been rarely used[84], mainly due to the general belief that the method looses its asymptotically exact properties by leaving the vicinity of the scale invariant critical point.

Our aim is to clarify the applicability of the Ma-Dasgupta-Hu (MDH) RG-method in the Griffiths phase of random quantum spin chains. We start with the RTIC, extend the method to the Griffiths phase and present the analytical solution of the RG-equations. Then, for general models, we analyze by scaling considerations the structure of the RG equations around the line of semicritical fixed points and arrive to the conclusion that the RG method becomes asymptotically exact in the whole Griffiths region. This statement is then checked numerically in the random quantum Potts model (RQPM) by solving the RG flow equations.

5.1 The Ma-Dasgupta-Hu RG-method

Investigating quantum phase transitions one is interested in the low-temperature properties of the system and would like to systematically eliminate high-energy degrees of freedom. A simple way of doing this the MDH RG-method firstly

developed for the random spin-$\frac{1}{2}$ Heisenberg chain [89] and later applied for other spin chains (RTIC, XX-, XY-, and XXZ chain) [33, 32].

The main idea of the method is to take the strongest term in the Hamiltonian, find the ground states of it, and take the coupling to the rest of the system perturbatively, and then throw out the excited states involving the strong coupling, yielding an effective Hamiltonian with couplings smaller then decimated ones. Thus iteration of the above operations leads to the successive decrease of energy scale.

We show here the implementation of the above procedure on the RTIC, where one distinguishes between two cases.

Strong bond decimation If the largest coupling is a bond, e.g. $\Omega = J_2$, one considers the block-Hamiltonian containing the two spins connected by J_2 (see Fig. 5.1):

$$H_{23} = -J_2\sigma_2^x\sigma_3^x - h_2\sigma_2^z - h_3\sigma_3^z. \tag{5.1}$$

We assume, that $J_2 \gg h_2, h_3$. The ground state of (5.1) lies in the subspace spanned by $|\uparrow\uparrow\rangle$ and $|\downarrow\downarrow\rangle$. Solving the eigenvalue problem in this subspace yields for the ground state energy:

$$E_0 = -\sqrt{J_2^2 + (h_2 + h_3)^2} = -J_2 - \frac{1}{2}\frac{(h_2 + h_3)^2}{J_2} + \dots \tag{5.2}$$

The first excited state is in the sector spanned by $|\uparrow\downarrow\rangle$ and $|\downarrow\uparrow\rangle$. The energy associated to this is

$$E_1 = -\sqrt{J_2^2 + (h_2 - h_3)^2} = -J_2 - \frac{1}{2}\frac{(h_2 - h_3)^2}{J_2} + \dots \tag{5.3}$$

Thus the excitation energy:

$$E_1 - E_0 = 2\frac{h_2 h_3}{J_2} + \dots \tag{5.4}$$

Dropping the two higher lying states with energies $E_3 \approx E_4 = J_2$, we are left with an effective Hamiltonian which acts on a single spin as

$$\tilde{H}_{23} = -\frac{h_2 h_3}{J_2}\sigma_{23}^x. \tag{5.5}$$

Strong field decimation If the strongest term in the Hamiltonian is a field, one has to consider the block (see Fig. 5.1):

$$H_{13} = -h_2\sigma_2^z - J_1\sigma_1^x\sigma_2^x - J_2\sigma_2^x\sigma_3^x. \tag{5.6}$$

Assuming $h_2 \gg J_1, J_2$ the last two term can be regarded as a small perturbation on the first one. These can be treated by second order degenerate perturbation theory in the subspace $|\sigma_1^z \uparrow_2 \sigma_3^z\rangle$ with $\sigma_1^z, \sigma_3^z = \uparrow$ or $\downarrow$. This yields for the effective Hamiltonian:

$$\tilde{H}_{13} = -\frac{J_1 J_2}{h_2}\sigma_1^x\sigma_3^x. \tag{5.7}$$

The same result can be obtained much easier by eliminating the strong coupling in the dual of (5.6), as shown in Fig. 5.1.

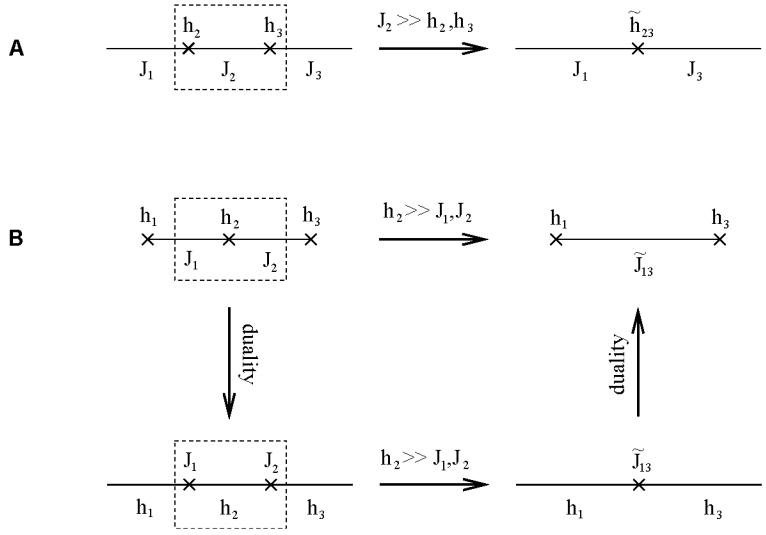

Figure 5.1: The course of MDH strong disorder RG-scheme for RTIC and RQPM. In case of a strong bond (A) one ends up with a single effective spin in a field $\tilde{h}_{23} = \frac{h_2 h_3}{\kappa J_2}$. For a strong field (B) the decimation is equivalent to eliminating a strong bond in the dual lattice. Then the central spin is eliminated, leaving an effective coupling $\tilde{J}_{13} = \frac{J_1 J_2}{\kappa h_2}$ between remaining spins.

Thus the basic RG-equations for coupling and field decimations are given by

$$\tilde{h} = \frac{h_i h_{i+1}}{\kappa J_i} \quad , \quad \tilde{J} = \frac{J_{i-1} J_i}{\kappa h_i} \, , \tag{5.8}$$

respectively, which are related through duality. Here, for the RTIM we have $\kappa = 1$. Note that for $\kappa \geq 1$ the generated new couplings are smaller than decimated ones[1], which leads to the gradual decrease of Ω during the procedure.

Under renormalization one follows the probability distributions of the couplings $R(J, \Omega)$, and that of the fields $P(h, \Omega)$, which are normalized, such that

$$\int_0^\Omega P(h, \Omega) dh = \int_0^\Omega R(J, \Omega) dJ = 1. \tag{5.9}$$

When the energy-scale is lowered as $\Omega \to \Omega - d\Omega$, which amounts to eliminating $d\Omega[P(\Omega, \Omega) + R(\Omega, \Omega)]$ spins, the distribution $R(J, \Omega)$ is changing as

$$\begin{aligned} & R(J, \Omega - d\Omega) = \\ & = \left\{ R(J, \Omega) + d\Omega P(\Omega, \Omega) \int_0^\Omega dJ_1 \int_0^\Omega dJ_3 R(J_1, \Omega) R(J_3, \Omega) \times \right. \\ & \left. \times \left[\delta \left(J - \frac{J_1 J_3}{\Omega} \kappa \right) - \delta(J - J_1) - \delta(J - J_3) \right] \right\} \frac{1}{1 - d\Omega[R(\Omega, \Omega) + P(\Omega, \Omega)]} \, . \end{aligned} \tag{5.10}$$

[1] Otherwise the procedure may fail. For details see Ref. [13, 69].

The first term in brackets accounts for generated new couplings, while the second and third term for decimated ones. The last factor is included in order to maintain normalization.

A similar equation for the field distribution follows from (5.10) through duality, which amounts to interchange $P \leftrightarrow R$ and $J \leftrightarrow h$.

Now expanding $R(J, \Omega - d\Omega)$ and $P(h, \Omega - d\Omega)$ we obtain the differential equations:

$$\frac{\mathrm{d}R(J,\Omega)}{\mathrm{d}\Omega} = R(J,\Omega)[P(\Omega,\Omega) - R(\Omega,\Omega)] \\ -P(\Omega,\Omega)\int_{J_\kappa}^{\Omega} \mathrm{d}J' R(J',\Omega) R(\frac{J\Omega\kappa}{J'},\Omega)\frac{\Omega\kappa}{J'} \ , \tag{5.11}$$

$$\frac{\mathrm{d}P(h,\Omega)}{\mathrm{d}\Omega} = P(h,\Omega)[R(\Omega,\Omega) - P(\Omega,\Omega)] \\ -R(\Omega,\Omega)\int_{h_\kappa}^{\Omega} \mathrm{d}h' P(h',\Omega) P(\frac{h\Omega\kappa}{h'},\Omega)\frac{\Omega\kappa}{h'} \ , \tag{5.12}$$

The fixed point ($\Omega \to 0$) solution to the above equations at the critical point ($R \equiv P$) of the RTIC ($\kappa = 1$) was found by Fisher [33, 31]. It is given in terms of the distribution $\rho(\eta)$ of the variable $\eta = -(\ln\Omega - \ln J)/\ln\Omega$ as

$$\rho(\eta)\mathrm{d}\eta = \exp(-\eta)\mathrm{d}\eta. \tag{5.13}$$

5.2 Analytical study of RTIC

For the RTIC ($\kappa = 1$) we found one class of solutions, which satisfy the RG equations also in the off-critical situation. They are of the form:

$$\begin{aligned} R(J,\Omega) &= R(\Omega,\Omega)\,(\Omega/J)^{1-R(\Omega,\Omega)\Omega} \\ P(h,\Omega) &= P(\Omega,\Omega)\,(\Omega/h)^{1-P(\Omega,\Omega)\Omega} \end{aligned} \ , \tag{5.14}$$

where the distributions involve the parameters, $\tilde{R}(\Omega) \equiv R(\Omega,\Omega)$ and $\tilde{P}(\Omega) \equiv P(\Omega,\Omega)$, which satisfy the relation $(\tilde{P} - \tilde{R})\Omega = 1/z = const.$ Thus the solution is characterized by a single parameter $z = z(\delta)$, which depends on the quantum control-parameter δ. At the critical point we have $1/z(0) = 0$, whereas in the paramagnetic phase $1/z(\delta) > 0$ and monotonically increases with δ.

In terms of the variables, $u = \tilde{R}\Omega + 1/2z = \tilde{P}\Omega - 1/2z$ and $v = -\ln\Omega$ we obtain the differential equation

$$\frac{\mathrm{d}u}{\mathrm{d}v} + u^2 = \frac{1}{4z^2} \ , \tag{5.15}$$

which has the solution, $u = 1/(v - v_0)$, $v_0 = \mathrm{const}$, *at the critical point* with $1/z = 0$. This is identical to the critical fixed point solution in (5.13). At this point we refer to Fisher's analysis [33, 31] and conclude that the functions in Eqs (5.14) indeed represent the fixed point distribution for all non-singular initial distributions. Another argument for Eqs. (5.14) representing the true fixed point distribution, is based on the numerical solution of Eqs. (5.11) and

(5.12), which are evolving towards the special solutions in (5.14) for different initial distributions. A third argument can be found in Ref. [52].

In the Griffiths phase, $\delta > 0$, the solution of Eq.(5.15) in terms of the original energy-scale variable, Ω, is given by

$$u = \frac{u_0/2z + 1/4z^2 \tanh\left[\ln(\Omega_0/\Omega)/2z\right]}{1/2z + u_0 \tanh\left[\ln(\Omega_0/\Omega)/2z\right]} \,, \tag{5.16}$$

where $u = u_0$ at a reference point $\Omega = \Omega_0$. Approaching the line of semicritical fixed points, i.e. for $\Omega/\Omega_0 \to 0$, we have in leading order:

$$\tilde{R}\Omega = \tilde{P}\Omega - 1/z = \tilde{R}(\Omega_0)/[\tilde{P}(\Omega_0)z]\,(\Omega/\Omega_0)^{1/z} + ... \tag{5.17}$$

thus $\tilde{P}$ and $\tilde{R}$ have different low energy asymptotics.

The *physical relevance* of $1/z$ can be obtained by studying the change of number of spins, $n_\Omega \to n_\Omega - \mathrm{d}n_\Omega$ connected with a change in the energy scale as $\Omega \to \Omega - \mathrm{d}\Omega$. This leads to the differential equation

$$\frac{\mathrm{d}n_\Omega}{\mathrm{d}\Omega} = n_\Omega \left[P(\Omega,\Omega) + R(\Omega,\Omega)\right], \tag{5.18}$$

the solution of which is given by:

$$n_\Omega = \left\{\cosh\left[\ln(\Omega_0/\Omega)/2z\right] + 2z\; y_0 \sinh\left[\ln(\Omega_0/\Omega)/2z\right]\right\}^{-2} \,, \tag{5.19}$$

which along the line of semicritical fixed points has the asymptotic behavior $n_\Omega = \mathrm{const} \cdot \Omega^{1/z}$, $\Omega \to 0$. Since the typical distance between remaining spins is $L_\Omega \sim 1/n_\Omega \sim \Omega^{-1/z}$, we can identify z as the *dynamical exponent*, which governs the relation between time- and length-scales as $\tau \sim L^z$.

Next we show that z is invariant along the RG trajectory and can be deduced from the original distributions. For this we consider the averages, $[J^\mu]_{\mathrm{av}}$ and $[h^{-\mu}]_{\mathrm{av}}$, and using Eqs.(5.11) and (5.12) we calculate the derivative:

$$\begin{aligned} &\frac{\mathrm{d}}{\mathrm{d}\Omega}\left[(J/h)^\mu\right]_{\mathrm{av}} = \left(1 - \left[(J/h)^\mu\right]_{\mathrm{av}}\right) \times \\ &\times \left(P(\Omega,\Omega)\Omega^{-\mu}[J^\mu]_{\mathrm{av}} + R(\Omega,\Omega)\Omega^\mu[h^{-\mu}]_{\mathrm{av}}\right), \end{aligned} \tag{5.20}$$

which is vanishing for $\mu = \tilde{\mu}$, if $[(J/h)^{\tilde{\mu}}]_{\mathrm{av}} = 1$. Consequently $\tilde{\mu}$ stays invariant along the RG trajectory until the fixed point, where using the distribution in Eqs.(5.14) we obtain $\tilde{\mu} = 1/z$. Thus the dynamical exponent for the RTIM is given by the solution of the equation (3.13), which is then exact, since the RG-transformation becomes asymptotically exact as $\Omega \to 0$. This latter statement follows from the fact that the ratio of decimated bonds, Δn_J, and decimated fields, Δn_h, goes to zero as $\Delta n_J/\Delta n_h = R(\Omega,\Omega)/P(\Omega,\Omega) \sim \Omega^{1/z}$. Then the probability, $Pr(\alpha)$, that the value of a coupling, J, being neighbor to a decimated field is $\Omega < J < \alpha\Omega$ with $0 < \alpha < 1$ is given by $Pr(\alpha) = 1 - \alpha^{\tilde{R}\Omega}$, which goes to zero for any non-zero α, since $\tilde{R}\Omega \sim \Omega^{1/z}$ at the fixed point. Consequently the decimations in Eq.(5.8) and the related RG equation in Eqs.(5.11) and (5.12) are indeed exact. Thus we presented here a derivation of (3.13), which is independent of that introduced in Section 3.4.

5.3 General scaling theory

Next, we consider general random quantum spin chains with a critical IRFP and analyze the structure of the RG equations close to the line of semicritical fixed points, thus as $\Omega \to 0$. As for the RTIM, the decimation for fields and couplings is asymmetric and for $\Omega \to 0$ exclusively fields are decimated out, which are typically infinitely stronger, than neighbouring couplings. Therefore the RG decimation equations in Eq.(5.8) are asymptotically exact. The second point is to show that the dynamical exponent stays invariant along the RG trajectory, even though in the starting phase the RG equations are approximative. For this we consider the low energy tail of the distribution function of the first gap, $P_L(\ln \epsilon_1)$, which involves the exponent z, and use the scaling result of Section 4.2. This states that the probability distribution of the second, third, etc. gaps are related to $P_L(\ln \epsilon_1)$ as $P_L(\ln \epsilon_2) \sim P_L^2(\ln \epsilon_1)$, $P_L(\ln \epsilon_3) \sim P_L^3(\ln \epsilon_1)$, etc, due to the fact that for a small second, third gap one needs two, three independent SCD-s and the corresponding probabilities are multiplied. In the RG decimation the SCD-s are only eliminated through coupling decimation, since their couplings are stronger than the average fields. If at some time a SCD with a small gap, ϵ_1, is eliminated then in the probability distribution, $P_L(\ln \epsilon_1)$, one should consider the former second gap and use the corresponding conditional probability, $P_L(\ln \epsilon_1) \to P_L(\ln \epsilon_2)/P_L(\ln \epsilon_1) \sim P_L(\ln \epsilon_1)$. Thus the small energy tail of the gap-distribution and consequently the dynamical exponent remains invariant under the renormalization procedure. The previously obtained exact results for the RTIM give strong support for the validity of these phenomenological considerations.

5.4 Numerical analysis of the random quantum Potts model

For a numerical demonstration of the validity of the above statement we considered two random quantum spin chains, the one-dimensional RQPM and the dimerized Heisenberg (XXX) chain, both having a set of RG equations very similar to that of the RTIM in (5.8).

The q-state RQPM was already introduced in Section 2.4.1. We study here its one-dimensional version given by the Hamiltonian

$$H = -\sum_{i=1}^{L} q J_i \delta(n_i, n_{i+1}) - \sum_{i}^{L} \frac{1}{q} h_i \sum_{k=1}^{q-1} M_i^k, \tag{5.21}$$

where periodic boundaries are considered, i.e. spins at site 1 and site $L+1$ are taken to be identical.

Fields and couplings play analogous role as for the RTIC. The quantum Potts chain is self-dual, and the quantum control parameter is the same as that of RTIC, given in (3.3). As it is shown in Appendix B, the recursion equations are of form of (5.8) and κ takes the value $\kappa = q/2$ [119].

At the critical point the RG-equations for $1 \leq \kappa < \infty$ have been solved by Senthil and Majumdar [119] with the result that κ is an irrelevant variable and the IRFP is the same as for the RTIM. In the Griffiths-phase we could not find a complete solution of the RG equations, in spite of the close similarity to that

of the RTIM. We could, however, show that up to an accuracy of $O(\Omega^{1/z})$ the solution is of the form of Eqs.(5.14) and thus there is infinite randomness along the line of fixed points.

This can be shown in an other way by using the numerical founding, that close to the fixed point $\Omega = \Omega^* = 0$ the distribution

$$p(x,\Omega)dx = \Omega P\left(\frac{h}{\Omega},\Omega\right) d\frac{h}{\Omega} \qquad 0 \le x \le 1 \tag{5.22}$$

has a non-vanishing value at x=1:

$$p(1,\Omega)\Big|_{\Omega=\Omega^*=0} = p^*(1) > 0, \tag{5.23}$$

while

$$r(y,\Omega)dy = \Omega R(\frac{J}{\Omega},\Omega)d\frac{J}{\Omega} \quad 0 \le y \le 1 \tag{5.24}$$

is zero at $r = 1$:

$$r(1,\Omega)|_{\Omega=\Omega^*=0} = r^*(1) = 0. \tag{5.25}$$

(See Fig. 5.2.) Then equation (5.18) reduces in the vicinity of the fixed point ($\Omega \to 0$) to

$$\frac{dn_\Omega}{d\Omega} = \frac{n_\Omega p^*(1)}{\Omega}, \tag{5.26}$$

with the solution

$$n_\Omega = \Omega^{p^*(1)} \times \text{const.} \tag{5.27}$$

Repeating the argument below Eq. (5.19), we can read off the dynamical exponent as

$$z = \frac{1}{p^*(1)}. \tag{5.28}$$

Now we derive the form of fixed point solution to (5.12) for general $\kappa \ge 1$, using the assumptions in (5.23) and (5.25), which was found by numerics.

In terms of the distribution functions (5.22) and (5.24), Eq. (5.12) can be written as

$$x\frac{\partial p}{\partial x} - \Omega\frac{\partial p}{\partial \Omega} + p = p(x,\Omega)[p(1,\Omega) - r(1,\Omega)] + r(1,\Omega)\int_{x\kappa}^{1} dx' p(x',\Omega)p(\frac{x}{x'}\kappa,\Omega)\frac{1}{x'}\kappa. \tag{5.29}$$

Close to the fixed point $\Omega = \Omega^* = 0$, where $r(1,\Omega^*) = 0$, $p(1,\Omega^*) = p^*(1)$ and $\Omega\frac{\partial p}{\partial \Omega}\big|_{\Omega=\Omega^*} = 0$, Eq. (5.29) becomes significantly simpler:

$$x\frac{\partial p^*}{\partial x} = -p^*(x)(1 - p^*(1)). \tag{5.30}$$

Its solution is

$$p^*\left(\frac{h}{\Omega}\right) = \frac{1}{z}\left(\frac{h}{\Omega}\right)^{-1+\frac{1}{z}}, \tag{5.31}$$

where we have used relation (5.28).

The exponent z, however, does depend on the parameter κ, since the validity of the condition in Eq.(3.13) is limited to $\kappa = 1$, thus in general $z = z_\kappa(\delta)$.

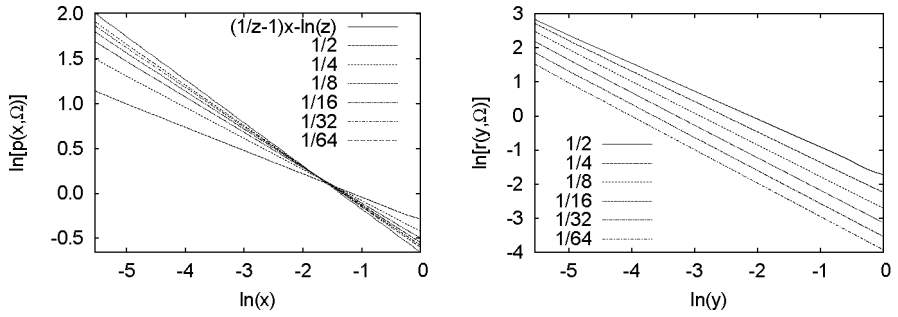

Figure 5.2: The distributions $p(x,\Omega)$ vs. x (left) and $r(y,\Omega)$ vs. y (right) on a log-log scale for different energy scales Ω denoted on the figures, obtained from the numerical solution of (5.11) and (5.12) with $\kappa = 3/2$ and uniform distribution with $h_0 = 2$. The solid line in figure left corresponds to (5.31) with the extrapolated value $z \approx 0.519$. In figure right $r(y,\Omega)$ evolves towards a power-law distribution with power -1 as $\Omega \to 0$.

We have calculated the dynamical exponent by solving numerically the RG flow equations (5.11) and (5.12). In a mathematical point of view these are connected integro-differential equations with singular kernels in the integrals.

In the numerical integration the bond and field variables are discretized, as $J_n = n \cdot \Delta J$ and $h_n = n \cdot \Delta h$, $n = 1, 2, \ldots$, where $N = \frac{1}{\Delta J} = \frac{1}{\Delta h}$ is the number of representative points in a unit interval, which we call *resolution*. The distribution functions R and P at a given energy-scale Ω are represented by a set of functional values $\{R(J_i,\Omega)\}$ and $\{P(h_i,\Omega)\}$, respectively.

Decreasing the energy scale by a small finite value $\Delta\Omega$ the evolution of distribution functions was computed by the standard forth-order Runge-Kutta method [98].

At each stage of the energy scale the integrals in (5.11) and (5.12) have to be evaluated, where the domain of integration vanishes as $\Omega \to 0$. To overcome this difficulty the resolution was doubled at energies $\Omega = \frac{1}{2}, \frac{1}{4}, \frac{1}{8}, \ldots$ by introducing new points into the sets $\{R(J_i,\Omega)\}$ and $\{P(h_i,\Omega)\}$ in between already existing points through polynomial fitting.

The normalization of distributions, which otherwise would deteriorate due to numerical errors, was restored after each Runge-Kutta step by integrating P and R over the whole domain of definition and renormalizing them. In the regions, where the integrand was slowly varying, a standard quadrature (Simpson formula [98]) was used, while the region containing the singularity was found to be able to be well approximated by a power-law. The border separating the two regions, were set automatically by monitoring the error of polynomial fitting.

The procedure was stopped at the final energy scale $\Omega_f = \frac{1}{1024}$, and the effective value of the dynamical exponent for various intermediate energy scales were extracted by fitting a straight line to $p(x,\Omega)$ in a log-log plot (Fig 5.2), where the slope is asymptotically related to z according to (5.31). These values were then extrapolated to $\Omega = 0$. The computation was then repeated with larger and larger resolutions, and finally the effective values were extrapolated to $N \to \infty$, by the BST-algorithm [8]. Starting with a uniform initial distribution in (4.19), the resulted values of z_κ are seen in Fig. 5.3.

We have also calculated the dynamical exponent by a numerical implemen-

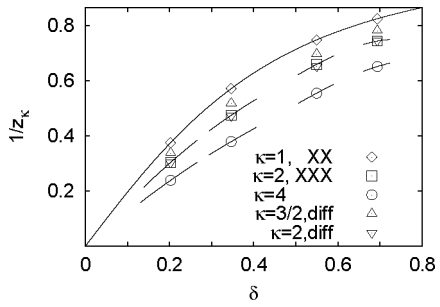

Figure 5.3: Dynamical exponents from numerical solution of Eqs. (5.11) and (5.12) (denoted by $\triangle$ and $\triangledown$), and from numerical iteration of recursion-equations (5.8) for different values of the parameter κ. For $\kappa = 1$ (RTIM and the random dimerized XX-chain) the exact result is given by the full line, for $\kappa = 2$ and 4 the broken lines are guide to the eye.

tation of the RG scheme over 50000 samples of length $L \leq 2^{14}$. Starting with the uniform probability distribution, we got the estimates shown in Fig. 5.3: $1/z_\kappa$ is a monotonously decreasing function of κ and eventually it is expected to go to zero in the whole Griffiths phase in the limit $\kappa \to \infty$.

These results were compared with dynamical exponents of the XXX-chain, calculated by P. Lajkó, directly from the asymptotic behaviour of the distribution of surface magnetization, as given in Eq. (3.14). For the dimerized XXX chain J and h in Eq.(5.8) are replaced by the Heisenberg couplings at odd and even positions, J_o and J_e, respectively, and the parameter takes the value $\kappa = 2$ [89, 32]. The distance from the critical point is measured similarly to (3.3). For numerical calculations of surface magnetization the DMRG method was used, for chains with $L \leq 64$ and some 20000 samples were considered. An overall agreement between dynamical exponents calculated by the two methods was found. As a demonstration we show in Fig. 5.4 the distribution of m_s for the XXX-chain and for the $q = 4$ state RQPM, where for both models we are at the same distance from the transition point. As seen in Fig. 5.4 the asymptotic behavior of the two distributions is identical, as expected on the RG basis, since $\kappa = 2$ for both models. Furthermore the dynamical exponents agree very well with those calculated by the RG method.

5.5 Summary

In this chapter we have pointed out by exact calculations on the RTIC and general scaling considerations, that MDH RG-method is applicable along the lines of semicritical fixed points of quantum spin chains, where it is asymptotically exact. We found the fixed point solutions to the RG flow equations governing the RTIC in the Griffiths region. We presented an exact result for the dynamical exponent, and showed, that z stays invariant along the RG procedure. By a general scaling argument on the gap distribution we suggest this later statements to be generally valid for other spin chains. We performed a numerical analysis of RG flow equations of the one-dimensional RQPM, and determined

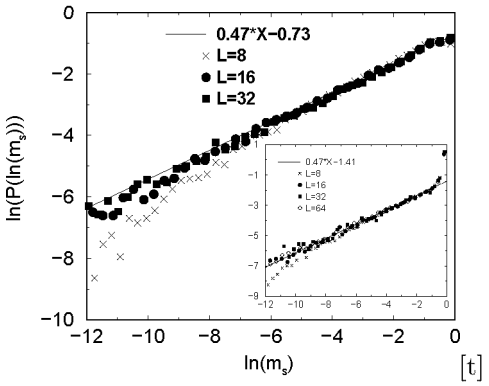

Figure 5.4: Probability distribution of the logarithm of the surface magnetization of the dimerized random XXX-chain with $\delta = -(\ln 2)/2$ for different finite systems calculated by the DMRG method by P. Lajkó. The slope of full straight line $1/z(\delta) = 0.47$ comes from the RG treatment. In the inset the same quantity is shown for the $q = 4$ state RQPM at the same distance from the critical point. The asymptotic slope of this distribution can be well fitted by the same exponent as for the XXX-model.

the κ-dependent dynamical exponents. For $\kappa = 2$ an excellent agreement was found with DMRG results on the dimerized XXX model, which is described by the same RG equations. These and other numerical results strongly support the asymptotic exactness of the procedure and the correctness of other exact and phenomenological findings.

Chapter 6

The random XX- and XY chain

In this chapter we are going to extend the methods and calculations brought out in Chapter 4 to other disordered quantum spin chains. Namely, we are going to study here XY- and dimerized XX spin-$\frac{1}{2}$ chains with random exchange couplings by analytical and numerical methods and by phenomenological scaling theory.

6.1 Phase diagram with non-random couplings

First we introduce a few well-known antiferromagnetic spin-$\frac{1}{2}$ models including those, which are the subject of investigation, then we give a brief survey of their zero-temperature phases.

We start with the general one-dimensional XYZ model, the other models under investigation are its special cases. It is given by the Hamiltonian

$$H_{XYZ} = \sum_l (J_l^x S_l^x S_{l+1}^x + J_l^y S_l^y S_{l+1}^y + J_l^z S_l^z S_{l+1}^z), \tag{6.1}$$

where $S_l^\mu \equiv \frac{1}{2}\sigma_l^\mu$ are the components of a spin-$\frac{1}{2}$ operator attached to site l. By rotating the spins at appropriate sites, one can always render the couplings J_l^x and J_l^y to be positive. If the couplings J_l^z are now positive, the model is antiferromagnetic, while if they are negative, it is ferromagnetic.

The special cases we consider are the following. Putting $J_l^x = J_l^y = J_l^z$ in (6.1) one gets the *Heisenberg (or XXX) model.* If $J_l^x = J_l^y \neq J_l^z$ in (6.1), the model is called *XXZ model.* Moreover if $J_l^z = 0$ one arrives to the simpler *XX model.* In the above models $S_T^z = \sum_l S_l^z$ is a conserved quantity. Keeping $J_l^z = 0$ but allowing J_l^x and J_l^y to be different, the resulting model is called *XY model.*

The homogeneous XYZ model (i.e. $J_l^x = J^x, J_l^y = J^y, J_l^z = J^z$) is controlled by two parameters: The parameter Δ given by

$$\Delta \equiv \frac{2J^z}{J^x + J^y} \tag{6.2}$$

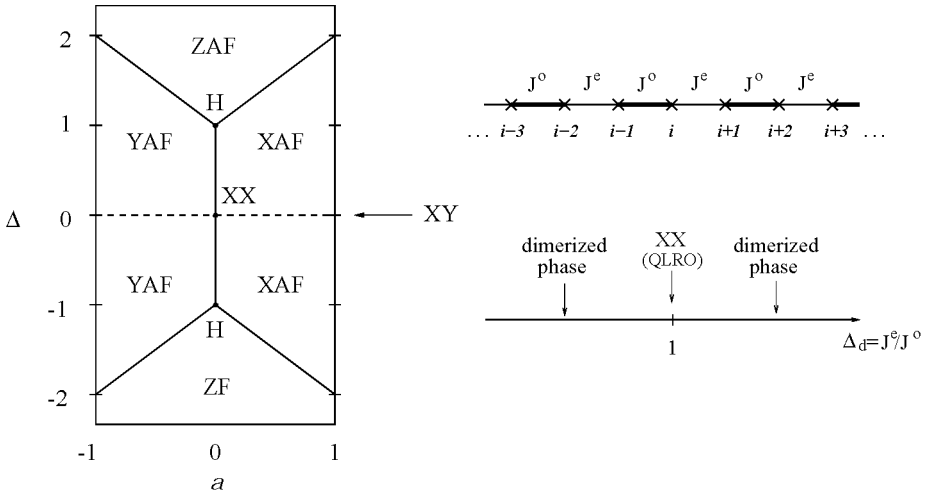

Figure 6.1: Left: Zero-temperature phase diagram of the pure antiferromagnetic XYZ chain. Phase boundaries are indicated by solid lines. XAF(YAF) refers to a phase with antiferromagnetic order in the x(y) direction. ZF(ZAF) denotes a phase with (anti)ferromagnetic order in the z direction. The points labeled by H have Heisenberg symmetry. Right: Phase diagram of the pure dimerized XX chain.

and the anisotropy parameter

$$a \equiv \frac{J^x - J^y}{J^x + J^y}. \tag{6.3}$$

The phase diagram is shown in Fig. 6.1 [4]. The system exhibits QLRO with continuously varying decay exponents along phase boundaries. These critical lines separate various long-range ferro- and antiferromagnetically ordered phases. The point $a = 0$, $\Delta = 1$ corresponds to the antiferromagnetic Heisenberg chain, whereas $a = 0$, $\Delta = -1$ can be transformed to a Heisenberg ferromagnet. The XY chain takes place along the line $\Delta = 0$ divided into two parts by the isotropic XX point.

Another issue in the context of XX chain is *dimerization.* (See Fig. 6.1 (right).) It was pointed out by Haldane, that isotropic antiferromagnetic chains of integer spins have an energy gap, whereas half integer spin chains are gapless [42]. However, alternating couplings in spin-1/2 chains enforce a dimerized ground state, and an energy gap is induced. See Fig. 6.1 (right). In the absence of disorder the spin-1 and dimerized spin-$\frac{1}{2}$ chains are in the same phase. This dimerized phase is characterized by a finite gap, exponentially decaying spatial correlations, and a non-vanishing string order parameter(see Ref. [47, 45]).

Now we shall focus on the line $\Delta = 0$ and summerize the existing results on the system subjected to randomness.

6.2 Previously known results for random couplings

The XX point is known to be unstable both against *symmetric randomness* $J_l^x = J_l^y$, and *asymmetric randomness*, i.e. when J_l^x and J_l^y are drawn from independent distributions, $\pi^x(J^x)$ and $\pi^y(J^y)$, respectively [29]. Furthermore in both cases the fixed point governing the critical behaviour is an IRFP.

In case of asymmetric randomness one obtains the random XY chain. The known results on this model are taking over from that of RTIC through the mapping of the XY chain into two decoupled RTIC. This mapping was developed in the thermodynamic limit and for finite chains with periodic boundaries [32, 103, 45].

The quantum control parameter of the model is the average anisotropy defined as:

$$\delta_a = \frac{[\ln J^x]_{\rm av} - [\ln J^y]_{\rm av}}{{\rm var}[\ln J^x] + {\rm var}[\ln J^y]} \ . \tag{6.4}$$

For $\delta_a > 0$ (< 0) there is long-range order in the x (y) direction, i.e. $\lim_{r\to\infty}[C^\mu(r)]_{\rm av} \neq 0$ for $\mu = x(y)$, where $[C^\mu(r)]_{\rm av}$ is defined in (3.46). $C^x(r)$ in the XY model can be expressed as the product of two independent Ising correlators (3.7). Thus at criticality ($\delta_a = 0$) the typical spin-spin correlations ($\mu = x, y$) decay as $\sim e^{-Ar^{1/2}}$, where the distribution of A is broad, like in the RTIC. Whereas average correlations decay algebraically (QLRO), with bulk decay exponents twice as that of RTIC, i.e. $\eta^x = \eta^y = 3 - \sqrt{5}$. The correlation length exponent is the same as that of RTIC, i.e. $\nu = 2$.

Considering the random XX model, where couplings are correlated as $J_l^x = J_l^y = J_l$, one can move the system away from criticality by introducing alternation such that even (e) and odd (o) couplings, connecting the site $2i, 2i+1$ and $2i-1, 2i$, respectively, are taken from distributions $\rho^e(J^e)$ and $\rho^o(J^o)$. The quantum control parameter is now the average dimerization defined as:

$$\delta_d = \frac{[\ln J^o]_{\rm av} - [\ln J^e]_{\rm av}}{{\rm var}[\ln J^o] + {\rm var}[\ln J^e]} \ . \tag{6.5}$$

At $\delta_d = 0$ the system is critical. According to the RG treatment by Fisher [32], in the resulting phase all spins are paired and form singlets, however, the distance between two spins in a singlet pair can be arbitrarily large. It is thus termed *random-singlet (RS) phase.* The long singlet bonds are typically much weaker than short ones and bonds cannot cross each other. The relation between length and time scale was found to be identical to that of RTIC in (3.11). Typical spatial correlation of spins decays as $\sim e^{-Ar^{1/2}}$, where the constant A is broadly distributed. Although rare widely separated pairs of spins, which have strong $\mathcal{O}(1)$ correlation lead to the algebraic decay of average correlations. Because of the singlet nature of pairs of spins, *all* components decay with the same power, which is $\eta^x = \eta^y = \eta^z = 2$. This phase is gapless, and there is no string order. The RG approach predicts the antiferromagnetic random XX fixed point to control the critical behavior of the antiferromagnetic Heisenberg model, too.

The region $\delta_d \neq 0$ corresponds to the *random dimer (RD) phase*, which is gapless like the *RS* phase, but has a non-vanishing string order.

In both random XX and XY chains, a Griffiths phase takes place around the critical point. As shown by an RG analysis [51, 135], applicable in the vicin-

ity of the RS fixed point, the Griffiths phase is characterized by a dynamical exponent predicted to be a continuous function of the quantum control parameter (anisotropy or dimerization) and the singular behavior of different physical quantities are all expected to be related to it.

The RG predictions [32, 51, 135] have been compared to the results of numerical studies [40, 118, 45], especially in the RS phase of isotropic chains. In the RS phase some numerical results are controversial: in earlier studies [118] a different scenario from the RG picture is proposed (in particular with respect to the transverse correlation function), later investigations on larger finite systems have found satisfactory agreement with the RG predictions [45], although the finite-size effects were still very strong.

6.3 Results

In this chapter we extend previous work in several directions. Here we consider open chains and study both bulk and surface quantities, as well as end-to-end correlations. We develop a phenomenological theory which is based on the scaling properties of rare events and determine the complete set of critical decay exponents. We calculate numerically (off-diagonal) spin-operator profiles, whose scaling properties are related to (bulk and surface) decay exponents [129] and compare the profiles with predictions of conformal invariance. Another new feature of our work is the study of dynamical correlations, both at the critical point and in the Griffiths phase, which are not accessible by the MDH RG-method. Finally, we perform a detailed analytical and numerical study of the Griffiths phase and calculate, among others, the exact value of the dynamical exponent.

6.3.1 Free-fermion representation

We consider an open XY chain (i.e. with free boundary conditions) with L sites described by the Hamiltonian:

$$H = \sum_{l=1}^{L-1} \left(J_l^x S_l^x S_{l+1}^x + J_l^y S_l^y S_{l+1}^y \right) \ . \tag{6.6}$$

We use two types of random distributions already introduced in Section 4.3, both for the XY and XX models. One of them is a binary distribution:

$$\begin{aligned} \pi^x(J^x) &= p\delta(J^x - \lambda) + q\delta(J^x - \lambda^{-1}); \\ \pi^y(J^y) &= \delta(J^y - J_0^y) \ , \end{aligned} \tag{6.7}$$

the other is a uniform one:

$$\begin{aligned} \pi^x(J^x) &= \begin{cases} 1, & \text{for } 0 < J^x < 1 \\ 0, & \text{otherwise} \end{cases} \\ \pi^y(J^y) &= \begin{cases} (J_0^y)^{-1}, & \text{for } 0 < J^y < J_0^y \\ 0, & \text{otherwise} \end{cases} \ . \end{aligned} \tag{6.8}$$

For the XX model the corresponding distributions $\rho^e(J^e)$ and $\rho^o(J^o)$ follow from correspondences:

$$J^x \to J^e, \quad J^y \to J^o,$$

$$\pi^x(J^x) \to \rho^e(J^e), \quad \pi^y(J^y) \to \rho^o(J^o)\ . \tag{6.9}$$

Note that the critical points of the two models ($\delta_a = 0$ and $\delta_d = 0$, respectively) are not equivalent due to the different disorder correlations.

Following a completely analogous way, as for the RTIC, i.e. performing the Jordan-Wigner transformation, and a subsequent canonical transformation, the Hamiltonian (6.6) is mapped into a system of non-interacting fermions with Hamiltonian (3.15). For details see Appendix A. The fermion excitations are non-negative and satisfy the set of equations

$$\begin{aligned} \epsilon_q \Psi_q(l) &= J^y_{l-1}\Phi_q(l-1) + J^x_l \Phi_q(l+1) \\ \epsilon_q \Phi_q(l) &= J^x_{l-1}\Psi_q(l-1) + J^y_l \Psi_q(l+1), \end{aligned} \tag{6.10}$$

with boundary conditions $J^x_L = J^y_L = 0$. These equations are nothing but (A.14) in components. Introducing a $2L$-dimensional vector V_q with components:

$$\begin{aligned} V_q(4l-3) = \Phi_q(2l-1), \qquad & V_q(4l-2) = \Psi_q(2l-1), \\ V_q(4l-1) = \Psi_q(2l), \qquad & V_q(4l) = \Phi_q(2l); \end{aligned} \tag{6.11}$$

Eqs.(6.10) then correspond to the eigenvalue problem of the matrix:

$$\mathbf{T} = \begin{pmatrix} 0 & 0 & J^y_1 & & & & & & & \\ 0 & 0 & 0 & J^x_1 & & & & & & \\ J^y_1 & 0 & 0 & 0 & J^x_2 & & & & & \\ & J^x_1 & 0 & 0 & 0 & J^y_2 & & & & \\ & & J^x_2 & 0 & 0 & 0 & J^y_3 & & & \\ & & & J^y_2 & 0 & 0 & 0 & \ddots & & \\ & & & & \ddots & \ddots & \ddots & \ddots & J^y_{L-1} & \\ & & & & & J^y_{L-2} & 0 & 0 & 0 & J^x_{L-1} \\ & & & & & & J^y_{L-1} & 0 & 0 & 0 \\ & & & & & & & J^x_{L-1} & 0 & 0 \end{pmatrix} \tag{6.12}$$

We confine ourselves to the positive part of the spectrum, as was argued in Appendix A. The eigenvalues of $\mathbf{T}$ in (6.12) are of two classes. For $q = 2i-1$, $i = 1, 2, \ldots, L$ the even components of the eigenvectors are zero, i.e. $V_{2i-1}(2j) = 0$, $j = 1, 2, \ldots, L$, whereas for the other class with $q = 2i$ the odd components are zero, $V_{2i}(2j-1) = 0$. Consequently $\mathbf{T}$ can be expressed as a direct product $\mathbf{T} = \mathbf{T}_\sigma \bigotimes \mathbf{T}_\tau$, with the tridiagonal matrices $\mathbf{T}_\sigma$, $\mathbf{T}_\tau$ of size $L \times L$. As a result one has to diagonalize these two matrices. Thus for chains with even number of sites, $L = 2N$, the two classes of eigenvectors are given in terms of the vectors Φ and Ψ via:

$$\begin{aligned} \epsilon_{2i-1}: \quad & \Phi_{2i-1}(2j) &&= \Psi_{2i-1}(2j-1) &&= 0 \\ \epsilon_{2i}: \quad & \Phi_{2i}(2j-1) &&= \Psi_{2i}(2j) &&= 0 \end{aligned} \tag{6.13}$$

for $i, j = 1, \ldots, N$.

For the XX model the even and odd sectors are degenerate, $\epsilon_{2i-1} = \epsilon_{2i}$, thus it is sufficient to diagonalize only one matrix. In this case one has the additional relations:

$$\begin{aligned} \Phi_{2i-1}(2j-1) &= \Psi_{2i}(2j-1)\ , \\ \Phi_{2i}(2j) &= \Psi_{2i-1}(2j)\ . \end{aligned} \qquad \mathrm{XX-model} \tag{6.14}$$

The matrices $\mathbf{T}_\sigma$ and $\mathbf{T}_\tau$ are in one-to-one correspondence with the eigenvalue problem of one-dimensional TIM-s. This exact mapping for finite open chains is presented in Appendix C.

Local order parameters Next we are going to study the long-range order in the ground state of the system. For similar reasons as for the RTIC, the local order parameter in a finite system is given by the off-diagonal matrix element:

$$m_l^x = \langle 1|S_l^x|0\rangle \ . \tag{6.15}$$

(Note that there is a difference of a factor of $\frac{1}{2}$ between the form of (3.21) and that of (6.15) since the former is defined in terms of Pauli operators instead of spin operators.) It can be calculated from the determinant (3.24) containing matrix elements in (3.25).

For surface spins the local order parameter is simply given by $m_1^x = \Phi_1(1)/2$, which can be evaluated in the thermodynamic limit $L \to \infty$ in the phase with long-range order, when $\epsilon_1 = 0$. Using the normalization condition $\sum_l |\Phi_1(l)|^2 = 1$ we obtain for the surface order parameter:

$$\begin{aligned} m_1^x &= \frac{1}{2}\left[1 + \sum_{l=1}^{L/2-1}\prod_{j=1}^{l}\left(\frac{J_{2j-1}^y}{J_{2j}^x}\right)^2\right]^{-1/2} && XY \\ m_1^x &= \frac{1}{2}\left[1 + \sum_{l=1}^{L/2-1}\prod_{j=1}^{l}\left(\frac{J_{2j-1}}{J_{2j}}\right)^2\right]^{-1/2} && XX. \end{aligned} \tag{6.16}$$

We note that this formula is *exact* for finite chains if we use fixed spin boundary condition, $s_L^x = \pm 1/2$, which amounts to have $J_{L-1}^y = 0$. In the fermionic description the two-fold degeneracy of the energy levels, corresponding to $s_L^x = 1/2$ and $s_L^x = -1/2$, is manifested by a zero energy mode in (3.15) and from the corresponding eigenvector we obtain m_1^x in (6.16) for any finite chain.

For non-surface spins the expression of the local order parameter (3.24) can be simplified by using the relations (6.13). Then, half of the elements of the determinant (3.24) are zero, the non-zero-elements being arranged in a checkerboard pattern, and m_l^x can be expressed as a product of two determinants of half-size, which reads for $l = 2j$ as:

$$\begin{aligned} m_{2j}^x = \frac{1}{2} & \begin{vmatrix} H_1 & G_{1,2} & G_{1,4} & \dots & G_{1,2j-2} \\ H_3 & G_{3,2} & G_{3,4} & \dots & G_{3,2j-2} \\ \vdots & \vdots & \vdots & \ddots & \vdots \\ H_{2j-1} & G_{2j-1,2} & G_{2j-1,4} & \dots & G_{2j-1,2j-2} \end{vmatrix} \\ \times & \begin{vmatrix} G_{2,1} & G_{2,3} & \dots & G_{2,2j-1} \\ G_{4,1} & G_{4,3} & \dots & G_{4,2j-1} \\ \vdots & \vdots & \ddots & \vdots \\ G_{2j,1} & G_{2j,3} & \dots & G_{2j,2j-1} \end{vmatrix} . \end{aligned} \tag{6.17}$$

The local order parameter m_l^y, related to the off-diagonal matrix-element of the operator S_l^y can be obtained from (3.24) and (6.16) by exchanging $J_l^x \leftrightarrow J_l^y$.

The local order parameter m_l^z is given as in (3.47), where $|\phi_z\rangle$ is now the ground state $|0\rangle$. Since $\langle 0|\sigma_l^z|0\rangle$ also contains a non-singular contribution, the scaling behaviour of its singular part is more convenient to determine by considering the *off-diagonal order parameter* $m_l^z = \langle\phi_z|\sigma_l^z|0\rangle$, where $\langle\phi_z|$ is now the first *excited* state of H, which has non-vanishing matrix element with $|0\rangle$ [57].

Using (4.6) the off-diagonal order parameter m_l^z is given by

$$m_l^z = \frac{1}{2}| - \Phi_1(l)\Psi_2(l) + \Psi_1(l)\Phi_2(l)| \; . \tag{6.18}$$

For the XX model one can obtain simple expressions using the relations in (6.14) as:

$$\begin{aligned} m_{2i-1}^z &= \tfrac{1}{2}[\Phi_1(2i-1)]^2 \; , \\ & \qquad\qquad XX-\text{model} \\ m_{2i}^z &= \tfrac{1}{2}[\Psi_1(2i)]^2 \; . \end{aligned} \tag{6.19}$$

In the context of XY and XX chains we shall call $m_l^{x,y}$ and m_l^z *transverse* and *longitudinal* order parameters, respectively, in the following.

Autocorrelations Next we consider the dynamical correlations $G_l^\mu(\tau) = \langle S_l^\mu(\tau) S_l^\mu(\tau)\rangle$ as a function of the imaginary time τ. For the x-component of the surface spins they are given following (3.28) as

$$\begin{aligned} G_1^x(\tau) &= \frac{1}{4}\sum_q |\Phi_q(1)|^2 \exp(-\tau\epsilon_q) \\ &= \frac{1}{4}\sum_i^{L/2} |\Phi_{2i-1}(1)|^2 \exp(-\tau\epsilon_{2i-1}) \; , \end{aligned} \tag{6.20}$$

where we have used the relations in (6.13).

The connected longitudinal correlation is given in a simple form for any position l in (4.8) as

$$G_l^z(\tau) = \frac{1}{4}\sum_{p>q} | - \Psi_p(l)\Phi_q(l) + \Psi_q(l)\Phi_p(l)|^2 \exp[-\tau(\epsilon_q + \epsilon_p)] \; . \tag{6.21}$$

6.3.2 Phenomenological theory from scaling of rare events

In this section we identify the rare events for the random XY (and XX) model, which dominate the average quantities, and use their properties to develop a phenomenological theory in an analogous way as it has been done for the RTIC.

Surface order parameter The local order parameter at the boundary is given by the simple formula in (6.16), which has the same structure like that of RTIC in (3.27). Thus using the extreme binary distribution (i.e. $\lambda \to 0$ and $J_0^y = 1$ in (6.7)) and following the same argumentations as for RTIC in Section 3.5.1, we conclude with the basic correspondences between the average surface order parameter of the XY (and XX) model and the surviving probability of adsorbing random walks:

$$[m_1^x(\delta, L)]_{av} \sim P_{\text{surv}}(\delta_w, L/2), \quad \delta \sim \delta_w \; . \tag{6.22}$$

The scaling properties of the average surface order parameter and the correlation length then follow from (3.39), (3.40) and (3.41) and will be evaluated in Section 6.3.3.

Scaling of low-energy excitations In order to estimate the scaling of low-energy excitations, we neglect the r.h.s. of the eigenvalue equation of matrix T in (6.12), which is reasonable, if ϵ_1 vanishes at least as fast as $\epsilon_1 \sim 1/l$, with the system size l. We shall see, that it is fulfilled. Deriving approximate expressions for Φ_1 and Ψ_1 we obtain, similarly to (3.42), the expression for the first gap:

$$\epsilon_1(l) \sim m_1^x m_{l-1}^x J_{l-1}^y \prod_{j=1}^{l/2-1} \frac{J_{2j-1}^y}{J_{2j}^x} \,. \tag{6.23}$$

Here m_1^x is given in (6.16) and the surface order parameter at the other end of the chain, m_{l-1}^x, is given by replacing J_{2j-1}^y/J_{2j}^x by J_{L+1-2j}^y/J_{L-2j}^x in (6.16).

The characteristic excitation energy of an SCD can be estimated from (6.23) as

$$\epsilon_1(l) \sim \prod_{j=1}^{l/2-1} \frac{J_{2j-1}^y}{J_{2j}^x} \sim \exp\Big\{-\frac{l_{\rm tr}}{2}\overline{\ln(J^y/J^x)}\Big\} \,, \tag{6.24}$$

where $l_{\rm tr}$ measures the size of transverse fluctuations of a surviving walk of length $l/2$ and $\overline{\ln(J^x/J^y)}$ is an average ratio of the couplings (it is $\overline{\ln(J^e/J^o)}$ for the XX model). Applying the properties of $l_{\rm tr}$ given in Section 3.5.2 we get similar behaviour as for the RTIC. At the critical point we arrive at (3.44), whereas in the Griffiths phase to (3.45), which now contains the dynamical exponent of the XY (XX) model.

6.3.3 Critical properties

Here we consider in detail the random XY and XX chains in the vicinity of the critical point. The off-critical properties in the Griffiths phase are presented in the following section.

Length- and time scales As we argued in Section 3.5 the rare events are SCD-s, having a coupling distribution of surviving RW character. The typical size of an SCD, as given by ξ_w in Eq. (3.41), is related to the average correlation length of the system ξ. Then using the correspondences in (6.22), (3.41) and (3.53) we get the relation:

$$\xi \sim |\delta|^{-\nu}, \quad \nu = 2 \,. \tag{6.25}$$

The *typical* correlation length, $\xi_{\rm typ}$, as measured by the average of the logarithm of the correlation function is different from the *average* correlation length. One can estimate the typical value by analyzing the formula (6.16) for the surface order parameter, where the products are typically of $\prod_j (J_{2j-1}^y/J_{2j}^x)^2 \sim \exp(\text{const} \cdot |\delta| L)$, thus $[m_s(L, \delta < 0)]_{\rm typ} \sim \exp(-\text{const} \cdot |\delta| L) \sim \exp(-L/\xi_{\rm typ})$. Therefore we obtain:

$$\nu_{\rm typ} = 1 \,. \tag{6.26}$$

We note that *at the critical point* the largest value of the above products is typically of $\prod_j (J_{2j-1}^y/J_{2j}^x)^2 \sim \exp(const \cdot L^{1/2})$, since the transverse fluctuations in the couplings are of $\mathcal{O}(L^{1/2})$. Therefore we have $[m_s(L, \delta = 0)]_{\rm typ} \sim \exp(-\text{const} \cdot L^{1/2})$.

As shown in Eq. (6.24) the value of the smallest gap is related to the size of transverse fluctuations of an SCD $l_{\rm tr}$. Close to the critical point ($\delta \to 0$) one

has $l_{\rm tr} \sim \xi^{1/2}$, and therefore the characteristic relaxation time of a sample scales with correlation length ξ as

$$\ln \tau_{rel} \sim \xi^{1/2} \ . \tag{6.27}$$

We note that the results in this part about length- and time scales are valid both for the XY- and XX models. They also hold in identical form for the RTIC, which can be understood as a consequence of the mapping of the XY chain into decoupled RTIC-s.

Quasi-long-range order

At the critical point the decay exponent of correlations are related to the scaling exponent x^{μ} of the fraction of rare events of the given quantity (see Eq. (3.50)) and its value generally depends on the type of correlations of the disorder, thus it could be different for the XY and the XX models. Analyzing the scaling properties of the rare events in the XY and XX chains we have calculated the critical decay exponents of different correlation functions, both between two spins in the volume and for end-to-end correlations. Our results are presented in Table 6.1.

In the following we are going to derive these exponents by analytical and scaling methods and then confront them with the results of numerical calculations based on the free fermion technique.

Longitudinal order parameter We start with the scaling behavior of the longitudinal order parameter m_l^z, which in the XX chain is given by the simple formula in (6.19). Summing over all sites one gets the sum-rule

$$\sum_{l=1}^{L} m_l^z = 1 \quad {\rm XX-model} \ , \tag{6.28}$$

where we have used (6.13) and the fact that the Φ_q and Ψ_q are normalized. Since this sum-rule is also valid for the average quantities, we get immediately

$$[m_l^z]_{\rm av} = L^{-1} \tilde{m}^z(l/L) \ , \tag{6.29}$$

where $\tilde{m}^z(\tilde{l})$ is a scaling function with $\tilde{l} = l/L$. Consequently for bulk spins the finite-size dependence of the local order parameter is $[m_l^z]_{\rm av} \sim L^{-1}$, thus we have $x^z(XX) = 1$ and from (3.50) the decay exponent is

$$\eta^z(XX) = 2.$$

	$\eta^x(XY)$	$\eta^x(XX)$	$\eta^z(XY)$	$\eta^z(XX)$
bulk	$3-\sqrt{5}^{(**)}$	$2^{(*)}$	4	$2^{(*)}$
surface	1	1	2	1

Table 6.1: Decay exponents of critical correlations in the random XY and XX chains. The exponents with a superscript $^{(*)}$ are those calculated by Fisher with the RG method [32], whereas $^{(**)}$ follows from the results of the RTIC in Ref. [33, 31].

A further consequence of the sum-rule is that the average value of the bulk order parameter is the same, if the averaging is performed over any single sample. Thus the order parameter m^z and the correlation function $\langle 0|S_l^z S_{l+r}^z|0\rangle$ are *self-averaging.* This is quite unusual in disordered systems where the correlations are generally not self-averaging [25].

The surface order parameter m_1^z for the XX model satisfies the relation $m_1^z = 2\,(m_1^x)^2$, which follows from relation $m_1^x = \Phi_1(1)/2$ and (6.19). Then a rare event with $m_1^x = \mathcal{O}(1)$ is also a rare event for the order parameter m_1^z. Consequently the fraction of rare-events P_1^z is given by the surviving probability in (3.39). Thus the scaling dimension is $x_1^z = 1/2$ and the decay exponent of critical end-to-end correlations is

$$\eta_1^z(XX) = 1.$$

We calculated the order-parameter profile $[m_l^z]_{\rm av}$ numerically for large finite systems up to $L = 256$. As shown in Fig. 6.2 the numerical points of the scaled variable $L[m_l^z]_{\rm av}$ are on one scaling curve $\tilde{m}^z(\tilde{l})$ for different values of L. The scaling curve has two branches for odd and even lattice sites, which cross at $l = L/2$. The upper part of the curves in the large L limit is very well described by the function $\tilde{m}^z(\tilde{l})_{\rm u} = \mathcal{A}\sin(\pi\tilde{l})^{-1/2}$, which corresponds to the conformal result on off-diagonal matrix element profiles [129]:

$$[m_l^\mu]_{\rm av} \sim \left(\frac{\pi}{L}\right)^{x^\mu} \left(\sin\pi\frac{l}{L}\right)^{x_1^\mu - x^\mu}, \tag{6.30}$$

with $x^z = 1$ and $x_1^z = 1/2$. On the other hand the lower part of the curves in Fig. 6.2 is given by $\tilde{m}^z(\tilde{l})_{\rm l} = \mathcal{A}\sin(\pi\tilde{l})$, which corresponds to Eq. (6.30) with $x_2^z = 2$. Thus we obtain that average critical correlations between two spins which are next to the surface are decaying as $[C^z(2, L-1)]_{\rm av} \sim L^{-4}$. Using the sum-rule for the profile in Eq. (6.28) and the conformal predictions one can determine the pre-factor $\mathcal{A}$ from normalization. Then from the equation $\mathcal{A}/2\int_0^1[(\sin\pi x)^{-1/2} + \sin\pi x]dx = 1$, one gets $\mathcal{A} = .86735$, which fits well the numerical data on Fig. 6.2.

These results about the conformal properties of the profile are in agreement with similar studies of the RTIC [57, 58]. Thus it seems to be a general feature that critical order-parameter profiles of random quantum spin chains are described by the results of conformal invariance, although these systems are strongly anisotropic (see Eq. (6.27)) and therefore not conformal invariant.

Next we turn to study the order parameter m_l^z and the longitudinal correlation function in the random XY model. In this model the disorder in the J_l^x and J_l^y couplings is uncorrelated, therefore one can perform averaging in the two subspaces $\mathbf{T}_\sigma$ and $\mathbf{T}_\tau$, or in the two decoupled RTIC-s, independently. Note that the expression for m_l^z in Eq. (6.18) is given as a product of two vector-components, where each vector belongs to different subspaces and have the same average behavior. Since the couplings entering the two separate eigenvalue problems are independent one gets for the disorder average

$$[m_l^z]_{\rm av} = [\Phi_1(l)]_{\rm av} \cdot [\Psi_2(l)]_{\rm av}\,. \tag{6.31}$$

The probability for m_l^z being of order one is the product of the probabilities for $\Phi_1(l)$ and $\Psi_2(l)$ being of order one hence we conclude that the scaling dimension

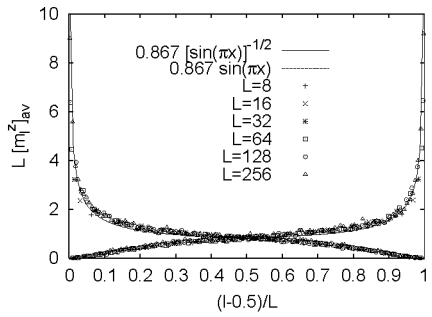

Figure 6.2: Finite-size scaling plot of the longitudinal order-parameter profiles $[m_l^z]_{\rm av}$ for the XX model at criticality for different system sizes calculated numerically with the fermion method using Eq. (6.19). The data are for the uniform distribution, averaged over 50000 samples. The profiles predicted by conformal invariance are indicated by full lines.

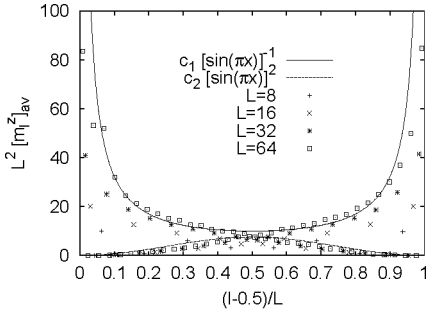

Figure 6.3: Finite size scaling plot of the longitudinal order-parameter profiles $[m_l^z]_{\rm av}$ for the XY model at criticality for different system sizes calculated numerically with the fermion method using Eq. (6.19). The data are for the uniform distribution, averaged over 50000 samples.

for m_l^z in the random XY chain is twice that for the random XX chain. Thus the decay exponents are

$$\eta^z(XY) = 4$$

and

$$\eta_1^z(XY) = 2$$

in the bulk and at the surface, respectively.

The numerical results about the order-parameter profile is shown in Fig. 6.3. The data collapse is satisfactory, although not as good as for the XX model. Similar conclusion holds for the relation with the profile predicted by conformal invariance, which is also presented in Fig. 6.3.

Transverse order parameter We start with the surface order parameter, m_1^x, as given by the simple formula in Eq. (6.16). This formula is identical both for the XY and XX models and its average behavior follows from the adsorbing

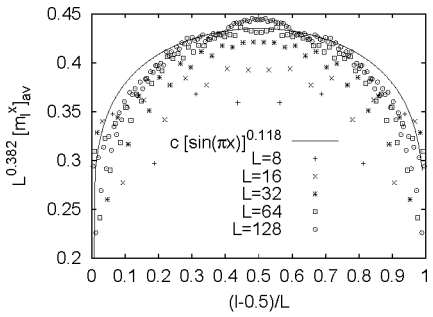

Figure 6.4: Transverse order-parameter profile $[m_l^x]_{\rm av}$ for the XY model at criticality for different system sizes calculated numerically with the fermion method using Eq. (6.17). The data are for the uniform distribution, averaged over 50000 samples.

random walk mapping in Section 6.3.2. Then from Eqs. (6.22) and (3.39) one gets $x_1^x = 1/2$ and

$$\eta_1^x = 1 \, ,$$

both for the random XY and XX models. The value of the decay exponents follows also from the mapping to two RTIC-s. As shown in Eq. (C.8) the correlation function $\langle S_{2l}^x S_{2l+2r}^x \rangle$ is expressed as the product of spin correlations in the two RTIC-s, one with open boundary conditions, but the other is taken with fixed-spin boundary conditions in terms of dual variables. For end-to-end correlations this second factor in the product is unity, since it is the correlation between two fixed spins. Therefore end-to-end correlations in the RTIC and the random XY and XX models are identical.

For bulk correlations one can easily find the answer for the XY model with the mapping in Eq. (C.1). When the two points of reference are located far from the boundary, the chosen boundary condition does not matter. After performing the independent averaging for the two factors of the product one obtains $[\langle S_{2l}^x S_{2l+2r}^x \rangle]_{\rm av} = 1/4[\langle \sigma_l^x \sigma_{l+r}^x \rangle]_{\rm av}^2$, thus we recover Fisher's result:

$$\eta^x(XY) = 2\eta(TIM) = 3 - \sqrt{5} \, . \tag{6.32}$$

The scaling exponent $x^x(XY)$ can identically be obtained from the expression of the order-parameter profile in Eq. (6.17), which is in the form of a product of the two Ising order parameters and for the XY model the two factors are averaged independently.

For the XY model the numerically calculated profile is shown in Fig. 6.4. The scaling plot with the exponents in Table 6.1 is reasonable, although larger systems and even more samples would be needed to reach the expected asymptotic behavior, as predicted by conformal invariance in (6.30).

The arguments leading to the prediction (6.32) for the transverse bulk order parameter exponent do not apply for the XX model and one cannot obtain a simple estimate for the bulk decay exponent from Eqs. (C.8) or (6.17) due to the following reason. The expressions with the parameters of the two quantum Ising chains contain real and dual variables for the two (σ and τ) systems. Since $J_l^x = J_l^y = J_l$ a domain of strong couplings in the σ chain corresponds

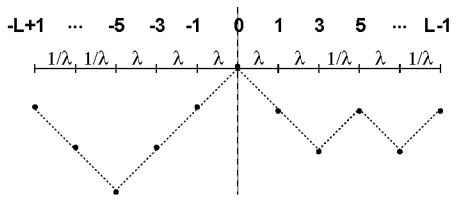

Figure 6.5: Sketch of a bond configuration for a chain of length $2L-1$ that gives a non-vanishing transverse magnetization $m^x \sim \mathcal{O}(1)$ for the central (bulk) spin. The example is for the extreme binary distribution. Weak couplings ($J_{2i-1} = \lambda$) correspond to downward steps of the random walk on both sides of the central spin (here at 0). Note that both, the right and the left half of the random walk have surviving character, i.e. do not cross the starting point.

to a domain of weak couplings in the τ chain and reverse. Therefore the rare events of the TIM can not be simply related to the rare-events of the XX chain.

The value for $\eta^x(XX)$, however, can be obtained by the following argument. For simplicity let us consider the extreme binary distribution in which $J_{2i} = 1$ and $J_{2i-1} = \lambda$ or $1/\lambda$ with probability $1/2$, taking the limit $\lambda \to 0$. Then from Eq.(6.16), one gets a non-vanishing transverse surface magnetization, only if the disorder configuration has a surviving walk character (meaning $\prod_{i=1}^{l} J_{2i-1} < \infty$ for all $l = 1, \ldots, L/2-1$). This implies, also for general distributions of couplings that $m_1^x \sim \mathcal{O}(1)$ only if the surface spin is *weakly* coupled to the rest of the system. It is instructive to note the difference to the surface magnetization in the RTIC, where $m_1^x \sim \mathcal{O}(1)$ when the surface spin is *strongly* coupled to the rest of the system, meaning that $\prod_{i=1}^{l}(1/J_i) < \infty$ for all $l = 1, \ldots, L-1$ for the extreme binary distribution.

The same remains true for a bulk spin, which also has non-vanishing transverse magnetization only if it is weakly coupled to the rest of the system (the trivial example being when both its couplings to the left and to the right are exactly zero, which gives the maximum value $m_1^x = 1/2$). Thus the central spin in a chain of length, say $2L-1$, has $m^x \sim \mathcal{O}(1)$ if and only if the bond-configurations on both sides have surviving character, as it is depicted in Fig. 6.5 for the extreme binary distribution. Since the probability $P_{surv}(L/2)$ for a configuration of $L/2$ couplings to represent a surviving walk is $P_{surv}(L/2) \sim L^{-1/2}$ it is

$$m_l^x \sim \{P_{surv}(L/2)\}^2 \sim L^{-1}, \quad \text{i.e.} \quad x^x(XX) = 1\,. \tag{6.33}$$

From this one obtains

$$\eta^x(XX) = 2. \tag{6.34}$$

We verified the strong correlation between weak coupling and non-vanishing transverse order parameter numerically in the following way: We considered a chain with $L+1$ sites and the couplings at both sides of the central spin were taken randomly from a distribution called SW[1], which represents those samples in the uniform distribution, which has a surface magnetization of $m_1^x(SW) > 1/4$. (Thus cutting one of the couplings to the central spin results in a local

[1] In the binary distribution SW denotes the set of coupling distributions with a *surviving walk* character.

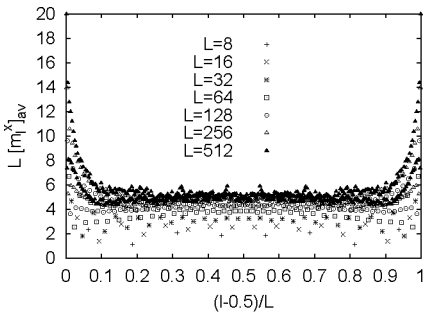

Figure 6.6: Transverse order-parameter profile $[m_l^x]_{\rm av}$ for the XX model at criticality for different system sizes calculated numerically with the fermion method using Eq. (6.17). The data are for the uniform distribution, averaged over 50000 samples.

magnetization greater than 0.25.) Then we calculated numerically the order parameter at the central spin and its average value over the SW configurations $[m^x_{L/2}]_{\rm sw}$ as given in Table 6.2.

As seen in the Table the averaged surface order parameter stays constant for large values of L, whereas the bulk order parameter decreases very slowly, actually slower than any power. The data can be fitted by $[m^x_{L/2}]_{\rm sw} \sim (\ln L)^{-\sigma}$, with $\sigma \approx 0.5$. Thus we conclude that the numerical results confirm the exponents given in (6.34), however there are strong logarithmic corrections, which imply for the average transverse correlations

$$[C^x(r)]_{\rm av} \sim r^{-2}(\ln r)^{-1} \qquad \text{XX model} . \tag{6.35}$$

These strong logarithmic corrections make the numerical calculation of the critical exponents very difficult [45, 118]. In earlier numerical work using smaller finite systems disorder dependent exponents were reported [118]. We believe that these numerical results can be interpreted as effective, size-dependent exponents and the asymptotic critical behavior is indeed described by Eq. (6.35).

Note that our results in Table 6.1 satisfy the relation $\eta^x(XX) = \eta^z(XX)$, both in the volume and at the surface, which corresponds to Fisher's RG result [32]. In this way we have presented an independent justification of Fisher's RS phase picture, where the average correlations are dominated by random singlets, so that the distance between the pairs could be arbitrarily large.

We checked numerically the above theoretical predictions in the random XX

L	$2[m^x_1]_{\rm sw}$	$2[m^x_{L/2}]_{\rm sw}$
16	0.817	0.531
32	0.806	0.471
64	0.799	0.431
128	0.792	0.413
256	0.791	0.383

Table 6.2: Surface and bulk transverse order parameters averaged over 50000 SW configurations for the uniform distribution.

L	$x^x(L)$
16	0.635
32	0.677
64	0.730
128	0.823
256	0.872
512	0.910

Table 6.3: Effective bulk scaling dimension of the transverse order parameter in the random XX chain.

model. In Fig. 6.6 we present the scaled m_l^x profiles for the binary distribution for finite systems up to $L = 512$. These have a broad plateau and the data for different system sizes do not perfectly fall on one single scaling curve due to strong finite-size effects. Even system sizes as large as $L = 512$ appear to be insufficient to get rid of such correction terms. Therefore we have calculated the effective size-dependent $x^x(L)$ exponents by a two-point fit. To do this we have averaged the order parameter in the middle of the profile for $L/4 < l < 3L/4$ and compared this average values for finite systems with $L/2$ and L sites. As seen in Table 6.3 the effective exponents are monotonously increasing with the size of the system and they are not going to saturate, even for $L = 512$[2].

From the data in Table 6.3 one can not make an accurate estimate about the limiting value of $x^x(L)$, but it is clear that $x^x(L)$ grows at least up to the theoretical limit $x^x = 1$, although it could, in principle, reach even a larger value. We note that similar observation was made by Henelius and Girvin [45] from the average S^x correlation function, where the effective η^x exponents seem to grow over the theoretically predicted value of $\eta^x = 2$. (See Fig. 2 of Ref [45].)

Autocorrelations

According to the scaling theory in Section 3.5.3 the decay of average critical autocorrelations in random quantum spin chains is ultra-slow, it takes place in logarithmic time scales, as given in (3.52). Here we compare these predictions with the results of numerical calculations. We start with the surface autocorrelation function $[G_1^x(\tau)]_{\rm av}$ for the XX model, which is calculated in the binary distribution ($\lambda = 4$) on finite systems up to $L = 128$. As seen in Fig. 6.7 (left) the logarithmic time-dependence is well satisfied and the decay exponent is found in agreement with $\eta_1^x(XX) = 1$ as given by the scaling result in Eq. (3.52). For bulk spin critical autocorrelations we considered $[G_{L/2}^z(\tau)]_{\rm av}$ for the XX model. Again the numerical results in Fig. 6.7 (right) are consistent with a logarithmic decay with an exponent $\eta^z(XX) = 2$.

Next we turn to study the *distribution* of critical autocorrelations. As we have seen the average behavior is logarithmically slow, but for typical samples, as described in Appendix D, one expects a faster decay with a power-law time-

[2]It is not feasible to increase the size of the system further, primary not due to computational demand, but due to inaccuracies in the numerical routines, even in 64-bit precision. The origin of this numerical difficulty are those samples with an extremely small excitation energy.

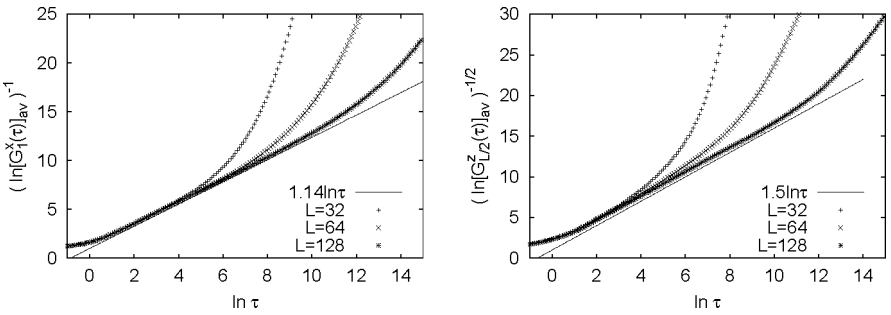

Figure 6.7: Spin autocorrelation function $[G_l^{\mu}(\tau)]_{\rm av}$ for the XX model for $L = 32, 64$ and 128 calculated numerically with the fermion method using Eqs. (3.28) and (6.21). The data are for the binary distribution ($\lambda = 4$), averaged over 50000 samples. a) (Left) shows $l = 1$, the surface transverse autocorrelations, b) (Right) shows $l = L/2$, the bulk longitudinal autocorrelations.

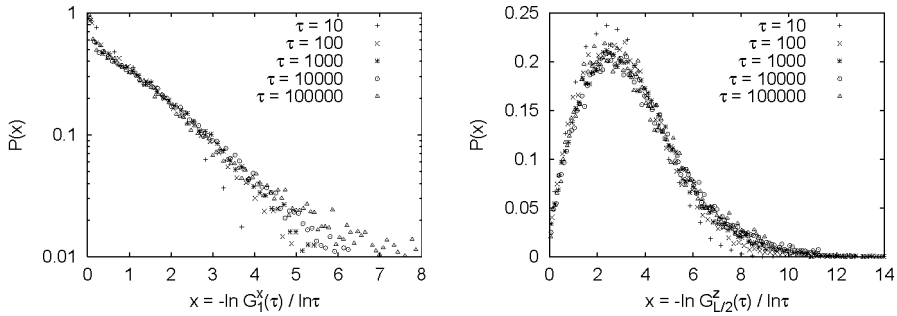

Figure 6.8: Scaling plot of the probability distribution of the autocorrelation function $G_l^{\mu}(\tau)$ for the XX model for different values of τ at criticality ($L = 128$). The data are for the uniform distribution averaged over 100000 samples. a) (Left) shows $l = 1$, the surface transverse autocorrelations, b) (Right) shows $l = L/2$, the bulk longitudinal autocorrelations.

dependence. Then $G_l^\mu(\tau) \sim \tau^{-\gamma}$ and the γ exponent could vary from sample to sample. Such type of "multi-scaling" behavior of the autocorrelations has been recently observed by Kisker and Young [78] in the random quantum Ising model. In Fig. 6.8 we have numerically checked this assumption for the critical autocorrelations $G_1^x(\tau)$ and $G_{L/2}^z(\tau)$, respectively, of the random XX chain, the average behavior of those have been studied before. As seen in Fig. 6.8 we have obtained indeed a good data collapse of the probability distributions $P^\mu(\gamma)$ in terms of the scaling variable $\gamma = -\ln G_l^\mu / \ln \tau$ for both type of autocorrelations, but the scaling curve in the two cases are different.

The average correlation function generally have a contribution from the scaling function $P^\mu(\gamma)$, but there could be also non-scaling contributions, as found for the random quantum Ising chain in Ref. [35]. The scaling contribution is coming from the small γ part of the scaling function, which according to Fig. 6.8 (left) for the autocorrelations $G_1^x(\tau)$ approaches a finite value linearly, $P^x(\gamma) \sim A + B\gamma$. Thus we have for the average autocorrelations:

$$\begin{aligned} [G_1^x(\tau)]_{\rm av} &= \int_0^\infty P^x(\gamma) G_1^x(\tau) d\gamma \\ &\sim \int_0^\infty (A + B\gamma) \exp(-\gamma \ln \tau) d\gamma \\ &\sim A(\ln \tau)^{-1} + B(\ln \tau)^{-2} , \end{aligned} \tag{6.36}$$

in agreement with the scaling result in (3.52) and with the numerical result in Fig. 6.8 (left) We note that the correction to scaling contribution to the average autocorrelations in (6.36) is also logarithmic.

For the critical autocorrelation $G_{L/2}^z(\tau)$ the scaling function in Fig. 6.8 (right) for small γ approaches linearly zero[3] $P^z(\gamma) \sim \gamma$. Thus the scaling contribution to the average autocorrelation, as evaluated along the lines of Eq. (6.36), is $[G_1^x(\tau)]_{\rm av} \sim (\ln \tau)^{-2}$, in agreement with the scaling result in (3.52).

6.3.4 Griffiths phase

Around the critical point both in the XY and XX chains a Griffiths phase can be found (See Fig. 6.9). Thinking of the mapping in (C.1) one observes, that the regions $0 < \delta_a(\delta_d) \leq \delta_G$ and $-\delta_G \leq \delta_a(\delta_d) < 0$ of the phase diagrams of the XY- and XX chain are mapped onto the Griffiths phase of the RTIC. Therefore one expects similar singularities in these regions like in the Griffiths phase of RTIC. The physical picture behind this singular phase in XY and XX chains is clear: similarly to the RTIC, the off-critical system contains rare islands of spins, which are locally in the opposite off-critical phase.

For the Griffiths phase of XY and XX chains all the phenomenological considerations, which were presented in Section 2.5.1 for the RTIC, are invariably valid here with $d = 1$. Thus all the singular quantities are described in this region by the dynamical exponent, which is a smooth function of the control parameter.

Dynamical exponent In the following we calculate the exact value of the dynamical exponent using the same strategy as for the random quantum Ising

[3] For a finite system the scaling function approaches a finite limiting value of $P^z(\gamma = 0, L) \sim L^{-1/2}$, which is checked numerically.

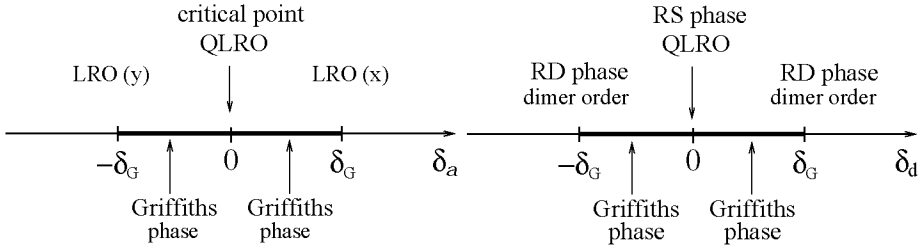

Figure 6.9: a) (Left) Phase diagram of the random XY chain. b) (Right) Phase diagram of the random dimerized XX chain.

model presented in Section 3.4. Our basic observation is the fact that the eigenvalue problem of the $\mathbf{T}_\sigma$ (or $\mathbf{T}_\tau$) matrix can be mapped to a Fokker-Planck operator, which appear in the Master equation of a Sinai diffusion. The transition probabilities of the latter problem are then expressed with the coupling constants of the spin model. The Griffiths phase of the spin model corresponds to the anomalous diffusion region of the Sinai walk and from the exact results on the scaling form of the energy scales in this problem one obtains for the dynamical exponent of the XY model:

$$\left[\left(\frac{J^x}{J^y}\right)^{1/z}\right]_{\rm av} = 1 \ , \tag{6.37}$$

whereas for the XX model the result follows with the correspondences in (6.9). For the binary distribution in (6.7) the Griffiths phase is for $1 < J_0^y < \lambda$ and z is given by

$$(J_0^y)^{1/z} = \cosh\left(\frac{\ln\lambda}{z}\right) \ . \tag{6.38}$$

For the uniform distribution (6.8)

$$z\ln\left(1-z^{-2}\right) = -\ln J_0^y \ , \tag{6.39}$$

and the Griffiths phase extends to $1 < J_0^y < \infty$.

Autocorrelations Next we are going to study numerically the Griffiths phase and to verify some of the scaling results described above. In this respect we shall not consider those quantities which have an equivalent counterpart in the RTIC (distribution of energy gaps, local susceptibility, specific heat, etc), since that model has already been thoroughly investigated numerically. The autocorrelation functions, however, are different in the two models and we are going to study those in the following.

The average bulk longitudinal autocorrelation function $[G^z_{L/2}(\tau)]_{\rm av}$ of the XX model is shown in Fig. 6.10 in a log-log plot at different points of the Griffiths phase. The asymptotic behavior in (3.55) is well satisfied and the dynamical exponents obtained from the slope of the curves are in good agreement with the analytical results in (6.37). Similar conclusion can be drawn from the average surface transverse autocorrelations, $[G^x_1(\tau)]_{\rm av}$, as shown in Fig. 6.10.

Next we study the distribution of the autocorrelation functions. In Fig. 6.11 the distribution of the bulk longitudinal autocorrelation function of the

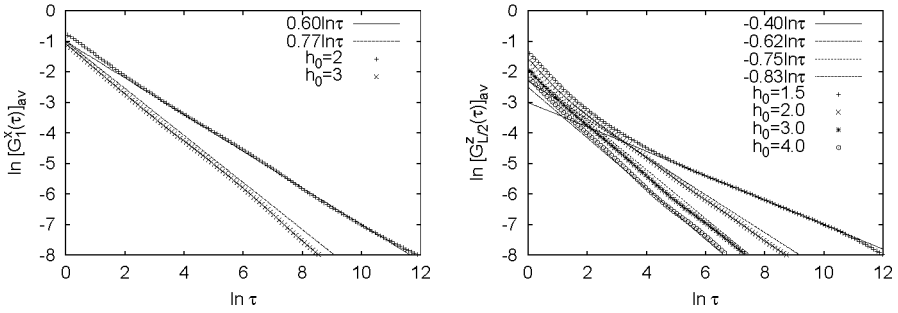

Figure 6.10: The average surface (left) and bulk (right) autocorrelation function $[G^{\mu}_{L/2;1}(\tau)]_{\rm av}$ of the XX model in the Griffiths phase for various values of h_0. The straight lines have a slope of $1/z(h_0)$, where the dynamical exponent $z(h_0)$ agrees well with the exact value determined via the formula (6.37). The data are for the uniform distribution averaged over 50000 samples of size $L = 128$.

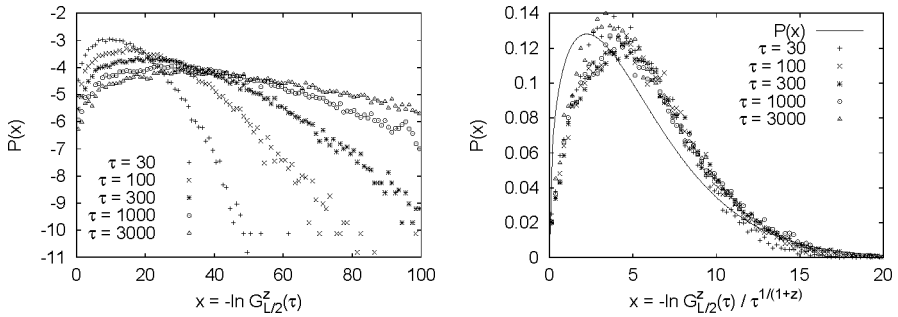

Figure 6.11: (Left): Probability distribution of the bulk longitudinal autocorrelation function of the XX model in the Griffiths phase for $h_0 = 1.5$. The data are for the uniform distribution from 100000 samples of size $L = 128$. (Right): Scaling plot of the data in the left figure. The scaling variable $[\ln G^z(\tau)]/\tau^{1/(z+1)}$ contains the dynamical exponent $z(h_0)$ known from the formula (6.37). The full curve is the theoretical prediction in (6.42) using the exact value of $z(h_0 = 1.5) = 2.659$ and a fit-parameter $c = 0.22$.

XX model is given at different times τ. As argued in Appendix D, the typical autocorrelations are of a stretched exponential form

$$G^{\mu}(\tau) \sim \exp\left[-(\tau\epsilon_0 z)^{1/(z+1)}\left(1+\frac{1}{z}\right)\right], \quad \delta \neq 0\ , \tag{6.40}$$

thus the relevant scaling variable is

$$\alpha = -\frac{\ln G^{\mu}(\tau)}{\tau^{1/(z+1)}}\ . \tag{6.41}$$

Using this scaling argument we obtained a good data collapse of the points of the distribution function as shown in Fig. 6.11 (right). We note that for the random quantum Ising model Young [138] has also derived the scaling function from phenomenological arguments,

$$P(x) = c(cx)^{1/z}\ \exp\left(-\frac{z}{1+z}(cx)^{1+1/z}\right) \tag{6.42}$$

which is also presented in Fig. 6.11. One can see considerable differences between the numerical and theoretical curves. Similar tendencies have been noticed for the RTIC in Ref. [138]. The discrepancies are probably due to strong corrections to scaling or finite-size effects. These corrections, however do not affect the scaling form in (6.41).

6.4 Summary

We have performed a detailed study of the scaling behavior of rare events appearing in the random XY and XX chains. We identified them as strongly coupled domains, where the coupling distribution has some surviving random walk character. From the scaling properties of the rare events we have identified the complete set of critical decay exponents and found exact results on the correlation length exponent and the scaling anisotropy.

Another new aspect of our work was the study of dynamical correlations. We have obtained the asymptotic behavior of the average autocorrelation function and determined the scaling form of the distribution of autocorrelations.

In the off-critical regime we investigated the singular physical quantities in the Griffiths phase. In particular we have obtained exact expression for the dynamical exponent z, which is a continuous function of the quantum control parameter and the singularities of all physical quantities can be related to its value.

Chapter 7

The Random-bond Potts model in the large-q limit

7.1 Introduction

So far we have dealt with quantum models, but in this chapter we turn our attention to a classical model, the two-dimensional q-state random-bond Potts model (RBPM) defined in (2.28). Much work has been devoted to this model, the transition point of which is known from self-duality also in its disordered version [76]. In the pure model an exact result by Baxter [4] ensures a first-order transition for $q > 4$. Although early Monte Carlo (MC) simulations [23, 27] left space for an interpretation [71] of a q-independent super-universal behavior in random systems, later extensive MC [105, 18, 19, 20, 101] and transfer matrix[12, 66] calculations consistently determined q-dependent magnetic exponents, whereas the correlation length exponent ν was found to be close to the pure Ising value $\nu_I = 1$ for all q.

In the large-q limit thermal fluctuations are reduced and as a consequence the pure model is soluble in any dimension and a perturbation expansion in powers of $1/q^{1/d}$ can be performed. In the same limit for the random model at the phase transition point an effective interface Hamiltonian has been constructed and mapped onto the interface Hamiltonian of the random-field Ising model [12, 66]. This mapping has then been used to relate the phase diagram of the two problems and to deduce the tricritical exponents of the RBPM at $d > 2$ dimensions. However, in the large-q limit no *direct* calculation to study the critical behavior has yet been performed. In two dimensions the presently known information is obtained via extrapolation of the results calculated at finite values for q. From these estimates no special type of critical behavior is expected in the large-q limit. For example the magnetization scaling dimension x_m seems to saturate at a finite, non-trivial limiting value [99, 67] $\lim_{q\to\infty} x_m(q) \approx 0.17 - 0.19$. However, at this point one should note on the presence of strong (logarithmic) corrections in the form of $1/\ln q$ (see Fig. 5 in Ref. [99]).

In this chapter we are going to present a direct investigation of the critical behaviour of the random-bond Potts model in the large-q limit. As will be shown, in this limit the thermal fluctuations are negligible and the calculation of the average thermodynamical and correlation properties of the model is ef-

fectively reduced to an optimization problem. Here the competition between ordering effects, originating from a tendency to clustering, and disordering effects, due to energy gain from quenched disorder, play an important role in determining the optimal structure. In two dimensions we perform a numerical study based on simulated annealing and a combinatorial algorithm, and also conformal aspects of the problem are investigated.

7.2 Cluster representation in the large-q limit

We consider the q-state Potts model on a d-dimensional hyper-cubic lattice with periodic boundary conditions given by the reduced Hamiltonian:

$$\frac{H}{kT} = -\sum_{\langle ij \rangle} K_{ij}\delta(\sigma_i, \sigma_j) \ , \tag{7.1}$$

where $K_{ij} > 0$ are reduced ferromagnetic couplings. The d-dimensional hyper-cubic lattice corresponds to a graph $\overline{G} = (V, E)$, where V is the set of vertices, which is identical to the lattice sites, and E is the set of edges, which is identical to the bonds between neighbouring sites on the lattice. As shown in Appendix E, in the *random cluster representation* [73] the partition sum of the model Z is expressed as a sum over all subsets $U \subseteq E$ of the set of edges (or bonds) as:

$$Z = \sum_{U \subseteq E} q^{n(U)} \prod_{(ij) \in U} v_{ij} \ , \tag{7.2}$$

where $n(U)$ denotes the number of connected clusters in the subgraph $G = (V, U)$ of $\overline{G}$, consisting of all lattice sites but the reduced set of bonds in U, and $v_{ij} = e^{K_{ij}} - 1$ is the Mayer function for the coupling K_{ij}. For the latter we use the parameterization:

$$v_{ij} = q^{1/d + w_{ij}} \ . \tag{7.3}$$

Then the contributions from the different graphs to Z are expressed in powers of q:

$$Z = \sum_{U \subseteq E} q^{F(U)} \tag{7.4}$$

with

$$F(U) = n(U) + \sum_{(ij) \in U} (\frac{1}{d} + w_{ij}) \ . \tag{7.5}$$

In the following we consider the large q-limit ($q \to \infty$), where the partition sum is dominated by the leading term given by the maximum value for F:

$$F_0 = \max_{U \subseteq E}\{F(U)\} \ , \tag{7.6}$$

where $-F_0$ corresponds to the free energy of the system, up to a prefactor of $1/(kT \ln q) = const.$ Let us denote with U_0 the subset of E that gives the optimum in (7.6), i.e. $F_0 = F(U_0)$, and with $G_0 = (V, U_0)$ the corresponding *dominant graph*. Then the energetic contribution to $-F_0$ is due to the couplings in the dominant graph, whereas the entropic term is related to the number of connected parts. In what follows, we use the word graph when we mean the subgraph $G = (V, U)$ of $\overline{G}$ defined by an edge subset U.

In the pure system, with $w_{ij} = w$, the structure of the dominant graphs in the different thermodynamic phases are trivial. Consider a lattice with $N = L^d$ spins with fully periodic boundary conditions, the number of bonds is dN. Then, in the low-temperature phase with $w > w_c$ the *fully connected graph* (V, E) is the dominant graph, thus $F_0 = F_c = [dN(1/d + w) + 1]$. On the other hand in the high-temperature phase, $w < w_c$, the dominant contribution is due to the *empty graph* $(V, \emptyset)$, with a value of $F_e = N$. At $w_c = -1/dN$, when $F_c = F_e$, there is phase coexistence, which means a sharp phase transition even in a finite system in the limit of $q \to \infty$. In the thermodynamic limit we have $w_c = 0$, and the latent heat per site is given by $\Delta L/N = 1$ in our units.

Introducing disorder, such that w_{ij} can take randomly positive and negative values, the question arises, whether this trivial structure of the dominant graph persists at the transition point, i.e.: Is there still a coexistence between two parts of the graph, one being fully connected, whereas the other is empty? To study this problem Cardy and Jacobsen [12, 66] have constructed the interface Hamiltonian, which is then mapped onto that of the random-field Ising model. This has lead to the answer that for $d > 2$ the effect of small disorder is irrelevant, thus there is still phase coexistence and thus the transition is of first order, whereas in $d = 2$ the phase coexistence is destroyed by any amount of disorder, in accordance with Aizenman and Wehr exact results [2].

In the following we are going to consider the problem in two dimension, where the dominant graph has a non-trivial structure. In particular we study the (fractal) properties of the largest connected cluster of G_0, denoted by Γ. In the low-temperature phase, $T < T_c$, Γ is compact, thus the average number of points in Γ is given by $[n_\Gamma]_{\rm av} \propto N = L^2$, where L is the linear size of the square lattice. In the high-temperature phase, for $T > T_c$, $[n_\Gamma]_{\rm av}$ stays finite and defines the average correlation length, ξ, through $[n_\Gamma]_{\rm av} \sim \xi^2$. At the transition point the average mass is expected to scale as

$$[n_\Gamma]_{\rm av} \sim L^{d_f} \ , \tag{7.7}$$

with a fractal dimension $d_f < 2$[1].

The properties of $[n_\Gamma]_{\rm av}$ are directly related to the asymptotic behavior of the average spin-spin correlation function, defined in the large-q limit as

$$[C(r)]_{\rm av} = [\langle \delta(\sigma_i, \sigma_j) \rangle]_{\rm av} \ , \tag{7.8}$$

where $\langle \ldots \rangle$ denotes the thermal and spatial average over all pairs of sites i and j with a distance r. We use the fact that correlations between two spins are generally zero, unless they belong to the same cluster, when $C(r) = 1$. In the case of $T \leq T_c$, when Γ is a spanning cluster the probability $Pr(L)$ that a spin belongs to Γ is given by $Pr(L) = [n_\Gamma]_{\rm av}/N$, whereas the same probability for two spins is $Pr(L)^2$. From this follows, that the average correlations between two spins separated by a large distance of $r = L$ is given by: $[C(r)]_{\rm av} \simeq Pr(L)^2 = ([n_\Gamma]_{\rm av}/N)^2$. In the low-temperature phase, $T < T_c$, where the average magnetization, $[m]_{\rm av}$, is defined as $[m]^2_{\rm av} = \lim_{r\to\infty}[C(r)]_{\rm av}$, we obtain:

$$[m]_{\rm av} = \lim_{L\to\infty} \frac{[n_\Gamma]_{\rm av}}{L^2}, \quad T < T_c \ , \tag{7.9}$$

[1] At the critical point the dominant graph is generally not unique, cf. with the bimodal distribution in Eq.(7.12) any two clusters having just one strong and one weak bond between them could be either connected or disconnected. We assume that the degenerate optimal graphs have the same asymptotic fractal properties.

whereas at the critical point the average spin-spin correlations decay as a power:

$$[C(r)]_{\rm av} \sim r^{-2x_m}, \quad x_m = 2 - d_f, \quad T = T_c \; . \tag{7.10}$$

Finally, in the high-temperature phase, where the average size of Γ is finite the probability to have a connected cluster of size r is exponentially small, which leads to an average correlation function of the form $[C(r)]_{\rm av} \sim \exp(-r/\xi)$, for $r \gg \xi$.

7.3 Methods

Next we specify the form of the disorder, where we make use of the simplification that arises due to self-duality that holds under special conditions. According to the results by Kinzel and Domany [76] the random model is at the critical point, if the distribution $P(w)$ of w_{ij} is an even function of w, i.e.

$$P(w) = P(-w). \tag{7.11}$$

For details see Appendix E. For convenience we use the bimodal distribution

$$P(w) = p\delta(w - \omega) + (1 - p)\delta(w + \omega) \; , \tag{7.12}$$

where the critical point is at $p = p_c = 1/2$, whereas the reduced temperature $t = (T - T_c)/T_c$ can be expressed as:

$$t = -\omega(p - 1/2), \quad |t| \ll 1 \; . \tag{7.13}$$

Generally we restrict ourselves to the range of disorder parameterized as $0 < \omega < 1/2$. We note that for $\omega = 0$ one recovers the pure model, whereas for $\omega > 1/2$ we are in the usual percolation limit. Indeed, for the latter range of parameters the dominant graph contains all the strong bonds, whereas the weak bonds are all absent.

According to the results presented in the previous Section the solution of the RBPM in the large-q limit is equivalent to an optimization problem with a non-local cost-function given by Eq.(7.5). To find the dominant graph of the problem we used standard, approximative procedures. Most of the results were obtained by the method of simulated annealing, but some calculations were performed by an approximative combinatorial optimization algorithm.

In the procedure of *simulated annealing* a hypothetical temperature variable T_h is introduced and, after thermalization, is lowered until the hopefully global minimum of the cost-function is reached. In practical applications we lowered the temperature as $T_h = 1/(\tau - 0.5)$, in finite time-steps $\tau = 1, 2, \ldots 60$, and checked that the resulting configuration does not change after further cooling. At a fixed temperature in the thermalization MC steps we generally used local rules by creating or removing bonds, but sometimes we also considered to move a full line of bonds. In order to arrive to the global minimum several different starting configurations are considered (at least three), and the best final configuration was taken. In the investigations generally $L \times L$ finite samples with linear size up to $L = 24$ were considered and periodic boundary conditions were used in both directions. For smaller sizes the averaging was usually performed over 10000 samples, whereas for larger sizes we used several thousands of realizations.

Alternatively, for $\omega < 1/4$ we used a combinatorial optimization algorithm that yields a configuration that is close to the optimum but not necessarily equal to it. Actually the worst case bound for the ratio of the value F_0 of the optimal solution U_0 to the value $F(U^*)$ of configuration U^* that is found by the algorithm is only $2/3$, which would be too bad for our purposes. However, in typical cases the configurations produced by the algorithm are much closer, as we checked by comparison with the configurations generated by the simulated annealing method. The algorithm works as follows [41]:

For all sites i let i_{x-}, i_{x+}, i_{y-} and i_{y+} be its left, right, lower and upper neighbour, respectively, and denote with (ii_{x-}), (ii_{x+}), (ii_{y-}) and (ii_{y+}) the bonds (edges) between these neighbouring sites and i. These constitute a minimal set of edges that, when removed from $\overline{G}$, cut the site i from the rest of the graph. Let us denote them by

$$E_i := \{(ii_{x-}), (ii_{x+}), (ii_{y-}), (ii_{y+})\} \tag{7.14}$$

and their weight

$$w(E_i) = \sum_{(ij)\in E_i} (\frac{1}{2} + w_{ij}) \; . \tag{7.15}$$

The *minimum cut* between any two pairs of sites, i and j, is defined as the set of edges that has a minimum total weight *and* whose removal from $\overline{G}$ cuts the graph into two disjoint subgraphs, one containing i and one containing j [1, 44, 3]. In our case it is then given either by E_i or E_j, as long as $|w_{ij}| < 1/4$, as one can easily convince oneselves.

The idea of the algorithm is as follows: Obviously the removal of the edges contained in a minimum cut, like in E_i for all i, increases the number of components in the graph by one, i.e. one wins one unit in the cost function $F(U)$ (7.5). On the other hand one looses $w(E_i)$ units and when increasing the number of components of the graph G, one should keep this weight loss as small as possible. Therefore we consider a collection of minimum cuts as possible candidates of edge sets to be removed from $\overline{G}$. Let the edge sets be ordered nondecreasing weight, such that $w(E_1) \leq w(E_2) \leq \ldots \leq w(E_{L^2})$ and define for all $r = 0, 1, 2, \ldots, L^2$ the edge subsets

$$U^r = E \backslash \bigcup_{i=1}^{r} E_i \; , \tag{7.16}$$

i.e. $U^0 = E$, and with increasing r successively edge sets of non-decreasing weight are substracted from E. When doing this, initially (i.e. for small r) most of the time a site will be isolated that before has been connected to a larger cluster and therefore frequently (depending on the weight of the substraced edges) $F(U)$ will increase, as desired. These are the trial configurations for our optimization problem and we take the best solution among them, i.e. U^* such that $F(U^*) = \max\{F(U^r) | r = 0, 1, \ldots, L^2\}$. It can be shown [41] that $F(U^*)/F_0) \geq 2/3$, also for $\omega > 1/4$, however, in this case the minimum cuts are not as simple as in (7.14).

With the combinatorial optimization method we could treat larger finite systems (up to 128×128), than by simulated annealing and the number of configurations we used were between 10000 and 1000 for smaller and larger systems, respectively.

For the purpose of cluster analysis we implemented the standard Hoshen-Kopelman labeling algorithm [49] in both methods.

7.4 Results at the critical point

First, we tested the relative accuracy of the two methods by comparing the value of the obtained cost-functions, F_0, for different finite sizes. As a general tendency simulated annealing has given higher, thus better estimates, but the relative difference for $L \leq 16$ was very small, less then 0.4%. For the largest system we studied by simulated annealing, $L = 24$, the relative difference has increased to about 0.6%. We shall later analyze consequences of the inaccuracy of the min-cut method in the magnetic properties of the RBPM. In the following we present results which are obtained by the more accurate simulated annealing method.

Microscopic length scale Typical optimal configurations for different values of ω calculated with the same disorder realization for $w_{ij}(= \pm\omega)$ are presented in Fig. 7.1. The position of the strong bonds ($w_{ij} = +\omega$) can be obtained

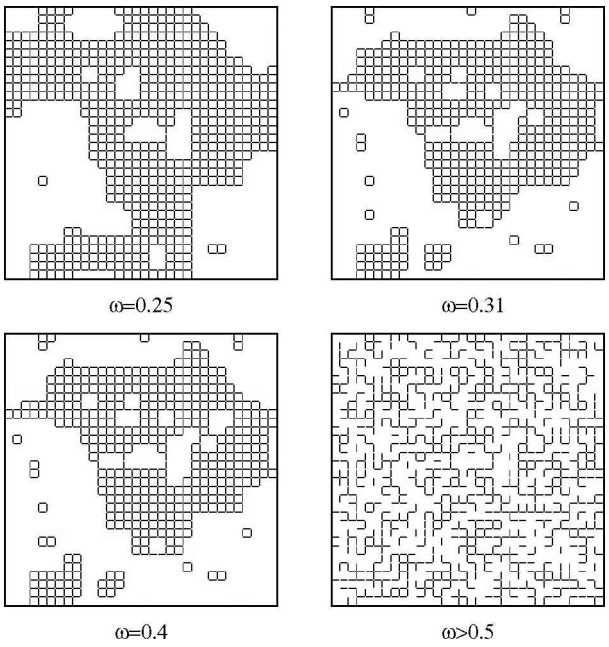

Figure 7.1: Typical optimal configurations for different values of ω calculated with the same disorder realization for $w_{ij}(= \pm\omega)$.

from the optimal configuration for $\omega > 1/2$, since in percolation only these bonds are occupied. As seen in the figure, for smaller disorder parameter the optimal graph looks to be more compact, whereas for stronger ω the optimal configurations are very close to each other. This fact is a consequence of the presence of a finite length-scale in the problem. For small ω the system behaves

uniformly up to a length-scale l_c which is given by estimating the size l of a step, which is located at the top of a straight surface of a connected cluster, see Fig. 7.2. Using the bimodal distribution in (7.12) the existence of the step is

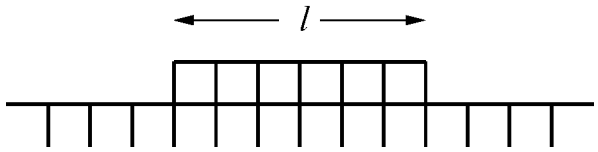

Figure 7.2: A connected cluster with a step of l-points on the top of a straight surface.

connected to the condition:

$$\sum_{i=1}^{2l-1} \left(\frac{1}{2} + w_i \right) > l \, , \tag{7.17}$$

where $w_i = \pm\omega$ with the same probability, or equivalently:

$$\sum_{i=1}^{2l-1} p_i > \frac{1}{2\omega} \, , \tag{7.18}$$

with $p_i = \pm 1$. For large l the probability distribution of the sum in the l.h.s. of Eq.(7.18) is Gaussian, with a variance of $\sqrt{2l-1}$. Consequently the average size of the step l_c scales with a small ω as

$$l_c \sim \left(\frac{1}{2\omega} \right)^2 \, . \tag{7.19}$$

To observe the true asymptotic behavior in the RBPM, the system size should be larger than this value, $L > l_c(\omega)$, therefore we restricted ourselves to not too small ω values.

Cluster size distribution Next we analyze the distribution of the largest connected cluster, Γ. Inspecting the structure of a typical optimal graph in Fig. 7.1 we arrive to the conclusion that Γ is a fractal, so that we take the scaling combination n_Γ / L^{d_f}, which corresponds to the form in Eq.(7.7). In Fig. 7.3 we present a scaling plot of the reduced cluster size distribution, where a data collapse can be obtained with a fractal dimension $d_f \approx 1.8$.

We note that the points, corresponding to the smallest system, deviate more from the hypothetical scaling curve, which can be attributed to the effect of the finite length scale l_c. In the inset of Fig. 7.3 a similar scaling plot is presented in the percolation region, i.e. for $\omega > 1/2$, where the fractal dimension of percolation [123], $d_p = 91/48$ is used. The scaling curves for $\omega < 1/2$ and $\omega > 1/2$ look different: for the RBPM the distribution is broad and there is a considerable weight for small clusters, whereas for percolation the distribution is single peaked without a relevant small cluster contribution.

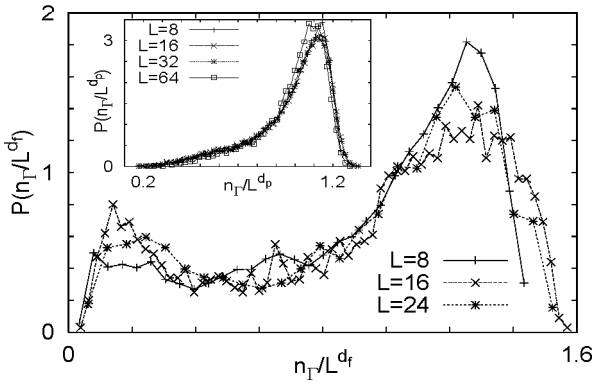

Figure 7.3: Scaling plot of the size distribution of the largest cluster at the critical point of the RBPM at $\omega = 0.4$ for different finite systems. A data collapse is obtained with a fractal dimension $d_f \approx 1.8$. In the inset the same quantity is plotted for percolation, when $\omega > 1/2$ and $d_p = 91/48$.

Magnetization exponent Next we calculated the average density of the largest connected cluster $[n_\Gamma]_{\rm av}/L^2$, from the size dependence of which the fractal dimension d_f in (7.7) and the magnetization exponent x_m in (7.10) follows. In Fig. 7.4 we have plotted $[n_\Gamma]_{\rm av}/L^2$ for different finite sizes in a log-log scale, using different values of the disorder parameter, ω. In this figure, besides the results obtained by simulated annealing, also points calculated by the approximate (min-cut) optimization algorithm are presented. As seen the min-cut algorithm works satisfactory for small systems, $L \leq 16$, when the difference in the cost-functions calculated by the two methods is also very small. For larger sizes, however, which are beyond the possibilities of simulated annealing, the error of the optimization algorithm increases. Based on the results presented in Fig. 7.4 the min-cut method tends to generate a *compact cluster* in the large system limit. Therefore we used the min-cut method only for limited sizes, which are anyhow manageable by the simulated annealing method, although with much longer computational time.

Returning to the average density in Fig. 7.4 one can observe that for the disorder parameter in the RBPM range, i.e. $0 < \omega < 1/2$, the points fall on nearly parallel straight lines having a slope of $-2 + d_f \simeq -0.2$, where $d_f \simeq 1.8$ corresponds to the value we used in the scaling plot of the reduced cluster-size distribution in Fig.7.3. The slope of the same line calculated in the percolation regime, with $\omega > 0.5$ is significantly different, it is $-2 + d_p \simeq -0.1$, where d_p is close to the fractal dimension of two-dimensional percolation.

The estimates of the magnetization scaling dimension x_m at different disorder parameter ω are summarized in Table 7.1.

As seen in Table 7.1 the magnetization exponent x_m is approximately independent of the disorder parameter for $0 < \omega < 1/2$, and its value is within the range of $x_m \approx 0.17 - 0.19$. This is in agreement with the estimates obtained by extrapolating the results calculated at finite q-s [99, 67], thus the two limits seem to be interchangeable. The apparent variation of x_m with ω can be attributed to cross-over effects: at $\omega = 0$ the pure system transition, whereas at

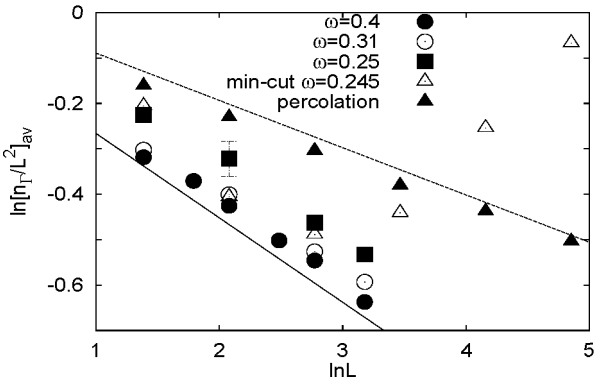

Figure 7.4: Size dependence of the average density of the largest connected cluster at different values of the disorder parameter, ω, calculated by simulated annealing and by the approximative optimization (min-cut) algorithm. Note that the min-cut method has a systematic error for larger systems. The slope of the curves, sl, for different $0 < \omega < 0.5$ is approximately identical and indicated by a straight line with $sl = -0.2$, but this slope differs from that of percolation, which corresponds to $\omega > 0.5$, and the related straight line has $sl = -5/48$. Typical error of the simulated annealing method is indicated by the error bar, whereas the error for percolation is smaller than the size of the symbol.

ω	x_m
0.2	0.185(30)
0.25	0.188(16)
0.31	0.165(15)
0.4	0.178(13)
> 0.5	0.103(2)

Table 7.1: Scaling exponent, x_m, of the average magnetization for different disorder parameter ω. The last row with $\omega > 0.5$ corresponds to normal percolation where the exact value is $x_m^p = 5/48 = 0.104$.

$\omega = 1/2$ the percolation fixed point is going to perturb the value of effective, finite-size dependent exponents.

The magnetization exponent x_m has been calculated by another method, which is based on conformal invariance. Here we use the result mentioned in Section 2.1.3, that in a long strip of width L_w and with periodic boundary conditions the average correlation function along the strip decay exponentially:

$$[\langle \sigma_i \sigma_{i+u} \rangle]_{\text{av}} \sim \exp(-u/\xi_{L_w}) \,, \tag{7.20}$$

where the correlation length ξ_{L_w} for large widths asymptotically behaves as:

$$\xi_{L_w} = \frac{L_w}{2\pi x_m} \,. \tag{7.21}$$

In practical calculations we used strips of widths, $L_w = 2, 3, 4$ and 5, and with such a lengths, that in the calculated correlation function the exponential decay

ω	x_m			
	$L_w = 2$	$L_w = 3$	$L_w = 4$	$L_w = 5$
0.400	0.263(9)	0.166(4)	0.165(5)	0.163(6)
0.423	0.267(1)	0.168(5)	0.167(2)	0.163(6)
0.452	0.266(1)	0.170(4)	0.169(2)	0.163(6)

Table 7.2: Numerical estimates for the average magnetization exponent, x_m, using the correlation length-exponent relation in Eq.(7.21) for different widths, L_w.

in (7.20) seemed not to change by further increase of the length. Generally we went at least up to a length of 64 sites, which has then limited the available widths L_w. The calculated exponents for some values of the disorder parameter are given in Table 7.2.

As we see the size dependence of x_m is very weak for $L_w \geq 3$ and the extrapolated value of $x_m \simeq 0.17$ is practically independent of the form of the disorder. This estimate is compatible with the previous one obtained by finite-size scaling. The fact, that this latter result lies close to the lower bound of the finite-size scaling one is probably due to the confluent singularity of the percolation fixed point, which is quite strong in the region of ω-s we used in the calculation on strips.

Central charge We have also calculated the central charge of the conformal anomaly c [11, 46] from the finite-size correction to the free energy per width:

$$f_0(L_w) = f_0(\infty) - \frac{\pi c}{6L_w^2} + \mathcal{O}(L_w^{-3}) \,, \tag{7.22}$$

with the result:

$$c = 0.74(1) = \frac{0.51(1)}{\ln 2} \,. \tag{7.23}$$

This is compatible with previous estimate [67] $c \simeq 0.5/\ln 2$, which is obtained by finite-q extrapolation.

7.5 Results outside the critical point

Finally we investigated the average magnetization, $[m(L,t)]_{\rm av}$, in the vicinity of the critical point. In the scaling region, defined as $L|t|^\nu = \mathcal{O}(1)$, where ν is the critical exponent of average correlations, the average magnetization is expected to behave as:

$$[m(L,t)]_{\rm av} = L^{-x_m} \tilde{m}(L|t|^\nu) \,, \tag{7.24}$$

where $\tilde{m}(y)$ is some scaling function. The calculated magnetizations at different finite size and temperature then should collapse to the same scaling function, provided the correct critical exponents x_m and ν are used. In Fig. 7.5 we show the result of such a scaling plot, where we used $\nu = 1$, as found approximately in finite-q calculations, whereas for x_m we used our previous estimate obtained through finite-size scaling at the critical point. The data collapse in Fig. 7.5 is satisfactory, however to obtain a precise estimate on ν one needs to extend the calculations for larger systems.

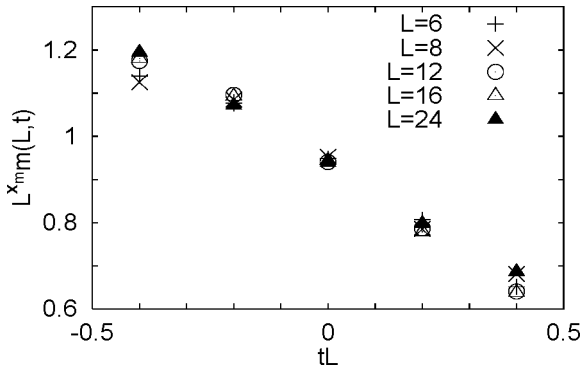

Figure 7.5: Scaling plot of the finite-size average magnetization in the vicinity of the critical point, for a disorder parameter $\omega = 0.4$. The scaling exponents we used here are $x_m = 0.177$ and $\nu = 1$.

7.6 Phase diagram

Working with the bimodal distribution in (7.12) our results are compatible with the RG-phase diagram drawn in Fig. 7.6.

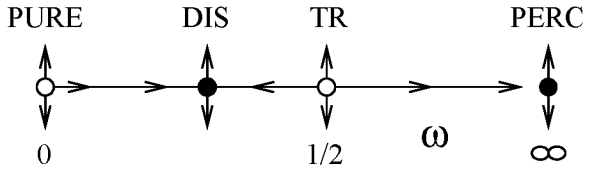

Figure 7.6: Schematic RG phase diagram of the two-dimensional RBPM with varying strength of bimodal disorder ω. For details see the text.

The pure systems fixed point ($PURE$), located at $\omega = 0$, is unstable against any weak disorder, thus the critical behavior in the range of $0 < \omega < 0.5$ is controlled by the disordered fixed point (DIS). Our numerical calculation indeed indicate a universality with respect of the strength of disorder. Increasing the disorder over $\omega = 0.5$ we reach the region of attraction of the normal percolation, and the corresponding fixed point ($PERC$) is located at $\omega = \infty$. Our RG phase diagram is completed by introducing a repulsive tricritical fixed point, TR, at $\omega = 0.5$, which separates the regions of attraction of the two non-trivial fixed points, DIS and $PERC$. The singular properties of the TR can be quite unusual, since the corresponding optimal graph is highly degenerate: the possible configurations include all which interpolate between that of the RBPM and that of normal percolation.

The behavior of the system at the fixed point DIS, which is the subject of the present study, is strongly dominated by disorder effects, whereas thermal fluctuations seem to be negligible. Similar, disorder dominated critical behavior occur in random quantum spin chains, the critical behaviour is controlled by an IRFP.

7.7 Summary

In this chapter the critical behavior of the Potts model with non-frustrated, random bimodal couplings was investigated in the large q-limit. We have shown how the calculation of the free energy and the correlation functions of the RBPM can be mapped onto an optimization problem, which was then numerically studied by simulated annealing and by an approximate combinatorial optimization algorithm. From the finite-size scaling of the average size of the dominant graph, we estimated the magnetization and correlation length exponent for different values of the disorder parameter, the former one also by measuring correlations in strip geometry. Moreover we calculated the central charge from the finite-size scaling of free energy. Our results are more precise than previous extrapolative estimates and are compatible with them. On the basis of the above results we presented the phase diagram of the model, where certain features the disordered fixed point controlling the $0 < \omega < 1/2$ region are reminiscent of an IRFP.

Chapter 8

Summary

In the present thesis we discussed random systems, where strong disorder leads to the possibility of obtaining exact or presumably exact results on the critical- and Griffiths-McCoy singularities, or at least considerably simplifies the treatment of the problem.

A large portion of our new results concerns the Griffiths phase of the RTIC and the closely related XX- and XY model. In these models, the critical behaviour of which is controlled by an infinite-randomness fixed point, the average quantities are dominated by the contribution of a vanishing fraction of rare samples, while other samples are irrelevant. A phenomenological scaling theory based on the properties of rare events was applied in order to determine the singular behaviour of higher gaps, non-linear susceptibility and autocorrelations in the Griffiths phase of the RTIC and the random XY- and XX chain. In addition to this extensive numerical analysis based on the free-fermion technique was performed. The results are consistent and show, that all singularities in the Griffiths phase are explained by the properties of rare strongly coupled domains, and this common origin manifests itself in the sufficiency of a single exponent for the complete description of Griffith-McCoy singularities.

On the other hand infinitely strong randomness is known to ensure the asymptotic exactness of the Ma-Dasgupta-Hu renormalization group treatment. We showed that the method is asymptotically exact also in the Griffiths phase due to the logarithmically broad distribution of couplings. We found that the dynamical exponent of the model, containing the information on the Griffiths-McCoy singularities, is invariant during the procedure, which makes possible to give an exact expression for calculating the dynamical exponent. The exact determination of dynamical exponents of the RQPM which is governed by similar RG equations like the RTIC, is still an open question.

Some of our results such as the invariance of dynamical exponent are supposed to be generally valid among disordered quantum spin chains, whereas others, e.g. the exponent relations for higher gaps, should be valid also in higher dimensions. Another field where the present results could be applied is the anomalous diffusion region of Sinai walk, which is closely related to the Griffiths phase of quantum chains.

The rare strongly coupled domains determine not only the properties of Griffiths phase but the average critical properties, as well. Using exact expressions for the surface order parameter of the XY- and XX chain, obtained by the free-

fermion technique, we identified the rare events with coupling sequences having a surviving walk character. Close to criticality, using the properties of random walk we determined the complete set of critical decay exponents of the above models. The numerically calculated off-diagonal operator profiles together with the results of conformal invariance give critical exponents, which are compatible with those obtained by the random-walk arguments. This fact is accordance with other experiences that in strongly anisotropic and therefore not conformal invariant disordered spin chains some results of conformal theory still hold.

In the other issue we discussed, the random-bond Potts model in the large-q limit, the special parameterization and the $q \to \infty$ limit converts the problem of calculating the thermodynamical and correlation properties into an optimization problem. The finding that a single graph describes the properties of the system is parallel to the important role of rare samples in the previous problem.

So we have dealt in this thesis with singular properties of strongly disordered models at criticality and in the Griffiths phase. Among our findings obtained in special models, there are a number of results which are supposed to reflect more general properties of random systems. Thus the information extracted from the above special models hopefully contributes to a better understanding of the cooperative behaviour of random systems with many degrees of freedom. Notwithstanding our analysis raise several new questions, such as the treatment of phenomena studied in our low-dimensional models in higher dimensional or in more realistic models.

Appendix A

Mapping the RTIC onto free fermions

A.1 Jordan-Wigner transformation

First we introduce the raising and lowering operators

$$a_i^+ = \frac{1}{2}(\sigma_i^x + i\sigma_i^y) \quad \text{and} \quad a_i = \frac{1}{2}(\sigma_i^x - i\sigma_i^y), \tag{A.1}$$

respectively, in terms of which $\sigma_i^x = a_i^+ + a_i$ and $\sigma_i^z = 2a_i^+ a_i - 1$. These operators commute on different sites like Bose operators, but on the same site they behave as Fermi operators: $\{a_i, a_i^+\} = 0$ and $(a_i)^2 = (a_i^+)^2 = 0$. In terms of a_i's and a_i^+'s the Hamiltonian (3.1) assumes a quadratic form:

$$H = -\sum_{i=1}^{L-1}[a_i^+ a_{i+1} + a_i^+ a_{i+1}^+ + h.c.] - \sum_{i=1}^{L} h_i(2a_i^+ a_i - 1), \tag{A.2}$$

where *h.c.* means hermitian conjugate.

Since canonical transformations do not preserve the mixed commutation rules among a_i's and a_i^+'s, it is not possible to diagonalize (A.2) directly. This difficulty can be avoided by introducing new variables after Jordan and Wigner[68]:

$$c_i = \exp\left[\pi i \sum_{j=1}^{i-1} a_j^+ a_j\right] a_i, \qquad c_i^+ = a_i^+ \exp\left[-\pi i \sum_{j=1}^{i-1} a_j^+ a_j\right]. \tag{A.3}$$

These are indeed Fermi operators, satisfying

$$\{c_i, c_j^+\} = \delta_{ij}, \qquad \{c_i, c_j\} = \{c_i^+, c_j^+\} = 0. \tag{A.4}$$

Then $c_i^+ c_i = a_i^+ a_i$, so the inverse transformation is simply

$$a_i = \exp\left[-\pi i \sum_{j=1}^{i-1} c_j^+ c_j\right] c_i, \quad a_i^+ = c_i^+ \exp\left[\pi i \sum_{j=1}^{i-1} c_j^+ c_j\right]. \tag{A.5}$$

Furthermore $a_i^+ a_{i+1} = c_i^+ c_{i+1}$ and $a_{i+1}^+ a_i^+ = c_i^+ c_{i+1}^+$. Thus the Hamiltonian can be arranged into a quadratic form of c_i's and c_i^+'s:

$$H = \sum_{i,j=1}^{L-1} \left[c_i^+ A_{ij} c_j + \frac{1}{2}(c_i^+ B_{ij} c_j^+ + h.c.) \right] + \sum_{i=1}^{L} h_i, \tag{A.6}$$

with matrices

$$\mathbf{A} = -\begin{pmatrix} 2h_1 & J_1 & & & \\ J_1 & 2h_2 & J_2 & & \\ & J_2 & \ddots & \ddots & \\ & & \ddots & & J_{L-1} \\ & & & J_{L-1} & 2h_L \end{pmatrix},$$

$$\mathbf{B} = -\begin{pmatrix} 0 & -J_1 & & & \\ J_1 & 0 & -J_2 & & \\ & J_2 & \ddots & \ddots & \\ & & \ddots & & -J_{L-1} \\ & & & J_{L-1} & 0 \end{pmatrix}. \tag{A.7}$$

The above steps can be achieved also for the XY chain defined in (6.6). In this case the above matrices read as

$$\mathbf{A} = \frac{1}{4}\begin{pmatrix} 0 & J_1^x + J_1^y & & & & \\ J_1^x + J_1^y & 0 & J_2^x + J_2^y & & & \\ & J_2^x + J_2^y & 0 & \ddots & & \\ & & \ddots & \ddots & & \\ & & & & J_{L-1}^x + J_{L-1}^y & \\ & & & J_{L-1}^x + J_{L-1}^y & 0 & \end{pmatrix},$$

$$\mathbf{B} = \frac{1}{4}\begin{pmatrix} 0 & J_1^x - J_1^y & & & & \\ J_1^y - J_1^x & 0 & J_2^x - J_2^y & & & \\ & J_2^y - J_2^x & 0 & \ddots & & \\ & & \ddots & \ddots & & \\ & & & & J_{L-1}^x - J_{L-1}^y & \\ & & & J_{L-1}^y - J_{L-1}^x & 0 & \end{pmatrix}. \tag{A.8}$$

The hermicity of H implies that $\mathbf{A}$ is a Hermitian matrix, while the commutation rules require that $\mathbf{B}$ is antisymmetric. Moreover for the RTIC and the XY chain both are real.

Note that it is not possible to obtain a simple quadratic form (A.6) in higher dimensions or with next-nearest-neighbour interaction or with an interaction containing also the z component of spin.

A.2 Bogoliubov transformation

The way of diagonalizing the quadratic Hamiltonian (A.6) is known as Bogoliubov-transformation [7]. One looks for a linear transformation

$$\eta_q = \sum_i (g_{qi} c_i + h_{qi} c_i^+), \quad \eta_q^+ = \sum_i (g_{qi} c_i^+ + h_{qi} c_i), \tag{A.9}$$

where g_{qi} and h_{qi} are real, and the η_q's and η_q^+'s are fermion operators (thus the transformation is canonical), in terms of which the Hamiltonian is expressed as

$$H = \sum_q \epsilon_q \eta_q^+ \eta_q + \text{constant}. \tag{A.10}$$

Applying the relation $[\eta_q, H] - \epsilon_q \eta_q = 0$ one obtains the equations for g_{qi} and h_{qi} [83]

$$\epsilon_q g_{qi} = \sum_j (g_{qj} A_{ij} - h_{qj} B_{ji}), \quad \epsilon_q h_{qi} = \sum_j (g_{qj} B_{ij} - h_{qj} A_{ji}). \tag{A.11}$$

Introducing the L-component vectors Φ_k and Ψ_k with components

$$\Phi_q(i) = g_{qi} + h_{qi}, \quad \Psi_q(i) = g_{qi} - h_{qi}, \tag{A.12}$$

chosen to be normalized to 1:

$$\sum_i \Phi_q^2(i) = \sum_i \Psi_q^2(i) = 1, \tag{A.13}$$

one obtains the equations for the one-fermion excitation energies ϵ_q in matrix notation:

$$\Phi_q(\mathbf{A} - \mathbf{B}) = \epsilon_q \Psi_q \quad \text{and} \quad \Psi_q(\mathbf{A} + \mathbf{B}) = \epsilon_q \Phi_q. \tag{A.14}$$

Combining these equations one arrives to

$$\Phi_q(\mathbf{A} - \mathbf{B})(\mathbf{A} + \mathbf{B}) = \epsilon_q^2 \Phi_q \quad \text{or} \quad \Psi_q(\mathbf{A} + \mathbf{B})(\mathbf{A} - \mathbf{B}) = \epsilon_q^2 \Psi_q. \tag{A.15}$$

Now the squares of excitation energies are given as the eigenvalues of an $L \times L$ matrix.

Creating a $2L$-component vector V_q, with components $V_q(2i-1) = -\Phi_q(i)$ and $V_q(2i) = \Psi_q(i)$, $i = 1, 2, \ldots, L$ (A.15) is reformulated as

$$\mathbf{T} V_q = \epsilon_q V_q, \tag{A.16}$$

where the matrix $\mathbf{T}$ of size $2L \times 2L$ is given in (3.16) [58].

It is easy to see, that if ϵ_q is an eigenvalue of $\mathbf{T}$, than $-\epsilon_q$ is also an eigenvalue and the corresponding eigenvector can be obtained from that of ϵ_q by transforming Φ_q to $-\Phi_q$. This means the interchanging of creation and annihilation operators, and reflects the particle-hole symmetry of the system. Therefore the whole information is contained in one half of the spectrum. We confine ourselves to positive fermion excitation energies $\epsilon_q > 0$.

The constant in (A.10) can be determined from the invariance of trace under canonical transformation. From (A.6) $\mathrm{tr}H = 2^{L-1} \sum_i A_{ii} + 2^L \sum_{i=1}^L h_i$, while from (A.10) $\mathrm{tr}H = 2^{L-1} \sum_q \epsilon_q + 2^L \times \text{constant}$. Comparing these two expressions the constant is thus $-\frac{1}{2} \sum_q \epsilon_q$ and one arrives to the final result in (3.15).

Appendix B

Renormalization of the RQPM

In order to derive the RG equations of the RQPM, it is expedient to represent the Hamiltonian (5.21) in the new basis

$$|n_l'\rangle = \frac{1}{\sqrt{q}} \sum_{n_l=1}^{q} \omega^{(n_l'-1)(n_l-1)} |n_l\rangle, \quad l = 1, 2 \ldots, L, \tag{B.1}$$

where $\omega = \exp\left[\frac{2\pi i}{q}\right]$ and $|n_l\rangle$, $n_l = 1, 2, \ldots, q$ stand for states of the Potts spin at site l [122]. In this basis (5.21) assumes the form

$$H = -\sum_{l=1}^{L-1} J_l \sum_{k=1}^{q-1} M_l^k M_{l+1}^{q-k} - \sum_{l=1}^{L} h_l R_l, \tag{B.2}$$

where operators M_l and R_l acting on $|n_l'\rangle$ are represented by the $q \times q$ matrices:

$$M_l = \begin{pmatrix} 0 & 1 & 0 & 0 & \ldots & 0 \\ 0 & 0 & 1 & 0 & \ldots & 0 \\ & & & \ddots & & \\ & & & & & 1 \\ 1 & & & & 0 & 0 \end{pmatrix} \quad R_l = \begin{pmatrix} q-1 & 0 & 0 & \ldots & 0 \\ 0 & -1 & 0 & \ldots & 0 \\ 0 & 0 & -1 & & \\ & & & \ddots & \\ & & & & 0 \\ 0 & & & 0 & -1 \end{pmatrix}. \tag{B.3}$$

In the following we work in this representation and primes are simply abandoned. We see that the terms in (B.2), through which the fields couple to the system are now diagonal, but the interactions are no longer. Instead they flip the spins.

Strong bond decimation If $J_2 \gg h_2, h_3$ one considers the block, similarly to the RTIC (see Fig. 5.1),

$$H = -J_2 \sum_{k=1}^{q-1} M_2^k M_3^{q-k} - h_2 R_2 - h_3 R_3. \tag{B.4}$$

This block has q^2 states. In the absence of fields $h_2 = h_3 = 0$, there are two levels in the spectrum: the ground state is q-fold degenerate and separated from

the $q(q-1)$-fold degenerate excited levels by J_2. If small fields are switched on, the lower nivou will split into a non-degenerate ground state and a $q-1$-fold degenerate multiplett. Dropping the higher lying $q(q-1)$ states one is left with a nivou-structure of a single Potts spin variable. The details of the calculation are the following. The eigenvalue problem separates into q orthogonal subspaces spanned by the vectors:

$$\begin{array}{ll} 1 & |11\rangle, |2q\rangle, |3(q-1)\rangle, \ldots, |q2\rangle \\ 2 & |12\rangle, |21\rangle, |3q\rangle, \ldots, |q3\rangle \\ \vdots & \\ \mathrm{q} & |1q\rangle, |2(q-1)\rangle, |3(q-2)\rangle, \ldots, |q1\rangle \end{array} \tag{B.5}$$

and subspaces $2, 3, \ldots, q$ are degenerate. The ground state is in the first subspace spanned by the vectors

$$\begin{aligned} \phi_0 &= |11\rangle \\ \phi_1 &= \frac{1}{\sqrt{q-1}}\{|2q\rangle + |3(q-1)\rangle + \ldots + |q2\rangle\}, \end{aligned} \tag{B.6}$$

where we have combined degenerate states. After solving the block eigenvalue problem, the ground state energy is given as

$$E_0 = -\frac{1}{2}\{J_2(q-2)+(q-2)(h_2+h_3)+[(qJ_2-(h_2+h_3)(q-2))^2+4(h_2+h_3)^2(q-1)]\}. \tag{B.7}$$

For $J_2 \gg h_2, h_3$ we get

$$E_0 = -J_2(q-1) - \frac{(h_2+h_3)^2}{qJ_2}(q-1) + \ldots \tag{B.8}$$

The $(q-1)$-fold degenerate excited state come from the ground states of the degenerate sectors $2, 3, \ldots, q$. Choosing sector 2, the ground state is spanned by the vectors

$$\begin{aligned} \psi_0 &= |12\rangle \\ \psi_1 &= |21\rangle \\ \psi_2 &= \frac{1}{\sqrt{q-2}}(|3q\rangle + 4(q-1)\rangle + \ldots + |q3\rangle). \end{aligned} \tag{B.9}$$

The solution of the block eigenvalue problem for $h_2 = h_3 = 0$ is

$$\begin{aligned} \varepsilon_0 = -J_2(q-1) \qquad & v_0 = (\frac{1}{\sqrt{q}}, \frac{1}{\sqrt{q}}, \sqrt{\frac{q-2}{q}}) \\ \varepsilon_1 = J_2 \qquad & v_1 = (\sqrt{\frac{q-2}{2q}}, \sqrt{\frac{q-2}{2q}}, -\frac{2}{\sqrt{2q}}) \\ \varepsilon_2 = J_2 \qquad & v_2 = (\frac{1}{\sqrt{2}}, -\frac{1}{\sqrt{2}}, 0). \end{aligned} \tag{B.10}$$

Now the fields can be treated as small perturbations given by the matrix

$$V = \begin{pmatrix} -(q-1)h_2 + h_3 & 0 & 0 \\ 0 & -(q-1)h_3 + h_2 & 0 \\ 0 & 0 & h_2 + h_3 \end{pmatrix}. \tag{B.11}$$

The first correction to ε_0 $\Delta\varepsilon_0^{(1)} = \langle v_0|V|v_0\rangle$ is zero, while the second correction is

$$\Delta\varepsilon_0^{(2)} = -\frac{|\langle v_0|V|v_1\rangle|^2}{\varepsilon_1 - \varepsilon_0} - \frac{|\langle v_0|V|v_2\rangle|^2}{\varepsilon_2 - \varepsilon_0} = -\frac{q-2}{2qJ_2}(h_2+h_3)^2 - \frac{1}{2J_2}(h_2-h_3)^2. \tag{B.12}$$

Thus the excitation energy is

$$\Delta E = E_1 - E_0 = 2\frac{h_2 h_3}{J_2} + \dots \tag{B.13}$$

Keeping now only the first q states, we are left with the energy spectrum of a single Potts spin in a field:

$$\tilde{h}_{23} = \frac{2}{q}\frac{h_2 h_3}{J_2}. \tag{B.14}$$

Strong field decimation In case of a strong field $h_2 \gg J_1, J_2$ one considers the block in Fig. 5.1 B, and uses the duality transformation of quantum Potts chain, which maps the high-temperature phase to the low-temperature one. Similarly to the RTIC, dual couplings J_i' and h_i' are related to original ones as

$$h_i' = J_{i-1} \quad \text{and} \quad J_i' = h_i. \tag{B.15}$$

Decimating out the strong bond $J_2' = h_2$ in the dual block, according to (B.14) one gets an effective Potts spin in a field $\tilde{h}_{23}' = \frac{2}{q}\frac{h_2' h_3'}{J_2'}$. In the direct lattice this procedure corresponds to the decimation of spin 2, and finally one is left with an effective bond between between spin 1 and spin 3, the value of which is, according to (B.15):

$$\tilde{J}_{13} = \frac{2}{q}\frac{J_2 J_3}{h_2}. \tag{B.16}$$

Thus we got the recursion equations (5.8) with $\kappa = \frac{q}{2}$ for the RQPC.

Appendix C

Mapping the XY chain into RTIC-s

We have seen in Section 6.3.1 that the matrix $\mathbf{T}$ in (6.12) can be represented as a direct product $\mathbf{T} = \mathbf{T}_\sigma \bigotimes \mathbf{T}_\tau$. Now one can observe that the tridiagonal matrices $\mathbf{T}_\sigma$, $\mathbf{T}_\tau$ of size $L \times L$ are of the form as the $\mathbf{T}$ matrix of an RTIC of size L (see (3.16)). The corresponding RTIC Hamiltonians read as

$$\begin{aligned} H_\sigma &= -\frac{1}{4}\sum_{i=1}^{L/2-1} J_{2i}^x \sigma_i^x \sigma_{i+1}^x - \frac{1}{4}\sum_{i}^{L/2} J_{2i-1}^y \sigma_i^z \\ H_\tau &= -\frac{1}{4}\sum_{i=1}^{L/2-1} J_{2i}^y \tau_i^x \tau_{i+1}^x - \frac{1}{4}\sum_{i}^{L/2} J_{2i-1}^x \tau_i^z \ . \end{aligned} \tag{C.1}$$

Here the $\sigma_i^{x,z}$ and $\tau_i^{x,z}$ are two sets of Pauli matrices at site i and there are free boundary conditions for both chains. We can then write $H_{XY} = H_\sigma + H_\tau$. Note the symmetry $\sigma_i^{x,z} \leftrightarrow \tau_i^{x,z}$ and $J_l^x \leftrightarrow J_l^y$, thus anisotropy in the XY model has different effects in the two Ising chains.

One can easily find the transformational relations between the XY and Ising variables:

$$\begin{aligned} \sigma_i^x &= \prod_{j=1}^{2i-1} \left(2S_j^x\right), \quad \sigma_i^z = 4S_{2i-1}^y S_{2i}^y \\ \tau_i^x &= \prod_{j=1}^{2i-1} \left(2S_j^y\right), \quad \tau_i^z = 4S_{2i-1}^x S_{2i}^x \ , \end{aligned} \tag{C.2}$$

whereas the inverse relations are the following:

$$\begin{aligned} 2S_{2i-1}^x &= \sigma_i^x \prod_{j=1}^{i-1} \tau_j^z, \quad 2S_{2i}^x = \sigma_i^x \prod_{j=1}^{i} \tau_j^z \\ 2S_{2i-1}^y &= \tau_i^x \prod_{j=1}^{i-1} \sigma_j^z, \quad 2S_{2i}^y = \tau_i^x \prod_{j=1}^{i} \sigma_j^z \ . \end{aligned} \tag{C.3}$$

We note that a relation between the XY model and two decoupled Ising quantum chains in the thermodynamic limit [102, 32] and for finite chains with periodic boundary condition [45] is known for some time, here we have extended this relation for finite chains with free boundary condition. These are essential to map local order parameters and end-to-end correlation functions.

End-to-end correlations are related as

$$\langle S_1^x S_L^x \rangle = \frac{1}{4} \langle \sigma_1^x \sigma_{L/2}^x \rangle \langle \prod_{i=1}^{L/2} \tau_i^z \rangle = \frac{1}{4} \langle \sigma_1^x \sigma_{L/2}^x \rangle \ , \tag{C.4}$$

since in the ground state $\langle \prod_{i=1}^{L/2} \tau_i^z \rangle = 1$. Similarly

$$\langle S_1^y S_L^y \rangle = \frac{1}{4} \langle \tau_1^x \tau_{L/2}^x \rangle \ , \tag{C.5}$$

thus the end-to-end correlations in the two models are in identical form. As a consequence the corresponding decay exponent η_1^x in the random models in Table 6.1 is the same in the two systems and the same conclusion holds also for the correlation length exponent ν in (6.25). These results are also independent of the type of correlation of the disorder, thus are valid both for the XY and XX models.

Correlations between two spins at general positions $2l$ and $2l+2r$ are related as

$$\langle S_{2l}^x S_{2l+2r}^x \rangle = \frac{1}{4} \langle \sigma_l^x \sigma_{l+r}^x \rangle \langle \prod_{i=1}^{r} \tau_{l+i}^z \rangle \ . \tag{C.6}$$

The second factor in the r.h.s., $\langle \prod_{i=1}^{r} \tau_{l+i}^z \rangle$, defines a string-like order parameter [47, 45] which can be expressed in a simpler form in terms of the dual Ising variables

$$\begin{aligned} \tilde{\tau}_i^z &= \tau_i^x \tau_{i+1}^x \\ \tau_i^z &= \tilde{\tau}_{i-1}^x \tilde{\tau}_i^x \ , \end{aligned} \tag{C.7}$$

already introduced in (3.2). Under the duality transformation fields and couplings are exchanged, therefore the vanishing bonds at the two ends of an open chain are transformed to vanishing fields, thus the dual chain has two end spins fixed to the same state. So we obtain for the correlations in Eq. (C.6)

$$\langle S_{2l}^x S_{2l+2r}^x \rangle = \frac{1}{4} \langle \sigma_l^x \sigma_{l+r}^x \rangle \langle \tilde{\tau}_l^x \tilde{\tau}_{l+r}^x \rangle^{++} \ , \tag{C.8}$$

where the superscript $^{++}$ denotes fixed-spin boundary condition. For non-surface points the average value of the correlation function in (C.8) depends on the type of disorder correlations. For the XY model, where the disorder is uncorrelated the two factors in (C.8) can be averaged separately, whereas this is not possible for the XX model. We treated this point in Section 6.3.3.

Appendix D

Scaling of autocorrelation functions

The autocorrelation functions are represented by the general form:

$$G^{\mu}(\tau) = \sum_{k} |M_k|^2 \exp(-\tau \Delta E_k) \tag{D.1}$$

where the dominant contributions to the sum in Eq. (D.1) are from SCD-s which are localized at some distance l from the spin and have a very small excitation energy, $\Delta E(l)$. The scaling form of $\Delta E(l)$ follows from the considerations in Section 3.5.2 and one obtains from (3.44) and (3.45)

$$\Delta E(l) \sim \begin{cases} \epsilon_0 \exp(-A l^{1/2}), \delta = 0 \\ \epsilon_0 l^{-z}, \delta < 0 \end{cases} \tag{D.2}$$

at the critical point and in the Griffiths phase, respectively, where ϵ_0 denotes the energy scale. Thus the larger the distance from the spin the larger the probability to have an SCD with a very small energy. For the matrix element, $|M(l)|^2$, the tendency is the opposite since the overlap with the wave function of the SCD is (exponentially) decreasing with the distance. The corresponding scaling form can be read from the typical behavior of the surface order parameter as given below and above (6.26) as

$$|M(l)|^2 \sim \begin{cases} \exp(-B l^{1/2}), & \delta = 0 \\ \exp(-l/\xi_{\rm typ}), & \delta < 0 \end{cases} . \tag{D.3}$$

Then $G^{\mu}(\tau)$ in (D.1) can be approximated by a sum which runs over SCD-s localized at different distances l and this sum is dominated by the largest term with $l = l_0$:

$$G^{\mu}(\tau) \sim |M(l_0)|^2 \exp(-\tau \Delta E(l_0)) . \tag{D.4}$$

Using the scaling forms in (D.2) and (D.3) one gets following result.

At the critical point the characteristic distance is $l_0 = [\ln(\tau \epsilon_0 A/B)/A]^2$ and the typical autocorrelation function decays as a power:

$$G^{\mu}(\tau) \sim \tau^{-B/A}, \quad \delta = 0 . \tag{D.5}$$

Thus the relevant scaling variable of the problem is

$$\gamma = -\frac{\ln G^{\mu}(\tau)}{\ln \tau}, \quad \delta = 0 \; . \tag{D.6}$$

In the Griffiths phase the characteristic distance has a power-law τ dependence, $l_0 = \xi_{\rm typ}(\tau\epsilon_0 z)^{1/(z+1)}$, which is however different from the average scaling form in (2.29). Thus the typical autocorrelations now are of a stretched exponential form, as presented in (6.40).

Appendix E

Duality of the RBPM

The two phases of the q-state random-bond Potts model can be mapped onto each other by a duality transformation, which makes possible the exact determination of the critical point. We present this in the framework of random cluster representation.

First we show, how to transform the partition function of the RBPM into (7.2), which is known as Fortuin-Kasteleyn transformation. The partition function of the RBPM reads as

$$Z = \sum_{\{\sigma_i\}} \exp\left(\sum_{\langle ij\rangle} K_{ij}\delta(\sigma_i,\sigma_j)\right) = \sum_{\{\sigma_i\}}\prod_{\langle ij\rangle}\left[\left(e^{K_{ij}\delta(\sigma_i,\sigma_j)}-1\right)+1\right]. \quad \text{(E.1)}$$

Introducing the new variable $v_{ij} \equiv e^{K_{ij}} - 1$ and using the identity $v_{ij}\delta(\sigma_i,\sigma_j) \equiv e^{K_{ij}\delta(\sigma_i,\sigma_j)} - 1$, Z is reformulated as

$$Z = \sum_{\{\sigma_i\}}\prod_{\langle ij\rangle}\left(v_{ij}\delta(\sigma_i,\sigma_j)+1\right). \quad \text{(E.2)}$$

Forgetting for a moment the sum over spin configurations in (E.2), and multiplying out the product, the resulting terms are products containing as many factors as the number of edges of the lattice. These factors are of two kind: whether 1 or $v_{ij}\delta(\sigma_i,\sigma_j)$. Now, to each such product a subgraph $G \subseteq \bar{G}$ can be associated. The rule for this one-to-one correspondence is that each edge (ij) of the graph is occupied, i.e. $(ij) \in U$, when it is counted with weight $v_{ij}\delta(\sigma_i,\sigma_j)$ in the product and unoccupied when it is counted with weight 1. Now considering a given product and performing the summation over spin states, only those configurations contribute (with $\prod_{(ij)\in U} v_{ij}$), in which, spins in all connected clusters take the same value. Then denoting the number of connected clusters by $n(U)$, one arrives to (7.2).

Now we introduce the concept of *dual lattice* $\bar{G}' = (V', E')$ the sites of which correspond to the plaquettes (squares) of G, and are located in the middle of them. Thus $\bar{G}'$ is also a square lattice, as $\bar{G}$, shifted by a half lattice spacing along both axes. A subgraph $G' = (V', U') \subseteq \bar{G}'$ is now said to be *dual* to $G = (V, U)$, if U' contains all edges $(ij)' \in U'$ which do not cross any edge $(ij) \in U$.

Since by construction each loop of G encircles a cluster of G', and vice versa, one has

$$n(U) = c(U') + 1, \qquad n(U') = c(U) + 1, \tag{E.3}$$

where c(U) denotes the number of loops in U. Furthermore the Euler relation

$$c(U) = b(U) + n(U) - N \tag{E.4}$$

holds for any graph, where N is the number of sites and $b(U)$ is the number of bonds in $G = (V, U)$. Using the above relations, and denoting the total product of weights as $V \equiv \prod_{(ij)\in E} v_{ij}$, Z can be rewritten in terms of dual graphs:

$$Z = \sum_{U\subseteq E} q^{n(U)} \prod_{(ij)\in U} v_{ij} = V \sum_{U'\subseteq E'} q^{c(U')+1} \prod_{(ij)'\in U'} v_{ij}^{-1} =$$
$$V \sum_{U'\subseteq E'} q^{b(U')+n(U')-N'+1} \prod_{(ij)'\in U'} v_{ij}^{-1} = Vq^{1-N'} \sum_{U'\subseteq E'} q^{n(U')} \prod_{(ij)'\in U'} \frac{q}{v_{ij}}. \tag{E.5}$$

We define the dual couplings K_{ij}^* through $q/v_{ij} = v_{ij}^* = e^{K_{ij}^*} - 1$, or equivalently

$$(e^{K_{ij}} - 1)(e^{K_{ij}^*} - 1) = q. \tag{E.6}$$

Considering now the pure model with reduced coupling $K_{ij} = K$, the first expression in (E.5) can be viewed as a high-temperature expansion with coupling K. According to the calculation in (E.5) it is then connected to a low-temperature partition function containing K^*. Provided that there is a single phase transition in the system, it must be at the fixed point of the duality transformation (E.6) $K^* = K$. Thus for the pure model the critical reduced coupling is $K_c = \ln(\sqrt{q} + 1)$. The random q-state Potts model with symmetric bimodal coupling distribution, i.e. with two equally probable couplings K_1 and K_2, is apparently critical, if $K_1^* = K_2$ and $K_2^* = K_1$, which is equivalent to

$$(e^{K_1} - 1)(e^{K_2} - 1) = q. \tag{E.7}$$

If we are given a continuous randomness distribution $\rho(K)dK$, the system is then at its critical point, if it is invariant against the transformation (E.6), i.e.

$$\rho(K)dK = -\rho(K^*)dK^*. \tag{E.8}$$

Now turning to the variable w_{ij} defined in (7.3), (E.8) reduces to the criticality condition presented in (7.11) [76].

Bibliography

[1] R.K. Ahuja, T.L. Magnanti, J.B. Orlin, *Network Flows*, Prentice-Hall (New Jersey, 1993).

[2] M. Aizenmann and J. Wehr, Phys. Rev. Lett. **62**, 2503 (1989).

[3] M.J. Alava, P.M. Duxbury, C. Moukarzel, and H. Rieger, in *Phase Transitions and Critical Phenomena*, vol. 18 eds C. Domb and J.L. Lebowitz, Academic Press, (New York, 1987).

[4] R.J. Baxter, Ann. Phys. (N.Y.) **70**, 193 (1972).

[5] R.J. Baxter, J. Phys. C**6**, L445 (1973).

[6] R.N. Bhatt: in *Spin Glasses and Random Fields*, Ed. A.P. Young (World Scientific, Singapore, 1998) p. 225.

[7] N.N. Bogoliubov, J. Phys. (USSR) **11**, 23 (1947).

[8] R. Bulirsch and J. Stoer, Num. Math. **6**, 413 (1964).

[9] G.G. Cabrera and R. Jullien, Phys. Rev. B **35**, 7062 (1987).

[10] C. de Calan, J. M. Luck, T. M. Nieuwenhuizen and D. Petritis, J. Phys. A **18**, 501 (1985).

[11] J.L. Cardy, in *Phase Transitions and Critical Phenomena*, vol. 11 eds C. Domb and J.L. Lebowitz (New York: Academic) (1987).

[12] J.L. Cardy and J.L. Jacobsen, Phys. Rev. Lett. **79**, 4063 (1997).

[13] E. Carlon, P. Lajkó, and F. Iglói, Phys. Rev. Lett. **87**, 277201 (2001).

[14] A.H. Castro Neto, G. Castilla, and B.A. Jones, Phys. Rev. Lett. **81**, 3531 (1998).

[15] A.H. Castro Neto, Proceedings of the VI International Summer School "Nicolás Cabrera" Miraflores de la Sierra, Madrid, 1999, cond-mat/9911092.

[16] A.H. Castro Neto and B.A. Jones, cond-mat/0003085.

[17] V. Cerny, J. Optimization Theory Appl. **45**, 41 (1985).

[18] C. Chatelain and B. Berche, Phys. Rev. Lett. **80**, 1670 (1998).

[19] C. Chatelain and B. Berche, Phys. Rev. E **58** R6899 (1998).

[20] C. Chatelain and B. Berche, Phys. Rev. E **60**, 3853 (1999).

[21] C. Chatelain, B. Berche, W. Janke and P.E. Berche, cond-mat/0103377.

[22] J. T. Chayes, L. Chayes, D. S. Fisher and T. Spencer, Phys. Rev. Lett. **57**, 299 (1986).

[23] S. Chen, A.M. Ferrenberg, and D.P. Landau, Phys. Rev. E**52**, 1377 (1995).

[24] C. Dasgupta and S.K. Ma, Phys. Rev. B **22**, 1305 (1979).

[25] B. Derrida, Phys. Rep. **103**, 29 (1984).

[26] B. Derrida and Y. Pomeau, Phys. Rev. Lett. **48**, 627 (1982).

[27] E. Domany and S. Wiseman, Phys. Rev. E**51**, 3074 (1995).

[28] Vl. Dotsenko, M. Picco and P. Pujol, Nucl. Phys. B**455** [FS], 701 (1995).

[29] C.A. Doty and D.S. Fisher, Phys. Rev. B **45**, 2167 (1992).

[30] M. Fabrizio and R. Mélin, Phys. Rev. Lett. **78**, 3382 (1997).

[31] D.S. Fisher, Phys. Rev. Lett. **69**, 534 (1992);

[32] D.S. Fisher, Phys. Rev. B**50**, 3799 (1994).

[33] D.S. Fisher, Phys. Rev. B **51**, 6411 (1995).

[34] D.S. Fisher, Physica A **263** 222 (1999).

[35] D.S. Fisher and A.P. Young, Phys. Rev. B **58**, 9131 (1998).

[36] S. Gopalan, T.M. Rice, and M. Sigrist, cond-mat/9312026.

[37] R.B. Griffiths, Phys. Rev. Lett. **23**, 17 (1969).

[38] M. Guo, R.N. Bhatt, and D.A. Huse, Phys. Rev. Lett. **72**, 4137 (1994).

[39] M. Guo, R.N. Bhatt, and D.A. Huse, Phys. Rev. B **54**, 3336 (1996).

[40] S. Haas, J. Riera and E. Dagotto, Phys. Rev. B **48**, 13174 (1993).

[41] T. Hagerup, unpublished.

[42] F.D.M. Haldane, Phys. Lett. **93A**, 464 (1983)

[43] A.B. Harris, J. Phys. C**7**, 1671 (1974).

[44] A.K. Hartmann and H. Rieger, *Optimization Algorithms in Physics*, WILEY-VCH (Berlin, 2001).

[45] P. Henelius and S.M. Girvin, Phys. Rev. B **57**, 11457 (1998).

[46] M. Henkel, *Conformal Invariance and Critical Phenomena*, Springer (Berlin Heidelberg, 1999).

[47] K. Hida, Phys. Rev. Lett. **83**, 3297 (1999).

[48] T. Hikihara, A. Furusaki and M. Sigrist, Phys. Rev. B **60**, 12116 (1999).

[49] J. Hoshen and R. Kopelman, Phys. Rev. B **14**, 3428 (1976).

[50] K. Hui and A.N. Berker, Phys, Rev. Lett. **62**, 2507 (1989).

[51] R.A. Hyman, K. Yang, R.N. Bhatt and S.M. Girvin, Phys. Rev. Lett. **76**, 839 (1996),

[52] F. Iglói, Phys. Rev. B **65**, 064416 (2002).

[53] F. Iglói, R. Juhász, and P. Lajkó, Phys. Rev. Lett. **86**, 1343 (2001).

[54] F. Iglói, R. Juhász, and H. Rieger, Phys. Rev. B **59**, 11308 (1999).

[55] F. Iglói, R. Juhász, and H. Rieger, Phys. Rev. B **61**, 11552 (2000).

[56] F. Iglói, I. Peschel, and L. Turban, Adv. Phys. **42**, No. 6, 683 (1993).

[57] F. Iglói and H. Rieger, Phys. Rev. Lett. **78**, 2473 (1997).

[58] F. Iglói and H. Rieger, Phys. Rev. B **57**, 11404 (1998).

[59] F. Iglói and H. Rieger, Phys. Rev. E **58**, 4238 (1998).

[60] F. Iglói and L. Turban, Phys. Rev. Lett. **77**, 1206 (1996).

[61] F. Iglói, L. Turban, D. Karevski and F. Szalma, Phys. Rev. B **56**, 11031 (1997).

[62] F. Iglói, L. Turban, and H. Rieger, Phys. Rev. E **59**, 1465 (1999).

[63] T. Ikegami, S. Miyashita and H. Rieger, J. Phys. Soc. Jap. **67**, 2761 (1998).

[64] Y. Imry and M. Wortis, Phys. Rev. B**19**, 3580 (1979).

[65] E. Ising, Z. Phys. **31**, 253 (1925).

[66] J.L. Jacobsen and J.L. Cardy, Nucl. Phys. B**515**, 701 (1998).

[67] J.L. Jacobsen and M. Picco, Phys. Rev. E**61**, R13 (2000).

[68] P. Jordan and E. Wigner, Z. Physik **47**, 631 (1928).

[69] R. Juhász and F. Iglói, Phys. Rev. E **66**, 056113 (2002).

[70] R. Juhász, H. Rieger, and F. Iglói, Phys. Rev. E **64**, 56122 (2001).

[71] M. Kardar, A.L. Stella, G. Sartoni and B. Derrida, Phys. Rev. E**52**, R1269 (1995).

[72] D. Karevski, R. Juhász, L. Turban, and F. Iglói, Phys. Rev. B **60** 4195 (1999).

[73] P.W. Kasteleyn and C.M. Fortuin, J. Phys. Soc. Jpn. **46** (suppl.), 11 (1969).

[74] S. Katsura, Phys. Rev. **127**, 1508 (1962).

[75] H. Kesten, Acta. Math. **131**, 208 (1973).

[76] W. Kinzel and E. Domany, Phys. Rev. B**23**, 3421 (1981).

[77] S. Kirkpatrick, C.D. Gelatt and M.P. Vecchi, Science **220**, 671 (1983).

[78] J. Kisker and A. P. Young. Phys. Rev. B **58**, 14397 (1998).

[79] J.B. Kogut, Rev. Mod. Phys. **51**, 659 (1979).

[80] H.A. Kramers and G.H. Wannier, Phys. Rev. **60**, 252 (1941).

[81] P. A. Lee and T.V. Ramakrishnan, Rev. Mod. Phys. **57**, 287 (1985).

[82] M.A. Lewis, Europhys. Lett. **43**, 189 (1998).

[83] E. Lieb, T. Schultz, and D. Mattis, Ann. Phys. (N.Y.) **16**, 407 (1961).

[84] Y.-C. Lin, N. Kawashima, F. Iglói, and H. Rieger, Prog. Theor. Phys. Suppl. **138**,479 (2000).

[85] Y. Liu *et al.* Phys. Rev. Lett. **67**, 2068 (1991).

[86] A.W.W. Ludwig, Nucl. Phys. B **285** [FS19], 97 (1987).

[87] A.W.W. Ludwig, Nucl. Phys. B**330** [FS19], 639 (1990).

[88] A.W.W. Ludwig and J.L. Cardy, Nucl. Phys. B**330** [FS19], 687 (1990).

[89] S.K. Ma, C. Dasgupta and C.-K. Hu, Phys. Rev. Lett. **43**, 1434 (1979);

[90] P.P. Martin, *Potts Model and Related Problems in Statistical Mechanics*, World Scientific (Singapore 1990).

[91] B. McCoy, Phys. Rev. Lett. **23**, 383 (1969).

[92] B.M. McCoy, Phys. Rev. **188**, 1014 (1969).

[93] B.M. McCoy and T.T. Wu, Phys. Rev. 176, 631 (1968).

[94] R. H. McKenzie, Phys. Rev. Lett. **77**, 4804 (1996).

[95] C. Monthus, O. Golinelli and Th. Jolicoeur, Phys. Rev. Lett. **79**, 3254 (1997).

[96] O. Motrunich, S.-C. Mau, D.A. Huse, and D.S. Fisher, Phys. Rev. B **61**, 1160 (2000).

[97] R. Mélin, Y.-C. Lin, P. Lajkó, H. Rieger, and F. Iglói, Phys. Rev. B **65**, 104415 (2002).

[98] Numerical Recipies in C: The Art of Scientific Computing, William H. Press (et al.), Cambridge, 1986.

[99] T. Olson and A.P. Young, Phys. Rev. B**60**, 3428 (1999).

[100] L. Onsager, Phys. Rev. **65**, 117 (1944).

[101] G. Palágyi, C. Chatelain, B. Berche and F. Iglói, Eur. Phys. J. B**13**, 357 (2000).

[102] I. Peschel, Phys. Rev. B **30**, 6783 (1984).

[103] I. Peschel and K. D. Schotte, Z. Phys. B**54**, 305 (1984).

[104] P. Pfeuty, Ann. Phys. (Paris) **57**, 79 (1970).

[105] M. Picco, Phys. Rev. Lett. **79**, 2998 (1997).

[106] C. Pich, A.P. Young, H. Rieger and N. Kawashima, Phys. Rev. Lett. **81**, 5916 (1998).

[107] R.B. Potts, Proc. Cam. Phil. Soc. **48**, 106 (1952).

[108] M. Randeira, J. P. Sentha and R. G. Palmer, Phys. Rev. Lett. **54**, 1321 (1985).

[109] H. Rieger and F. Iglói, Europhys. Lett. **39**, 135 (1997).

[110] H. Rieger and F. Iglói, Europhys. Lett. **45**, 673 (1999).

[111] H. Rieger and F. Iglói, Phys. Rev. Lett. **83**, 3741 (1999).

[112] H. Rieger, R. Juhász, and F. Iglói, Europ. Phys. J. B **13**, 409 (2000).

[113] H. Rieger and N. Kawashima, Europ. Phys. J. B **9**, 233 (1999).

[114] H. Rieger and A.P. Young, Rev. Mod. Phys. **58**, 801 (1986).

[115] H. Rieger and A.P. Young, Phys. Rev. Lett. **72**, 4141 (1994)

[116] H. Rieger and A.P. Young, Phys. Rev. B **54**, 3328 (1996).

[117] H. Rieger and A. P Young, in *Complex Behavior of Glassy Systems*, ed. M. Rubi and C. Perez-Vicente, Lecture Notes in Physics **492**, p. 256, Springer-Verlag, Heidelberg, 1997.

[118] H. Röder, J. Stolze, R.N. Silver and G. Müller, J. Appl. Phys. **79**, 4632 (1996).

[119] T. Senthil and S.N. Majumdar, Phys. Rev. Lett. **76**, 3001 (1996).

[120] J.P. Bouchaud and A. Georges, Phys. Rep. **195**, 127 (1990).

[121] R. Shankar and G. Murthy, Phys. Rev. B **36**, 536 (1987).

[122] J. Sólyom and P. Pfeuty, Phys. Rev. B **24**, 218 (1981).

[123] D. Stauffer and A. Aharony, *Introduction to Percolation Theory*, (London: Taylor & Francis) (1992).

[124] J. Stolze, A. Nöppert and G. Müller, Phys. Rev. B **52**, 4319 (1995).

[125] M. Suzuki, Prog. Theor. Phys. **56**, 1454

[126] M.J. Thill and D.A. Huse, Physica A **214**, 321 (1995).

[127] L.C. Tippie and W.G. Clark, Phys. Rev. B **23**, 5846 (1981).

[128] L.C. Tippie and W.G. Clark, Phys. Rev. B **23**, 5854 (1981).

[129] L. Turban and F. Iglói, J. Phys. A: Math. Gen. **30**, 105 (1997).

[130] A. Weinrib and B.I. Halperin, Phys. Rev. B **27**, 413 (1983).

[131] E. Westerberg, A. Furusaki, M. Sigrist and P.A. Lee, Phys. Rev. B**55**, 12578 (1997).

[132] F.Y. Wu, Rev. Mod. Phys. **54**, 235 (1982).

[133] W. Wu, D. Bitko, T.F. Rosenbaum, and G. Aeppli, Phys. Rev. Lett. **71**, 1919, (1993).

[134] W. Wu, B. Ellmann, T.F. Rosenbaum, G. Aeppli, and D.H. Reich, Phys. Rev. Lett. **67**, 2076 (1991).

[135] K. Yang and R.N. Bhatt, Phys. Rev. Lett. **80**, 4562 (1998).

[136] A.P. Young, in *Statphys 19*, ed. Hao Bailin (World Scientific, 1995).

[137] A. P. Young and H. Rieger, Phys. Rev. B **53**, 8486 (1996).

[138] A. P. Young, Phys. Rev. B **56**, 11691 (1997).

Acknowledgements

In the first place I thank Prof. Dr. Ferenc Iglói for supervising this thesis. I am grateful for his precious suggestions and constant helping in my work throughout my PhD study.

I thank the co-authors of our publications, Dr. Dragi Karevski, Dr. Péter Lajkó, and Prof. Dr. Loïc Turban for the fruitful cooperation.

I especially thank Prof. Dr. Heiko Rieger for his collaboration and hospitality during the half-year period I spent in his research group.

I thank all members of the Institute for Theoretical Physics, University of Szeged for providing an inspiring working atmosphere and for their helpfulness.

I am grateful to Dr. Ludger Santen for his careful reading of the manuscript and for his useful comments.

Rendezetlenség dominálta szinguláris viselkedés kvantum- és klasszikus rendszerekben
Összefoglalás

A természetben előforduló anyagokat és folyamatokat kevés kivételtől eltekintve mindig bizonyos fokú inhomogenitás jellemzi. A leggyakrabban említett példa erre a kristályokban megfigyelhető szennyező atomok és egyéb rácshibák jelenléte. A valós rendszerek ezen tulajdonságának elméleti leírása hívta létre a *rendezetlenség* koncepcióját, majd indította útjára a—mára már széleskörűen alkalmazott—*rendezetlen modellek* vizsgálatát, mely lassanként önálló diszciplinává növi ki magát.

A rendezetlen rendszerek elméleti leírása során külön kezelendők azon rendszerek, melyekben a rendezetlenséggel kapcsolatos relaxációs idő lényegesen nagyobb a termikus szabadsági fokokhoz társuló relaxációs időnél. Az ilyen rendszereket leíró ún. "befagyott" rendezetlenségű modellekben a fizikai mennyiségek termikus várható értéke függ a rendezetlenség konkrét megvalósulásától. Ilyen modellekben előfordulhat, hogy némely mennyiség *nem önátlagoló*, azaz átlagos- és tipikus értéke különböző. Ezen mennyiségek jellemzéséhez a teljes eloszlásuk ismerete szükséges. A továbbiakban az ilyen modellek tulajdonságait tárgyaljuk.

A rendezetlen modelleken belül különös érdeklődés indult meg a *fázisátalakulást* mutató modellek iránt, melyeknél természetes módon vetődik fel a kérdés, hogy a rendezetlenség bevezetése milyen változásokat eredményez (ha eredményez egyáltalán) a rendezetlenségtől mentes, ún. tiszta rendszer tulajdonságaihoz képest.

A tapasztalatok szerint a rendezetlenség változó mértékben befolyásolja a tiszta rendszer fázisátalakulását: Előfordul, hogy a rendezetlenség a fázisátalakulási pont megszűnéséhez vezet, vagy az átalakulás rendűségének megváltozásához: nevezetesen az elsőrendű fázisátmenet folytonossá válik. Alapvető kérdés itt, hogy egy folytonos fázisátalakulás esetén (amelyet a rendezetlenség nem mos el), a kritikus pont *univerzális* tulajdonságai mily módon változnak. Véletlen-csatolású modellekben a választ erre a kérdésre egy—Harris nevéhez fűződő—heurisztikus stabilitási kritérium adja, mely a rendezetlenség releváns voltát a megfelelő tiszta rendszer fajhő exponensével hozza kapcsolatba.

A klasszikus rendszerekben lezajló—termikus fluktuációk által kontrollált—fázisátalakulásoktól számos vonatkozásban különböznek az—abszolút nulla fokon végbemenő—ún. *kvantum-fázisátalakulások*. Itt—hőtartály nem lévén—az aktiválási dinamikát az alagútazás váltja fel, ami a klasszikustól merőben eltérő fázisátalakulási mechanizmushoz vezet. A rendezetlen kvantum-fázisátalakulások kritikus tulajdonságait a termikus fluktuációk helyett a *kvantum-fluktuációk* és a rendezetlenség fluktuációinak összjátéka alakítja ki.

A kvantum-fázisátalakulási ponttal rendelkező rendezetlen modellek egy csoportja különleges nagyléptékű és alacsony energiás viselkedést mutat. Míg a legtöbb rendszert a—hosszúságegység növekedésével járó—valós-tér renormálási-csoport transzformációk olyan fixpont felé sodorják, ahol a Hamilton-függvényben szereplő lokális paraméterek hányadosa *véges* marad, addig ezen modellekben a fenti transzformáció során a Hamilton-operátor paramétereinek eloszlása, logaritmikus skálán, minden határon túl szélesedik, midőn az energiaskála nullához tart. A fixpontban ekkor a paraméterek hányadosa tipikusan

végtelen vagy nulla; a rendszer viselkedését egy ún. *végtelenül erős rendezetlenségű fixpont* írja le. A széles eloszlások maguk után vonják az *önátlagolás hiányát*, és a mennyiségek átlagértékét az ún. ritka minták extrém járulékai határozzák meg. A modellek ezen osztályába alacsony dimenziós kvantumrendszerek tartoznak, zömében spinlácok és spinlétrák.

Azonban a rendezetlenség hatása nem csupán a a fázisátalakulási pont jellemzőinek befolyásolására korlátozódik. Griffiths ill. McCoy mutatta ki a rendezetlen klasszikus- ill. kvantum-Ising-modellben, hogy a kritikus pont körül egy kiterjedt tartomány található, ahol számos fizikai mennyiség szingulárisan viselkedik. Ennek a—kizárólag rendezetlen rendszerekben megfigyelhető—ún. Griffiths-fázisnak a létét azok a ritka domének okozzák, melyek lokálisan a kritikus pont túloldalán lévő fázisban vannak. A Griffiths-McCoy szingularitások a klasszikus modellekkel szemben lényegesen hangsúlyozottabban jelentkeznek a kvantummechanikai rendszerekben, ahol a dinamika és sztatika összekapcsolódik. Itt a rendezetlenség fent vázolt fluktuációi következtében az átlagos időbeli korrelációk—a kritikus viselkedéssel megegyező módon—hatványfüggvény szerint csengenek le. Ezzel szemben a térbeli korrelációkat rövidtávú rend jellemzi, így a Griffiths-fázist "szemikritikus" fixpontok sorozatának nevezik. Egy fenomenologikus skálaelmélet szerint az összes vizsgált fizikai mennyiség szinguláris viselkedése közös fizikai alapra vezethető vissza, és az ezt leíró exponensek kapcsolatba hozhatók a rendszer dinamikai exponensével, mely folytonosan változik a Griffiths-fázisban.

Az értekezés túlnyomó részében rendezetlen kvantum-spinláncok Griffiths-fázisbeli- és kritikus viselkedését vizsgáljuk, melyet a fent említett végtelenül erős rendezetlenségű fixpont kontrollál. Az értekezés második részében egy klasszikus modell, a véletlen-csatolású ferromágneses q-állapotú Potts-modell kritikus viselkedését tanulmányozzuk a nagy q határesetben, amikor a termikus fluktuációk jelentéktelenné válnak. Mindkét probléma közös vonása, hogy a rendszer viselkedését a rendezetlenség alakítja ki döntő módon a kvantumfluktuációkkal ill. a klasszikus problémánál a termikus fluktuációkkal szemben.

A fenti kérdéskörök tanulmányozására számos módszert alkalmaztunk. A kvantum-spinláncok viselkedését a szabadfermion-reprezentáción alapuló analitikus és numerikus módszerekkel, valamint fenomenologikus skálaelmélet segítségével tanulmányozzuk. A Griffiths-fázis tulajdonságait renormálási-csoport transzformáció keretein belül elemezzük, analitikusan és numerikus úton. A véletlen-csatolású Potts-modell megoldását a nagy q határesetben optimalizálási problémára vezetjük vissza, amit aztán numerikus sztochasztikus- és kombinatorikus optimalizációs módszerekkel vizsgálunk.

Az értekezés felépítése a következő. Rövid bevezetést követően, a második fejezetben összefoglaljuk a tiszta- és rendezetlen klasszikus- és kvantumrendszerekben megfigyelhető kritikus viselkedés sajátosságait, majd ismertetjük a Griffiths-McCoy szingularitások fenomenologikus elméletét.

A harmadik fejezetben az egydimenziós rendezetlen kvantum-Ising-modellre vonatkozó eddigi ismereteket gyüjtjük össze. Ezen belül bemutatjuk a fenti modell leképezését szabad fermionok rendszerére, kapcsolatát a véletlen bolyongással, és egy—a ritka eseményekre épülő—fenomenologikus skálaelméletet.

A negyedik fejezettel kezdődően rátérünk az új eredmények ismertetésére. Elsőként az előző fejezetben bemutatott modell Griffiths-fázisában vizsgálunk olyan mennyiségeket, melyek szinguláris viselkedése nem hozható közvetlenül kapcsolatba az energiarés—ismert—viselkedésével. Ezen mennyiségek a követ-

kezőek: a második- és magasabb energiarések eloszlása, a nemlineáris szuszceptibilitás és az energiasűrűség autokorrelációs függvény. Fenomenologikus skálázási érveléssel kimutatjuk a fenti mennyiségek szinguláris viselkedését, és az ezt leíró exponenseket kapcsolatba hozzuk a dinamikai exponenssel. Szabadfermion-reprezentációban a fenti mennyiségekre zárt formulát vezetünk le, majd ezeket numerikus vizsgálatnak vetjük alá. A fenomenologikus- és az azokkal összhangban álló numerikus eredményeink szerint a Griffiths-fázisban szinguláris mennyiségek egyetlen—a kontroll-paraméterrel folytonosan változó—exponenssel jellemezhetőek.

Ezt követően a Ma-Dasgupta-Hu-féle közelítő valós-tér renormálási-csoport transzformációt alkalmazzuk a fenti modellre. A renormálási-csoport egyenletek fixponti megoldásai ismertek a modell kritikus pontjában, ahol az eljárás aszimptotikusan egzakt, azonban általánosan elterjedt az a felfogás, hogy ez kizárólag a kritikus pontban és közvetlen közelében igaz. Ebben a fejezetben megadjuk a renormálási-csoport egyenletek analitikus megoldását a rendezetlen kvantum-Ising-modell Griffiths-fázisában, majd megmutatjuk, hogy az eljárás itt is aszimptotikusan egzakt. Bizonyítjuk, hogy a dinamikai exponens invariáns marad a renormálás során, majd ezt felhasználva egzakt kifejezést adunk a dinamikai exponens számítására. Az energiarés eloszlására épülő fenomenológiai megfontolások alapján a fenti állításokat általános érvényűnek gondoljuk a kvantum-spin-láncok körében. Ezt ellenőrizendő, numerikusan megoldjuk a rendezetlen kvantum-Potts-lánc renormálási-csoport egyenleteit, és becslést adunk a modell q-tól függő dinamikai exponensére. Ezen értékek jó egyezésben állnak más módszerrel (sűrűségmátrix renormálási csoporttal) kapott megfelelő becslésekkel, ily módon a numerikus eredmények alátámasztják az elméleti megfontolások helyességét.

Ezután a rendezetlen XY- és a rendezetlen dimerizált XX-lánc tanulmányozására térünk át. Vizsgálataink alapját az átlagos mennyiségek—a ritka domének skálázási viselkedésén alapuló—fenomenologikus elmélete képezi, melyet kiterjesztünk az XY- és XX-modellekre. A fenti modellek és a véletlen bolyongás között talált kapcsolat révén azonosítjuk a ritka doméneket, mint olyan tartományokat, melyekben a csatolások sorozata túlélő bolyongással reprezentálható. Ezen elmélet segítségével meghatározzuk a fenti modellek tömbi- és felületi kritikus exponenseit. Ezeket azután összevetjük az operátor profilokra—szabadfermion-reprezentáción alapuló számítással—kapott numerikus eredményeinkkel. Eredményeink szerint a kritikus nemdiagonális rendparaméter-profilok követik a konform elmélet által megjósolt viselkedést, annak ellenére, hogy a modell nem konform invariáns. Mindezek mellett vizsgáljuk a dinamikai korrelációkat. A kritikus állapotban ezek átlagának logaritmikusan lassú csökkenését találjuk, míg a korrelációs függvény eloszlásában multi-skálázás figyelhető meg. Ezzel szemben a Griffiths-fázisban az átlagos autokorrelációs függvény a távolság valamely hatványaként cseng le, ahol a kitevő kapcsolatba hozható a dinamikai exponenssel. Felhasználva, hogy a vizsgált modellek alkalmas transzformációval, két Ising-lánccá csatolhatók szét, analitikus összefüggést adunk a dinamikai exponens számítására.

Az értekezés utolsó fejezetében a kétdimenziós rendezetlen q-állapotú Potts-modellt tanulmányozzuk. Ismert, hogy ezen modell tiszta változata $q > 4$ esetén elsőrendű fázisátalakulást mutat, mely a rendezetlenség hatására folytonossá válik. Korábbi, véges q-ra kapott eredmények szerint a korrelációshossz-exponens q-tól alig függ, míg a mágnesezettségi exponens q-függést mutat, és a $q \to \infty$

határesetben véges értékhez tart. Itt a fenti modellt közvetlenül a $q \to \infty$ határesetben vizsgáljuk, a *véletlen klaszter reprezentáció* segítségével. Ekkor megmutatható, hogy a termikus fluktuációk irrelevánssá válnak, és a kritikus viselkedést a rendezetlenség fluktuációi szabják meg döntő módon, ami abban nyilvánul meg, hogy a fizikai tulajdonságokat egyetlen domináns gráf határozza meg. Megmutatjuk, hogy ezen gráf megtalálása egy—a gráfok halmazán értelmezett—globális, nemkonvex költségfüggvény optimalizálási problémájával egyenértékű. Ezen optimalizálási feladatot két numerikus módszerrel, egy standard sztochasztikus optimalizációs eljárással és egy közelítő kombinatorikus optimalizációs módszerrel oldjuk meg. A domináns gráf fraktáltulajdonságainak számításával becslést adunk a Potts-modell mágnesezettségi- és korrelációshossz-exponensére, különböző mértékű rendezetlenség mellett. A korábbi extrapolatív becslésekkel összhangban álló, de annál pontosabb eredményeink szerint a fenti exponensek függetlenek a rendezetlenség alakjától.

Összefoglalva, jelen értekezésben erősen rendezetlen modellek kritikus pontbeli- és Griffiths-fázisbeli tulajdonságait tanulmányoztuk. A speciális modellekre kapott eredményeink között számos olyan található, mely a véletlen modellek általánosabb érvényű vonásait tükrözi. Így eredményeink, reményeink szerint, hozzájárulnak a rendezetlen, sok szabadsági fokú rendszerek koorepatív viselkedésének mélyebb megértéséhez. Mindamellett az értekezésben vázolt elemzéseink számos új kérdést vetnek fel. Így például az alacsony dimenziós modellek fent leírt jelenségei magasabb dimenziós, valamint a valóságot pontosabban tükröző modellekben javarészt továbbra is feltáratlanok.

Disorder dominated singular behaviour in random quantum and classical systems
Summary

The bulk of substances and processes in nature is often characterized by certain degree of inhomogeneity: one might say, it is rather the rule than the exception. The most frequently mentioned example is the almost always inevitable presence of impurities or other lattice defects in crystals. The theoretical description of this kind of feature of real systems established the concept of *disorder*, and started on its way the investigation of the—nowadays widespread—*disordered models*, which is gently developing to be an independent discipline.

From a theoretical point of view those systems in which the characteristic relaxation time associated to impurities is negligible to that of thermal degrees of freedom, has to be treated separately. In the so called "quenched" disordered models describing these systems, the thermal expectational value of a given quantity is apparently depends on the particular realization of disorder. Some quantities may be non-self-averaging, i.e. the typical and average values are different. In this case one has to consider the whole distribution of the quantity instead of the average value.

Among disordered models special attention was payed for models which exhibit a *phase transition*, where the obvious question arises, what consequences the introduction of disorder has (if it has at all) on the properties of the *pure* (i.e. homogeneous) system. According to the experiences quenched disorder has effects on the nature of phase transitions in varying degrees. It may lead to the elimination of the transition by smearing out singularities. Or it may cause the change of order of the transition: a first order transition can turn to a continuous one. In case of a continuous transition (which is not "smeared out" by randomness), a basic question is, how *universal* properties, such as critical exponents are influenced by disorder. Here, for random coupling models a general heuristic relevance-irrelevance criterion was formulated by Harris, which relates the stability of pure system fixed point to the specific heat exponent of the pure system.

Quantum phase transitions occurring at zero temperature differ from thermally driven transitions in several respects. Here, there is no heat bath and activated dynamics is replaced by quantum tunneling through energy barriers, which leads to an entirely different mechanism of phase transition. The random quantum critical behaviour is formed by the interplay between disorder and *quantum fluctuations* instead of thermal ones.

A special class of low-dimensional disordered quantum models is known to have an unconventional coarse-grained behaviour. By coarse-graining, most systems flow toward a fixed point, where the ratio of local parameters in the Hamiltonian remains finite. Contrary to this it turned out, that in these models, the distribution of parameters becomes arbitrarily broad on a logarithmic scale as the fixed point is approached. The ratio of parameters is typically infinite or zero at the fixed point, and the system is said to be governed by an *infinite-randomness fixed point.* Broad distributions involve the lack of self-averaging and average quantities are dominated by the extreme contribution of a vanishing fraction of rare samples. This class of models comprises mainly quantum spin

chains and spin ladders.

Disorder influences however not only the critical behaviour. Griffiths and McCoy pointed out in the random classical and quantum Ising model, respectively, that there exists an extended region around the critical point, where several physical quantities are singular. The origin of *Griffiths phase*, which has no counterpart in pure systems, is the presence of such rare domains, which are locally in the opposite phase. The so called Griffiths-McCoy singularities are much more enhanced in quantum systems, where statics and dynamics are inherently linked. Here, the fluctuations of disorder described above give rise to a power-law decay of average temporal correlations, which is reminiscent of criticality, while in the spatial direction there is short-range order. For this reason Griffiths phase is termed as a line of "semicritical fixed points". According to a phenomenological scaling theory the singular behaviour of quantities studied so far, were reduced to a common physical ground, and the exponents characterizing the singularities are all related to the dynamical exponent of the system, which is a continuous function of the control parameter in the Griffiths phase.

In the bulk of the thesis we deal with the Griffiths phase and the critical behaviour of quantum spin chains, which is controlled by an infinite-randomness fixed point. In the second part a classical model, the random-bond q-state Potts model is studied in the large-q limit, where thermal fluctuations become irrelevant. A common feature of both problems, that the critical behaviour is strongly dominated by fluctuations of disorder as opposed to quantum fluctuations (resp. thermal fluctuations in the classical model).

In order to investigate the above problems, several different approaches have been used. The quantum spin chains are studied by the help of free-fermion representation in analytical and numerical way, and in the framework of a phenomenological scaling theory. The properties of Griffiths phase are investigated analytically and numerically by renormalization group transformation. The problem of random-bond Potts model in the large-q limit is mapped onto an optimization problem, which is solved by stochastic and combinatorial optimization methods.

In Chapter 2 we shortly summerize the theory of critical phenomena in disordered classical- and quantum systems, and give a general phenomenological description of Griffiths phase.

In Chapter 3 previously known results on the random transverse-field Ising chain are reviewed, including the free-fermion description of the model, the relation with random walk, and the phenomenological scaling theory of rare events.

In Chapter 4 we present our numerical and phenomenological results on the Griffiths phase of random transverse-field Ising spin chain. We consider here quantities, the singular behaviour of which is not trivially related to that of the energy gap, such as the second energy gap, non-linear susceptibility, and energy-density autocorrelation function. By using phenomenological scaling arguments we relate the exponents describing the singular behaviour of the above quantities to the dynamical exponent. In the free-fermion picture closed forms for these quantities are derived, which are then analyzed numerically. The numerical results support the validity of scaling considerations.

Subsequently we extend the Ma-Dasgupta-Hu type real-space renormalization group scheme to the Griffiths phase, which is presented in Chapter 5. This

method was applied at the critical point of several quantum spin chains, where it works asymptotical exactly, and generally believed to lose its asymptotical exactness by leaving the vicinity of critical point. We give an analytic solution for the flow equations of the random transverse-field Ising chain in the Griffiths region, where we show that the procedure is asymptotically exact, and the dynamical exponent stays invariant during renormalization. By the help of this an exact expression for the determination of dynamical exponent is given. On the ground of phenomenological considerations we propose the above assertions to be generally valid for quantum spin chains. In order to check this we solve numerically the renormalization group flow equations of random quantum Potts chain, and estimate the value of q-dependent dynamical exponents. Our results are compatible with that of obtained by density-matrix renormalization group calculations, supporting the validity of theoretical considerations.

Chapter 6. is devoted to the study of random XY- and random dimerized XX chain. Our investigations rest on the phenomenological theory of average quantities developed in Chapter 3, which relies on the scaling behaviour of rare events. Establishing a relation with random walks, rare events are identified as regions corresponding to surviving walks. By the help of this theory we determine the complete set of bulk- and surface critical exponents. These are then compared to results on operator-profiles, which are obtained by numerical calculations based on the free-fermion technique. We find that critical order-parameter profiles follow the conformal predictions, although the models under investigation are not conformal invariant. Furthermore we determine the average behaviour and the distribution of dynamical correlations at criticality and in the Griffiths phase. Average autocorrelations are found to decay logarithmically slowly at criticality, whereas they decay as a power-law in the Griffiths phase with a power related to the dynamical exponent. Via decoupling the models into two Ising chains, we give an analytical expression for the dynamical exponent.

In Chapter 7 we turn to study the q-state random Potts model, where after appropriate parameterization the $q \to \infty$ limit is sensible, and the q-dependent magnetization exponent is known to converge to a finite value. Contrary to previous finite-q calculations we perform here a *direct* investigation in the $q \to \infty$ limit by the help of *random cluster representation* of the model. We show that in this limit thermal fluctuations becomes irrelevant, and critical behaviour is determined by a single dominant graph in the geometric representation of the model. To find this graph is equivalent to an optimization problem of a non-convex cost-function defined on the set of graphs. We solve this problem by a stochastic- and a combinatorial optimization method. Analyzing the fractal properties of dominant graph we give a more accurate estimation for critical exponents, than previously.

We have dealt in this thesis with singular properties of strongly disordered models at criticality and in the Griffiths phase. Among our findings obtained in special models, there are a number of results, which are supposed to reflect more general properties of random systems. Thus the information extracted from the above special models hopefully contributes to a better understanding of the cooperative behaviour of random systems with many degrees of freedom. Notwithstanding our analysis raise several new questions, such as the treatment of phenomena studied in our low-dimensional models in higher dimensional or in more realistic models.